Studies of the Gold-Sulphur Bonding in Nanotechnology

Amanda Bard

A thesis submitted in partial fulfillment of the requirements for the
Master's degree of Science in Chemistry

Department of Chemistry and Biomolecular Sciences
Faculty of Science
University of Ottawa

Abstract

This thesis explores the kinetics of gold nanoparticle surface modification with thiols and its potential applications in nanotechnologies. In chapter 3 the ideal functionalization time for thiols to bind to the surface of the AuNP was found to take more than one hour for completion. 7-mercapto-4-methylcoumarin was used to follow the process by fluorescence spectroscopy and serves as a convenient molecular probe to determine relative kinetics. Fluorescence spectroscopy studies with various thiols, such as aliphatic and aromatics, further support the slow surface modification kinetics observed by fluorescence spectroscopy. The formation of thiolate bonds is a relatively slow process; we recommend one to two hour wait for thiol binding to be essentially complete, while for disulfides, overnight incubation is suggested.

The application of gold nanoparticle surface modification was further investigated with its application in a Nanopore Assay as an amplification method for low concentration target proteins. Gold sulphur binding was utilised as a method to attach DNA on the surface of a AuNP in order to increase signalling 100 fold or more. Following low signal results, testing involving the loss of DNA to plastic tubing was investigated and it was noted that interactions with plastic can cause significant loss of sample to the surface of plastic non binding materials.

Acknowledgments and Contributions

I would first and foremost like to take a moment to thank my family and friends, in particular my parents who let me make my own path and supported me no matter the outcome. Thank you for allowing me to explore without fear and thrive in ways I could not have known without your love and support. And to my husband, Karl, for all the late night support, making sure supper was taken care so that I could focus, thank you. For always being there through the tough times when I thought I couldn't, for pushing me to continue even when I did not want to, thank you. Thank you for always listening to my chemistry talk and even sparking a debate from time to time. Here's to the next adventures together!

Tito, I'm not sure if I would have even embarked on such a journey without your encouragement and support, for this I will always be grateful. Thank you for your guidance and endless knowledge, I have yet to find a question that you could not answer. Your investigative nature and curiosity inspires me and reminds me there is always opportunity to continue learning.

I will never forget the Scaiano Group, to this great group of individuals of which I have shared countless memories. I would like to take the time to thank you in particular Anabel with your support and guidance throughout my work. Your input and critical feedback allowed me to grow as a scientist and persevere where I wasn't sure I could.

I would also like to acknowledge the contribution and help from the Tabard-Cossa Group, their knowledge on nanopores and the development of nanopore assays were essential in the development of DNA materials to be quantified. They were also responsible for all gel electrophoresis testing.

Contents

List of Figures

List of Schemes

List of Tables

List of Abbreviations

AuNP Gold Nanoparticles

C-SMe S-methyl-7-mercapto-4-methylcoumarin

BSA Bovine serum albumin

C-SH 7-mercapto-4-methylcoumarin

DMSO Dimethyl sulfoxide

dsDNA Double stranded DNA

I-2959 Irgacure-2959

LA Lipoic acid

LFP Laser flash photolysis

LSPR Localised surface plasmon resonance

ME 2-mercaptoethanol

MMP Magnetic microparticle

NH_2-DNA Amino terminated DNA

NP Nanoparticle

PA Polyallomer

PBS Phosphate-buffered saline

PEG Polyethylene glycol

PhSH Thiophenol

Rh Rhodamine

SAMs Self-assembled monolayers

SH-DNA Thiol terminated DNA

SPR Surface plasmon resonance

ssDNA Single stranded DNA

TEM Transmission electron microscopy

TSH Thyroid stimulating hormone

Chapter 1: General Introduction

Table Contents

1. Introduction

1.1 Nanomaterials

Materials with at least one dimension lower than 100 nm are commonly known as nanomaterials. Nanomaterials span a large variety of materials, shapes and sizes. For comparison, Figure 1.1 demonstrates the breadth of nanomaterials in contrast to everyday items.

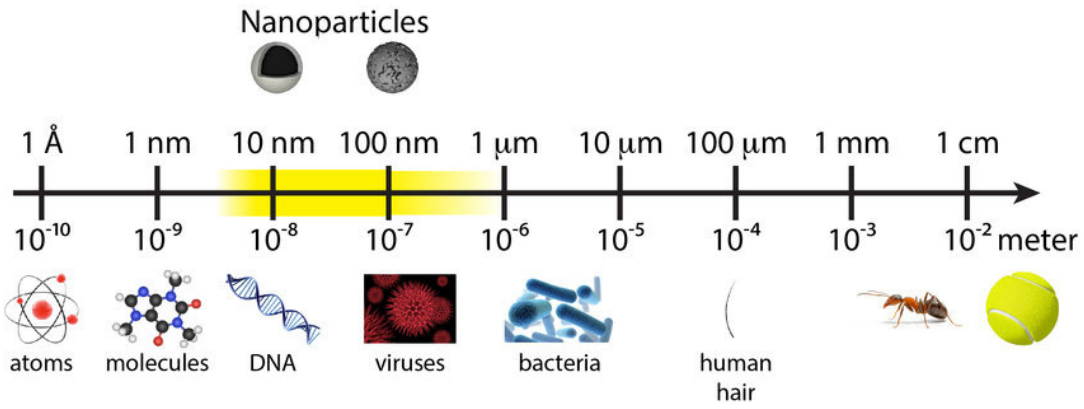

Figure 1.1: Size of nanomaterials in relation to common objects. Reprinted with permission from ref. 1 Copyright (2015).

In general, nanoscale materials show different physical, chemical and biological properties than those of the bulk material. The fundamental difference in chemical composition as well as morphological properties when going to the nanoscale has brought a lot of attention to the research and development of nanotechnology over the past few decades. [2-5]

Historically nanoparticles were commonly used, though they had not been identified at the time. A great example of this is the use of gold nanoparticles (AuNP) for the wide variety of colors they display in the presence of light and different treatments. The Lycurgus Chalice created in the 4th Century A.D., depicted in Figure 1.2, demonstrates the use of 70 nm spherical gold and silver nanoparticles imbedded in the glass. The chalice appears green with reflected light however if light is shone directly through the chalice it appears red. These ruby red colors have been used for centuries in stained glass and other applications. In recent years, a deeper understanding of AuNP has emerged, revealing that the ruby red color stems from the reduction of gold during the glass production process.

Figure 1.2 Lycurgus Chalice Department of Prehistory and Europe, The British Museum © The Trustees of the British Museum.

The various properties of these materials is what makes nanoparticles quite promising. Interest remains due to their high versatility and small size (1-100 nm); they have potential to be used across a wide variety of applications, such as catalysis, self-assembly structures, biological and chemical sensing, among many others [3-5]. Distinct applications often require specific materials, for example, nanoparticles are commonly used for targeted transport applications, which optimise the nanoparticles properties as an electron carrier in electrochemical applications.[6] However, nanoparticles can also have biological applications as a drug carrier. Scientific interest in nanoparticles has increased and has pushed the development of nanoscale devices that bridge the gap between chemical and biological systems.

For centuries, gold nanoparticles have been incorporated in stained glass for their vibrant colors, which are due to an optical interaction with visible light. Their optical properties have been extensively studied. [7] Nanoparticles have a variety of properties that can change depending on size, capping layer, pH and solvents. The key difference relates to the interfaces; it is this layer that allows the modification of properties of the nanoparticle based on size, shape and composition. A nanoparticle (NP) is typically made of an inorganic metal (Au, Ag, Cu, etc.) with an exterior capping agent. Organic molecules are used as a capping agent and stabilizer for the inorganic core. One distinguished property of some of the metal nanoparticles is their plasmon absorption. This optical property is responsible for the visible colour of colloidal metal (Au, Ag, Cu, etc.) nanoparticles and is widely used in most of the metal nanoparticle applications.

1.2 Plasmon

Plasmonics relies heavily on processes involving the plasmon of metals. The plasmon is considered as a collective oscillation of electrons following changes in the electric field vector of the incident beam. [6] It resembles ripples on the surface of a pond. The pond water acts as a collective mode of water molecules, which is comparable to the electrons of the metal surface. Plasmons are most commonly found in metals, where electrons are usually bound weakly to the atoms and move freely. A plasmon can be considered as an electronic ripple, where the electrons follow a well-defined wavelength. The wave is created by the excitation of electrons and the associated positive charges generated that deploy a force on the electrons. The nuclei act as a restoring force to bring the electron back, the movement of electrons creates plasmon oscillation. It is important to first understand the plasmon of the bulk materials. Surface plasmon resonance (SPR) is generated from a layer of bulk noble metals in particular gold and silver, upon the absorption of light. Bulk material carry both bulk plasmons and surface plasmon polaritons on a flat surface, which contains a collection of positive charges periodically dispersed on the surface. Upon irradiation with light, light interacts with the surface of the metal and can displace the electrons following Figure 1.3.

The phenomenon of localised surface plasmon resonance (LSPR) has been of considerable interest. [8] LSPR is typically used for the detection of molecular interactions close to the surface on gold or silver nanoparticles. LSPR occurs near the surface of a nanoparticle, as demonstrated in Figure 1.3.

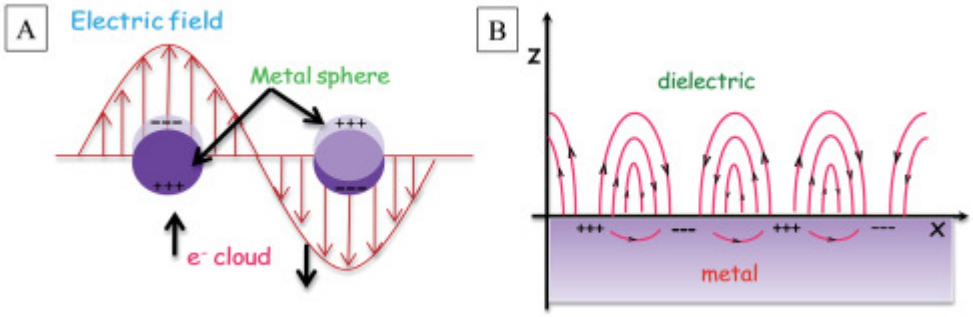

Figure 1.3: Illustration of A) localized surface plasmon resonance and B) surface plasmon resonance. Reprinted from ref. 9 with permission from RSC Adv. 2016, (89) Copyright (2016).The Royal Society of Chemistry.

Metal NP resemble miniature films which absorb light, similar to SPR, however as NPs get smaller their surface curvature becomes increasingly important. The surface is no longer planar in relation to the light exciting it. The free electrons form and participate in the oscillation of the plasmon, which affects NP optical properties. The nanoparticles have a negligible bulk effect, which makes then a good tool for monitoring surface attachment to AuNP.

As depicted in Figure 1.4, the incident electromagnetic field generates the oscillation of the electrons on the nanoparticle surface, which in turn produces an induced electromagnetic field. Since the NP size is much smaller compared to the wavelength of the incident electromagnetic field, it can be assumed that all electrons will sense a constant electric field (Figure 1.4, inset). This phenomenon is responsible for the absorption of light by the NP. Thus, when the NP absorbs the proper light frequency there is a great response in the electric oscillations of the electrons. The induced electromagnetic field generated on the NP surface can drastically affect the optical properties of any species in close proximity to the NP surface and is usually related to the enhancement of Raman signals as well as quenching of fluorescence. [10]

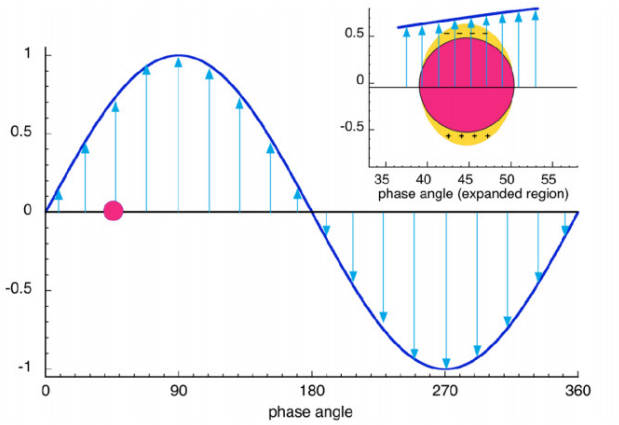

Figure 1.4: Illustration of plasmon effect produced on nanoparticles in the presence of an electromagnetic field. Reprinted from ref. 6 with permission from J Phys Chem Lett 2013, 4 (7), 1177-87 Copyright (2016) American Chemical Society.

This phenomenon is known as plasmon enhancement, and allows for the detection of molecules at low concentrations (*vide infra*). Nanoparticle characteristics such as shape, size, chemical nature and environment influence the effect of LSPR. Marquez *et al.* have demonstrated some of the effect seen when changing the shape of a nanomaterial. [11] A change in morphology results in a change in plasmon absorption. Therefore, it is expected that plasmon absorptions differ

when nanoparticles change from spheres to other morphologies. For instance, rod-like particles show two distinguishable plasmon bands that correspond to the longitudinal and the transversal plasmon resonances which can be seen in Figure 1.5 below.

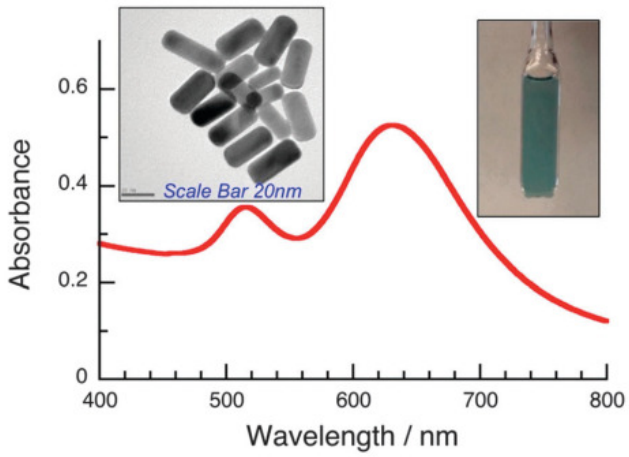

Figure 1.5: Spectrum of silver nanorods. From ref. 11 Reprinted with permission from Chem Commun (Camb) 2015, 51 (10), 1911-3. Copyright (2015) The Royal Society of Chemistry.

LSPR strongly depends on the rod aspect ratios, as light can generate different electronic motions at the tip of the rods compared to their length. Thus, depending on the orientation of the rod, it can be considered invisible to certain wavelengths. This generates the two main absorption bands in Figure 1.5, known as transversal and longitudinal bands at ~520 nm and ~650 nm, respectively. The phenomenon is observable through the various colours that occur when there is a change in the aspect ratio or, as shown in Figure 1.6, when the particles can adopt certain alignment with respect to the incident electromagnetic field.

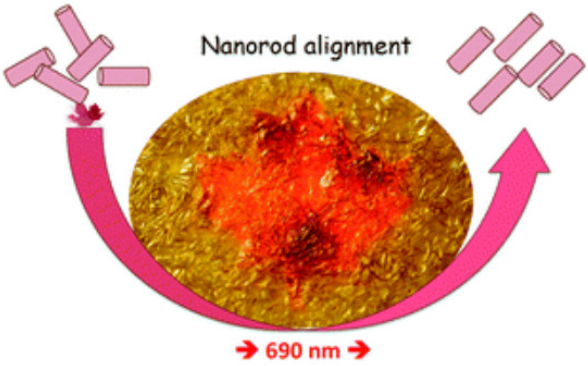

Figure 1.6: Illustration of nanorod alignment upon radiation where the red leaf represents the alignment of AuNR upon exposure to 690 nm light. From ref. 10. Reprinted with permission from Chem Commun (Camb) 2015, 51 (10), 1911-3. Copyright (2015) The Royal Society of Chemistry.

The irradiation of the sample seen in Figure 1.6, in a specific pattern, allows the alignment of randomly oriented nanorods. The alignment is caused by the heat generated by the plasmon absorption. This heat is enough to melt the polymer allowing the nanorods to move and align within the incident electromagnetic field. When excitation is stopped, the polymer cools down fixing the rods in the aligned position.[11]

It is important to note that not only the shape will affect optical properties. Dielectric medium such as high salt concentration can cause the NP to aggregate. In the presence of high salt concentration, the overall charge of the surface of the NP is affected. The standard Zeta potential for a stable colloidal solution should be greater than 25 mV; [12, 13] however, if there is a change in the dielectric media, the environment felt by the particles will have a change in the overall charge. The resulting aggregation is due to a change in the surface charge. At values lower than 25 mV, the NP no longer has the proper balance of charge to repel one another to maintain stability, resulting in the aggregation and eventual precipitation of the colloidal solution, unless other repulsion forces can take place.[12] Controlling the environment of the NP is crucial to properly maintain stability and their optical properties.

1.2.1 Mie's Solution to Maxwells Equation

To be able to properly understand LSPR we must consider Mie's theory. Plasmon absorption of small spherical particles was described by Gustav Mie in 1908 when he solved

Maxwell's equation.[14] The electronic cloud is affected by the absorbance of light and can fluctuate depending on that absorbed light.

$$C_{ext} = C_{abs} + C_{sca} \quad (1.1)$$

Where C_{ext} is the nanoparticle extinction, C_{abs} is the absorption component of the optical extinction and C_{sca} stands for the scattering of the optical extinction, respectively. Mie theory involves the scattering and absorption of light when considering their interaction with the plasmon waves. Mie solutions of AuNP follow Rayleigh approximations which state: diameter much less than the wavelength (<<λ), or approximately one twentieth of the wavelength (~1/20 λ). [8] It was not before his publication in 1908 that the color of colloids was able to be described.

$$C_{sca} \propto a^6 n^4{}_{med}/\lambda^4{}_0 (m^2 - 1)/(m^2 + 2) \quad (1.2)$$

$$C_{abs} \propto a^3 n_{med}/\lambda_0 Im(m^2 - 1)/(m^2 + 2) \quad (1.3)$$

Where α is the radius of the particle, *n* is the refractive index of the media and *m* is the refractive index of the solution. As per equation 1.2, the scattering predicted by the Mie solution is inversely proportional to the fourth power of the wavelength of light, whereas the absorption is an inverse function of the wavelength (λ). These factors govern not only the color of the colloids but also their properties which changes as a function of size, shape and dielectric media. As discussed later, these inherent properties will directly affect the plasmon enhancement.

1.2.2 Enhancement and Quenching of Fluorescence or Raman Signals

Optical signals obtained using fluorophores have become an industry standard for imaging and for high sensitivity models, which has brought to light the effects of enhancement and quenching. Figure 1.7 illustrates the relation between the distance and the fluorescence intensity of the fluorophore in proximity to a metal NP. At an infinite distance from the nanoparticle, there is a given fluorescence/scattering of the AuNP. As the fluorophore approaches, the fluorophore sees an enhancement from the AuNP plasmon. As fluorophores approach to the NP surface (10 nm), which has a strong plasmon field, there is an interaction with the electrons of the fluorophore and the NP. The interaction leads to changes in the fluorescence of the fluorophore (enhancement or quenching). The cause of quenching or enhancement is related to the plasmon of the NP. When the fluorophore reaches a critical distance from the NP surface, quenching of the fluorescence is experienced. Upon binding to the AuNP there is an interaction with the fluorophore, which leads

to the complete fluorescence quenching (*i.e.*, no fluorescence). When the fluorophore reaches larger distances (> 20 nm) from the surface of the AuNP, the fluorophore can still see dipole-dipole interactions from neighboring molecule on AuNP. Quenching and enhancement are competing effects; however, the key between their relationship is the distance of the fluorophore to the particle. Each has a relationship that differs in function of distance. Quenching dominates at distances less than 1 nm, whereas enhancement dominates at larger distances. [15]

The strength of the induced electromagnetic field of the metal NP is controlled by the absorbance of incident light. However, the field strength is also dependent on the structure and composition of the NP; metal composition, particle size, capping agents and surface of the NP as well as the wavelength of incident light used. Enhancement and quenching have been utilized in a wide variety of studies such as kinetic studies and ligand quantification. Enhancement can be attributed to greater sensitivity and reduced signal-to-noise in fluorescent samples. Quenching allows for a variety of potential testing and can be used in areas such as negative sensing or selective quenching. [16, 17]

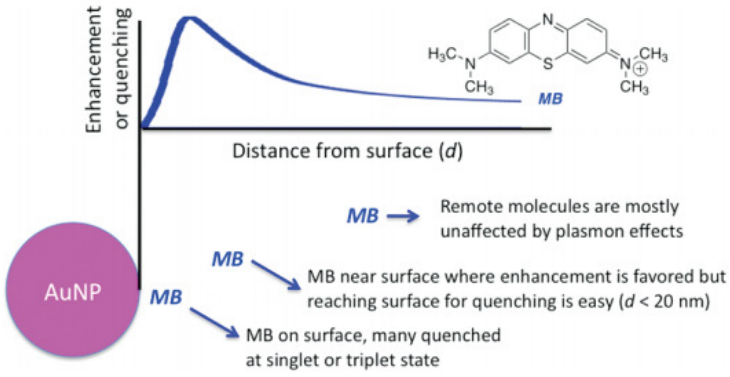

Figure 1.7: Illustration of the relationship of fluorescent enhancement and quenching with distance from the surface. From ref. 14. Reprinted with permission from J Am Chem Soc 2010, 132 (18), 6298-9. Copyright (2010) American Chemical Society.

1.3 Nanoparticle Synthesis

The synthesis of nanoparticles can be categorised into two different types of methods: *top down* and *bottom up*. In the case of *top down* synthesis, there are two main methods, which are laser ablation and E-beam lithography.[18] In both cases, the particles are made from etched out bulk

material, ultimately removing crystal planes until a nanostructure is created. It is often referred to as the removal of building blocks from a substrate to form nanoparticles.

The *bottom up* method involves the synthesis of nanoparticles onto a substrate or solution, which requires the building blocks to come together to form nanoparticles. Bottom up synthesis generally allows for more control of the system leading to nanoparticles with less defects and a more homogenous composition. The bottom up synthesis is more commonly used for chemical applications and catalysis. [19-21]

1.3.1 Nanoparticle Nucleation and Ripening

For nanoparticles to be created they require ripening time, which is the time the particles require to grow to the thermodynamically stable size and shape and can be controlled in a few different manners. Oswald ripening follows a spontaneous thermodynamic process, where larger particles are favored over smaller particles. Adding a capping agent can be a simple method to stop NP growth. Other methods include temperature control, often using sodium borohydride as reducing agent. [22, 23] The nucleation and ripening processes of NP over time as a function of atom concentration can be seen in Figure 1.8 below.

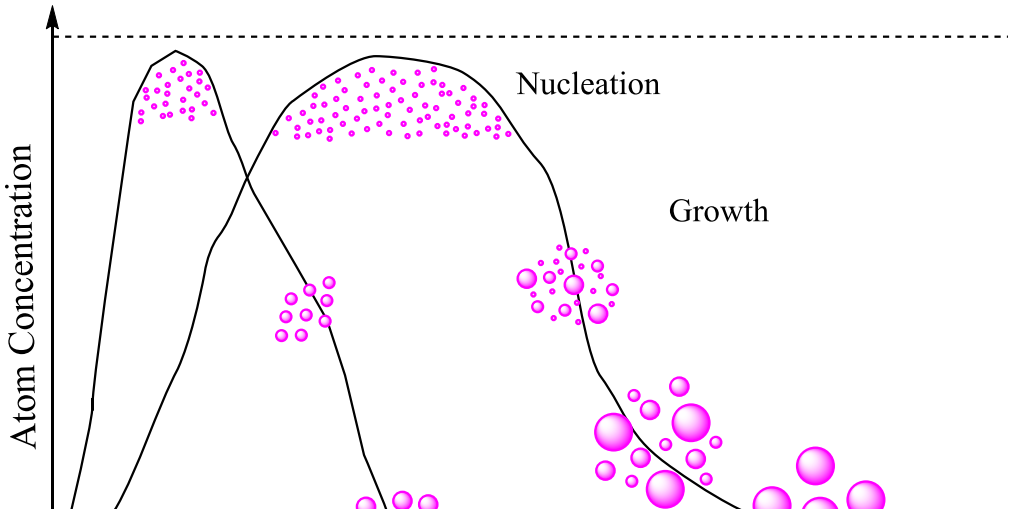

Figure 1.8: Nucleation and ripening processes over time of nanoparticles as a function of atom concentration Adapted from ref. 24 Chikan, V.; McLaurin, E. J., Rapid Nanoparticle Synthesis by Magnetic and Microwave Heating. Nanomaterials (Basel) 2016, 6 (5).

1.3.2 Synthesis of Gold Nanoparticles

Nanoparticles' size and coverage are adjusted during the synthesis method using different precursors, or after synthesis by ligand exchange. Colloidal gold nanoparticles are commonly synthesised by reducing gold chloride salt.[25] The aqueous colloidal process is one of the more commonly used syntheses due to its simple and cost-effective procedure. It also allows for easy tailoring of nanoparticle size. The size of nanoparticles can be crucial for various applications; thus controlling the size through the synthesis methods as well as capping agent can be helpful to tailor NP size to a given application. Extensive control over the composition, size and surface properties of the NP allows for optimal usage.[26] Studies have also been done to be able to calculate a given concentration of the AuNP in solution.

1.3.2.1 Effect of Capping Agent

The capping agent used can affect the properties of the AuNP by changing both the environment as well as the active surface of the particle. Common capping agents include citrate, PEG and thiols.

1.3.2.2 Sodium Citrate

Sodium citrate capped gold nanoparticles can be synthesized using a simple method that requires very little effort.[25] To begin, gold chloride salt is dissolved with milli-Q water. The gold chloride solution is heated and placed under reflux for two hours. After heating, a reducing agent is added to reduce the gold salt from Au (III) to Au (0). Citrate, in this case, is a reducing agent as well as stabilizer meaning the citrate simultaneous reduces and stabilizes the AuNP. The citrate solution is added to the hot gold chloride solution; upon the addition of the citrate, the solution color will begin to change from golden yellow to a ruby red over the course of the next hour under reflux. The time required for the particle to ripen is demonstrated in the Figure 1.8, resulting in particles of 15-20 nm of diameter.

1.3.2.3 Sodium Borohydride

Other syntheses include the use of sodium borohydride ($NaBH_4$); similarly to sodium citrate, sodium borohydride is a reducing agent, however it is qualified as a strong reducing agent which results in smaller AuNP (5-10 nm). The gold chloride solution must be kept cool before the addition of a sodium borohydride solution. The gold chloride solution will go from golden yellow to a pink-red after the addition of sodium borohydride; this is a result of the reduction of Au(III)

to Au(0). The temperature control allows the reaction to occur in a timely manner that enables proper ripening of the AuNP of a smaller size.

The use of $NaBH_4$ allows for a variety of capping agents, following the reduction of the Au. The AuNP are considered bare after being reduced by $NaBH_4$ and a variety of stabilisers can be added. However, the naked particles that are produced after reduction are more susceptible to aggregation.

The different capping agents can also affect the tolerance of nanoparticles to changes in the dielectric environment. Looking at citrate versus DNA coated AuNP there is a small shift in the peak.

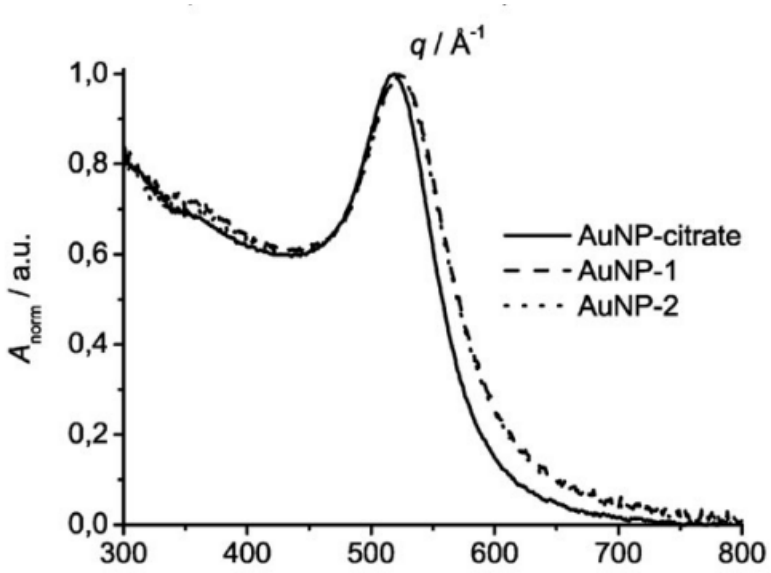

Figure 1.9: Absorbance peak shift of AuNP with various stabilizer coatings. From ref. 27 Reprinted with permission from the Phys Chem Chem Phys 2008, 10 (14), 1870-5. Copyright (2008) Physical Chemistry Chemical Physics.

The effect of different capping agents can be seen in Figure 1.9; the replacement of citrate can lead to a small shift in the absorbance spectra. Upon the addition of a capping agent with a greater negative charge, the UV-spectrum experiences a red shift. The application of UV techniques can be complementary in confirming the proper adhesion of a capping agent. Furthermore, studies have shown that the stabilisation of AuNP via the Au-S bond is quite strong

due to the bond energy associated (130 kJ/mol). [28] It is the robust nature of the Au-S bond that allows for the stabilization and easy modification of the surface using thiols.

Capping agents can also be used to prevent NP etching as shown by Lanterna *et al*.[29] The use of a variety of capping agents can allow both stability and protection of the AuNP core. Selectivity and agglomeration are some of the main concerns when modifying the surface of NP. If the solution of AuNP and capping agent is not given enough time to modify the surface of the AuNP it can leave parts of the surface of the AuNP bare. A bare surface often leads to agglomeration and/or aggregation.

1.3.2.4 Dielectric Media

Studies have shown AuNP to be highly influenced by its surrounding environment. This is because AuNP are commonly made in solution, such as colloidal solutions. It has been shown by various studies that high concentration of salt leads to the agglomeration of AuNP. Concentrations of salt in the μM range have been used as an industry standard and maintains stable AuNP. At higher concentrations, there is a change of the optical properties, which is related to the aggregation of the nanoparticles.

1.3.2.5 Size Effect

The relationship between AuNP size and color has been characterized, which is demonstrated in Figure 1.10. The wavelength (correlated to the color seen) of the nanoparticles increases as the particle size increases, but there is a limit to which the nanoparticle reach properties that resemble those of the bulk material. The solutions then have a translucent color and can often have particles that are not in suspension.

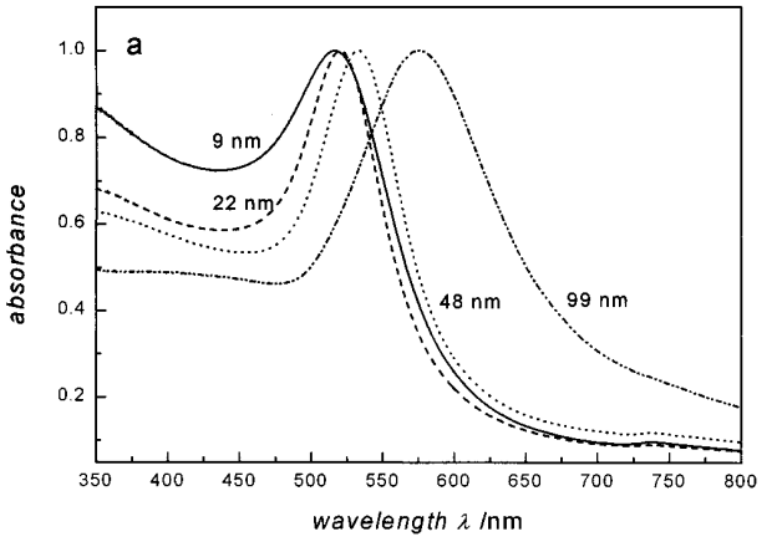

Figure 1.10: Plasmon band shift with varying size of AuNP. From ref. 30 Reprinted with permission from J. Phys. Chem. B, 1999, 103, 4212-4217. Copyright (1999) American Journal Society.

1.3.3 Photochemical synthesis

The use of photo-initiators is another method used to produce gold nanoparticles. The particles synthesised generally range from 5-10 nm in size. A commonly used synthesis for gold nanoparticles uses Irgacure-2959 (I-2959). Upon irradiation with light, the I-2959 generates ketyl radical, 2-hydrox-2-propyl radical, which is a powerful electron donor. For the reduction of gold to proceed there must be an efficient transfer of the electron in the presence of an acceptor, Au(III) in the form of $AuCl_4^-$ in this case.

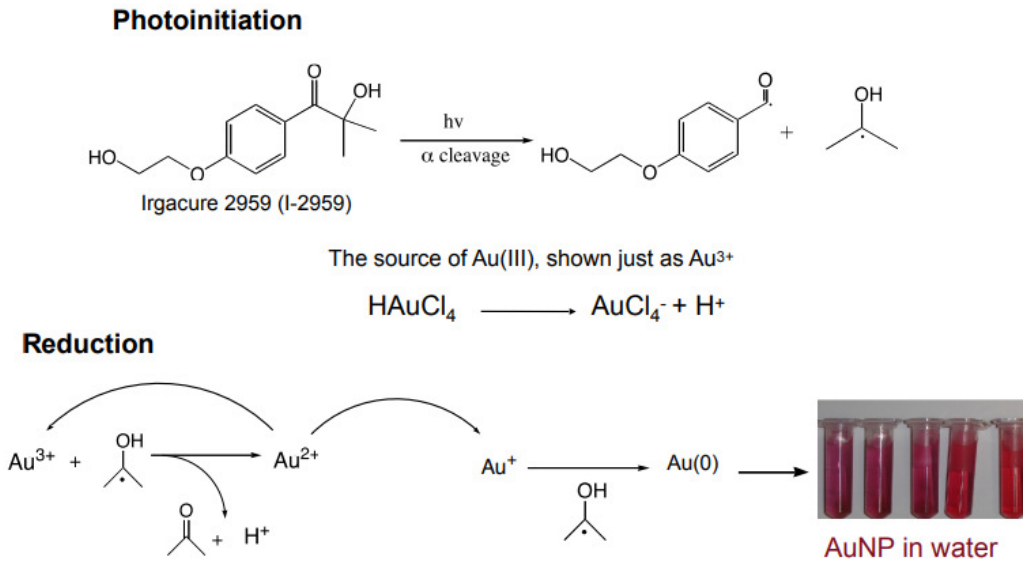

Figure 1.11: Photochemical synthesis mechanism of the reduction of Au to make AuNP. From ref. 31. Reprinted with permission J Am Chem Soc 2006, 128 (50), 15980-1. Copyright (2006) American Chemical Society.

For the process in Figure 1.11 to be efficient, the transfer of an electron from the ketyl radical to the Au(III) must be efficient and occur faster than other radical chemistry. The synthesis of photo-initiated nanoparticles requires the photo-initiation of the I-2959, followed by the reduction of Au(III) to Au(0) giving colloidal AuNP. The ratios of I-2959 to gold salt must be kept in stoichiometric amounts to obtain good nanoparticles (3:1 for the case of gold nanoparticles since it requires three electrons to reduce Au(III) to Au(0)).

Under UVA irradiation, the synthesis of AuNP can be completed in minutes. Interestingly the NP size can also be controlled by changing the illumination strength, with stronger light generally leading to smaller particles.[31] Another benefit of using light is that the nanoparticles created do not have a surface coating and can be easily modified.

1.4 Gold-Sulphur Bonding

The sulphur-gold bonding is extremely important and has been well characterized through various studies. Xue *et al.* [32] explored the strength of the gold-sulphur bond in relation to the gold-gold bond. Studies were done using a flexible PEG linker to able to apply adequate resistance. It was discovered, with the aid of an AFM tip functionalized with a thiolated PEG linker, that the Au-S bond was much stronger than the Au-Au bond. [32] The AFM tip was placed onto a gold surface allowing for the thiol to bind to with Au. Following the binding of the thiol from the AFM

tip was removed causing stretching which applies tensions; as seen in the Figure 1.12 below. The Au-Au bond is broken upon stretching, leaving the Au-S bond intact.

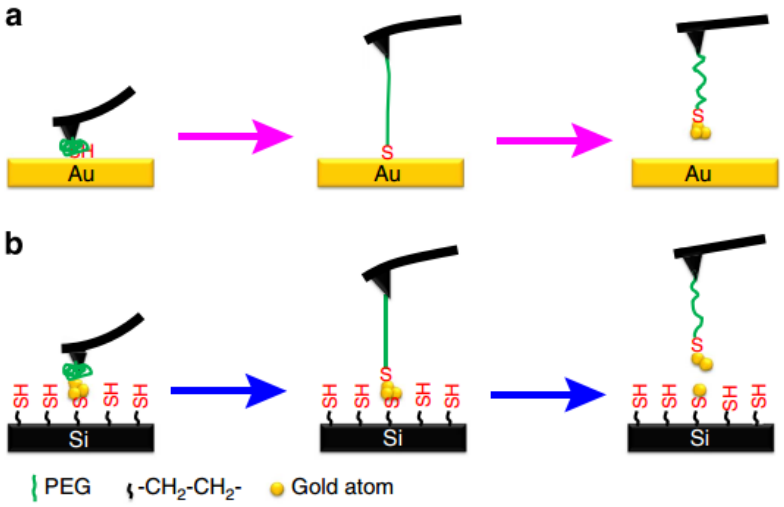

Figure 1.12: Illustration of AFM-tip experiment, which allowed for the determination of Au-Au bond strength. From ref. 32 Reprinted by permission from Nat Commun 2014, 5, 4348. Copyright (2014) Nature Communications.

1.4.1 Self-Assembled Monolayer

The industry standard currently believes the Au-S bond forms rapidly (in minutes), however my studies have shown that this is not true. This becomes important when creating self-assembled monolayers (SAMs) and to have a uniform monolayer surrounding the NP. SAMs rely heavily on the bonding kinetics of the gold-sulphur bond. [33]

Self-assembled monolayers on gold have shown their potential for a wide range of applications in sensing. SAMs are made via the simple ligand exchange of the AuNP to the new ligand; those most commonly used have a thiol due to the bond strength of Au-S interaction. SAMs in the case of AuNP are often prepared from a thiolated organic molecule, which varies depending on final function. Due to the gold sulphur affinity, the thiolated marker will displace other stabilizing molecules, such as citrate.

1.5 Characterization of AuNP

1.5.1 Transmission Electron Microscopy

Transmission electron microscopy (TEM) is a high-resolution microscopy technique that uses a beam of electrons to generate an image. From the interactions between the electrons and the sample an image is created. The features of the samples used in TEM are commonly in the µm range, and can be used on samples as small as a few of nm range. Grids are utilised to hold samples or to obtain proper readings. TEM imaging allows to determine the size of the nanoparticles by measuring their dimensions with proper imaging software. Image J software was used to take an average of approximately 100 nanoparticles.

1.5.2 UV-Vis Spectroscopy

UV-Vis spectroscopy is one of many techniques that are used to be able to estimate AuNP size, concentration and level of aggregation. A simple method can allow for a quick check on the colloidal AuNP solution, to verify whether they are stable and/or if they have agglomerated. It is often used to ensure particles are stable over the course of experiments, and over the period of multiple experiments using the same batch of nanoparticles. As seen in Figure 1.10 particle size and coatings result a shift in the absorbance peak. Two absorbance peaks were monitored in order to follow the colloidal AuNP solution, stable particles for the given synthesis gave a distinct peak at 525 nm and a broader peak at ~700 nm demonstrates the agglomeration of AuNP.

UV-Vis spectroscopy measure the extinction of light (scattered and absorbed) that passes through a sample. The optical properties of nanoparticle are dependant on various characteristics such as size, shape, concentration and agglomeration state. This allows UV-Vis to be a useful tool to identify and characterize nanomaterials. It is the distinct optical property, LSPR mentioned in section 1.2 that results in a strong absorbance between 500nm-600nm in the visible region allowing measurement by UV-Vis spectroscopy. From the maximum absorbance peak the size of the AuNP can be estimated. The concentration of the sample can be correlated linearly to particle peak absorbance.[41] The stronger the absorbance peak the higher the concentration of AuNP.

1.5.3 Fluorescence Spectroscopy

Fluorescence spectroscopy can be utilised to measure both the excitation spectrum and the emission spectrum of a sample. It is a fast, simple and inexpensive method to quantify the concentration of a sample based on the intensity of its fluorescence. The excitation spectrum

provides information on the wavelength of light absorbed that is responsible for the emission of the sample, whereas the emission spectrum demonstrates the wavelengths the sample emits.

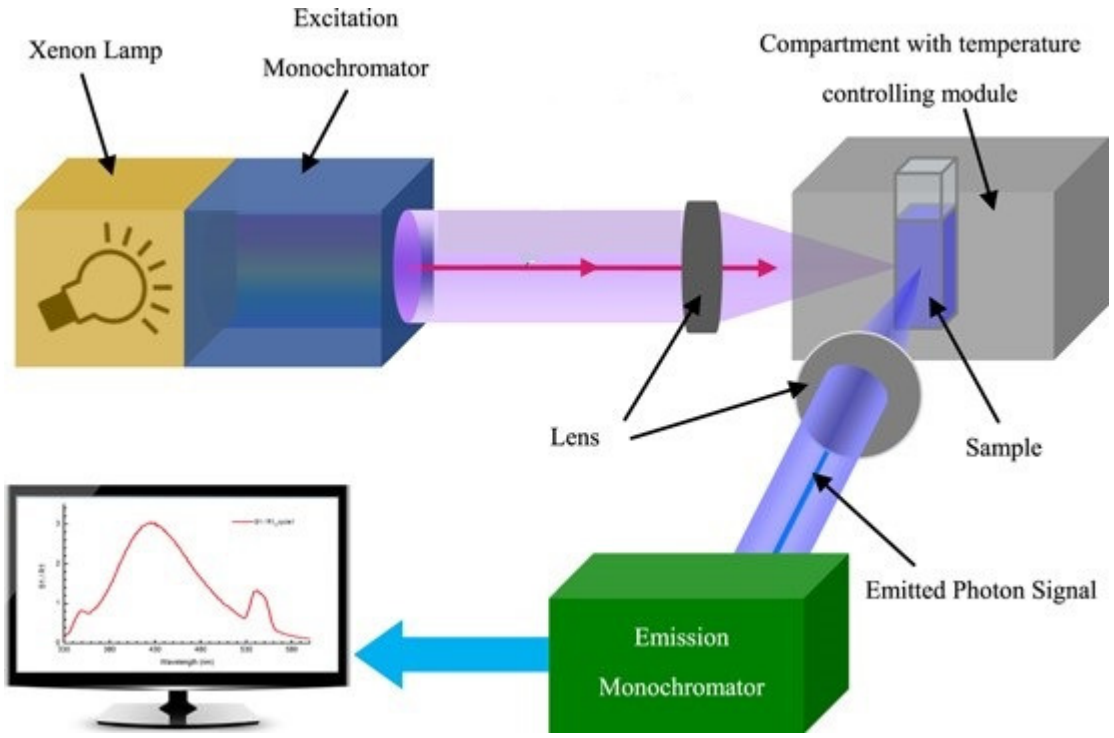

Figure 1.13 Illustration of inner working of a typical fluorimeter. From ref. 34 Reprinted with permission from. Nanotechnology 2014, 25 (43), 435703. Copyright (2014) Nanotechnology.

When considering a fluorescent molecule, the concept of fluorescence must first be understood. A molecule that absorbs light at a given wavelength will get excited to an excited state that exists for a short duration of time (generally nanoseconds) and can relax to the ground state through different processes. A simplified Jablonski diagram illustrated in Figure 1.14 demonstrates the light absorption pathways.

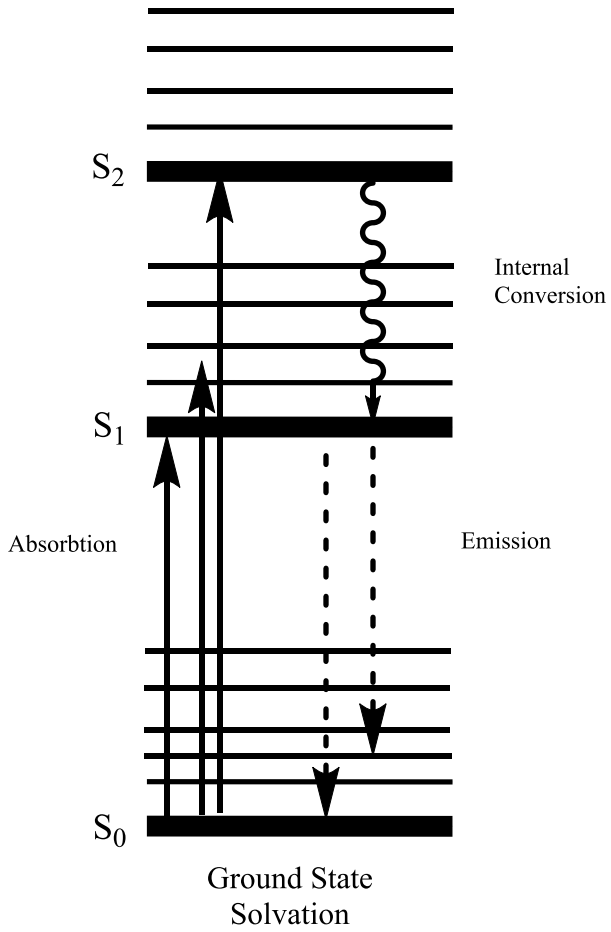

Figure 1.14: Simplified Jablonski diagram: ground state and excited state of a fluorescent molecule upon absorption of a photon. Adapted from ref. 35 with permission from J Chem Educ 1966, 43 (9), 469. Copyright (1966) American Chemical Society.

The excited state of a molecule generally can go through non-radiative processes to lose any excess energy. Some of these processes include the release of heat to the solvent, however when a photon from the excited state relaxes to the ground state it releases energy as emits light, this decay to the lower ground state while maintaining spin is considered fluorescence. To further understand such process consider the simplified Jablonski diagram in Figure 1.14. Beginning in the ground state (S_0), molecules absorb light which allows for an electron from the ground state to be excited to the higher states (S_1, S_2, S_n). Every electronic state contains multiple vibrational and rotational energy levels. Electrons excited into energy states higher than S_1 will relax back down into the S_1 following Kasha's rule, that states *that photon emission (fluorescence or phosphorescence) occurs in appreciable yield only from the lowest excited state of a given*

multiplicity. [36] The light absorbed is associated to a photon that has the same energy or greater than the difference between the ground state and the first excited state. The energy (E) of a photon is given by:

$$E=h\upsilon \quad (1.4)$$

where h is Planck's constant ($6.27*10^{-34}m^2$ kg/s) and υ is the light frequency.

Once a molecule has absorbed the required photon, the photon can be excited and relaxed to a given energy level to be emitted. A Stokes shift is the consequence of S_0 and S_1 having different geometries. The photon that is absorbed, relaxes from the excited state to produce light, however there is some energy lost to other processes, such as heat. This loss of energy is what produces the Stokes shift between the excitation and emission fluorescence spectra, as seen in the Figure 1.15.

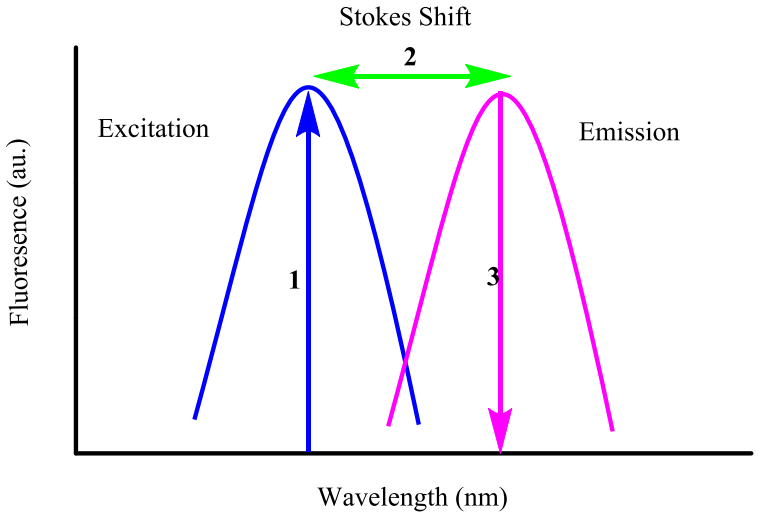

Figure 1.15: Diagram of Stokes shift Adapted from ref. 37 with permission from Proc Natl Acad Sci USA 2007, 104 (51), 20189-94. Copyright (2007) National Academy of Sciences.

Fluorescence is susceptible to quenching or enhancement as a fluorophore approaches the surface of a NP, which can be exploited to quantify a sample that does not fluoresce. In the presence of a non fluorescent competitive reactant there is a decrease in fluorescence because the flurophore can no longer see plasmon enhancement. This principle was applied to quantify testing completed in Chapter 3.

1.5.4 Raman Spectroscopy

Raman spectroscopy allows the observation of the vibrational and rotational modes of a given structure and is most commonly used to give the structural fingerprint of a given sample. The system relies on Raman scattering of monochromatic light. The light is generally provided from a laser in the visible or near infrared. It is most commonly used to visualise interactions between molecules. Gold-sulphur bonding shows good Raman signal and has been used as a quantification method in previous reports. [10, 38, 39] What makes Raman useful is the fact that samples can be monitored in many forms (solid, liquid or in solution), however each type of sample incurs its own set of problems.

Unlike fluorescence spectroscopy, which relies on the relaxation of an electronic state, Raman can detect the various vibrational modes that occur in the rigid crystal lattice of a sample. Moreover, Raman spectroscopy also allows for a larger sensitivity in the scattering fingerprint of the molecule. This fingerprint allows for a more in-depth understanding of the mechanics and bonding of a sample. However, a drawback of Raman is the low signal intensity, which can be several magnitudes lower than those seen in fluorescent markers. [38] Nevertheless, the use of a high power laser can circumvent the low signal issue.

Figure 1.16 below demonstrates the general process of Raman spectroscopy in a simplified Jablonski Diagram. To begin, there are generally three lasers used: the 532 nm (green), 635 nm (red) or 785 nm. The specific laser is chosen depending on the application. The laser is used as an excitation source, which allows high power in a localised area. Following excitation, the use of filters allows the removal of high intensity laser light but enables the transmission of the slightly Raman shifted wavelength from the sample. The filter ensures the proper wavelengths reach the detector without being saturated by residual light of the laser. From the detector, the spectrometer can produce a spectral fingerprint of the crystal lattice structure of the sample, which shows the various bonding kinetics occurring in the sample.

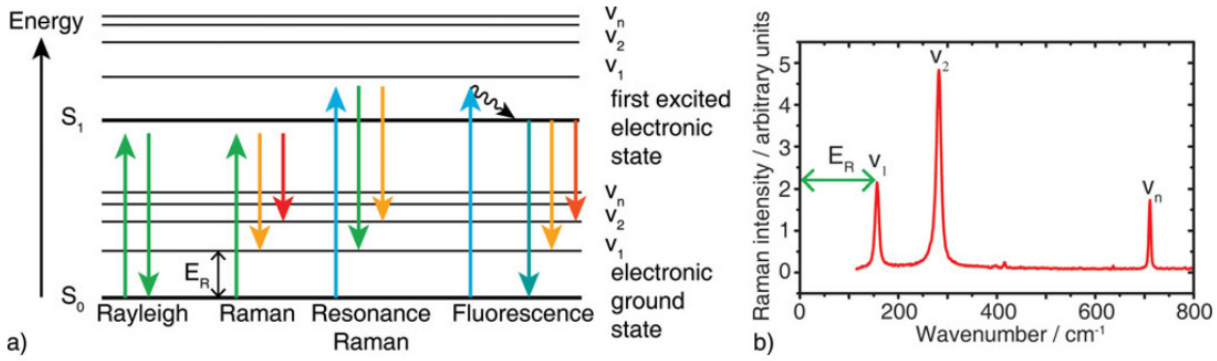

Figure 1.16: Illustration of Jablonski Diagram of Raman from ref. 40. Reprinted with permission from Neth J Geosci 2015, 95 (2), 141-151.

Raman interactions can have one of two outcomes: a material can absorb energy and emit a photon with a lower energy, this is called Stokes Raman or a material can lose energy and emit a photon that has a higher energy, this is called anti-Stokes Raman. The change in energy is related to the vibrational energy levels in the ground electronic state. The observed Raman shift of either Stokes or anti-Stokes can give you insight on the vibrational modes of a molecule thus giving a chemical footprint of what is being measured.

This general introduction gives a good overview of the various concepts utilised to complete the research of the various projects developed in this thesis. Nanomaterials have shown a great diversity and my work explores one of many aspects. To begin my work will assess the functionalization of AuNP with thiols and the role the structure of the thiols plays on functionalization time. Currently, most research follows a simple mix and use method of functionalization, however as my work has show there is a minimum time required for the functionalization of the surface to occur. The reaction time was established by using UV-Vis and fluorescent spectroscopy.

Moreover, this thesis will develop on methods to easily quantify gold nanoparticle loading utilizing UV and fluorescence spectroscopy, as well as the potential applications for the various coatings that can be used to functionalize the surface of gold nanoparticles in particular relating to the strength of gold-sulphur bonds.

1.6 References

1. Bloemen, M. Immunomagnetic separation of bacteria by iron oxide nanoparticles. KU Leuven, 2015.
2. Schwirn, K.; Tietjen, L.; Beer, I., Why are nanomaterials different and how can they be appropriately regulated under REACH? *Environ Sci Eur* **2014,** *26* (1) 4.
3. Giljohann, D. A.; Seferos, D. S.; Patel, P. C.; Millstone, J. E.; Rosi, N. L.; Mirkin, C. A., Oligonucleotide loading determines cellular uptake of DNA-modified gold nanoparticles. *Nano Lett* **2007,** *7* (12), 3818-3821.
4. Yu, H.; Xu, X.; Liang, P.; Loh, K. Y.; Guntupalli, B.; Roncancio, D.; Xiao, Y., A Broadly Applicable Assay for Rapidly and Accurately Quantifying DNA Surface Coverage on Diverse Particles. *Bioconjug Chem* **2017,** *28* (4), 933-943.
5. Hinterwirth, H.; Kappel, S.; Waitz, T.; Prohaska, T.; Lindner, W.; Lämmerhofer, M., Quantifying thiol ligand density of self-assembled monolayers on gold nanoparticles by inductively coupled plasma-mass spectrometry. *ACS Nano* **2013,** *7* (2), 1129-1136.
6. Scaiano, J. C.; Stamplecoskie, K., Can Surface Plasmon Fields Provide a New Way to Photosensitize Organic Photoreactions? From Designer Nanoparticles to Custom Applications. *J Phys Chem Lett* **2013,** *4* (7), 1177-1187.
7. Njoki, P. N.; Lim, I.-I. S.; Mott, D., Size Correlation of Optical and Spectroscopic Properties for Gold Nanoparticles *J Phys Chem* **2007,** *111*, (40) 14664-14669.
8. Mayer, K. M.; Hafner, J. H., Localized surface plasmon resonance sensors. *Chem Rev* **2011,** *111* (6), 3828-3857.
9. Jana, J.; Ganguly, M.; Pal, T., Enlightening surface plasmon resonance effect of metal nanoparticles for practical spectroscopic application. *RSC Adv* **2016,** (89) 86174-86211.
10. Bard, A.; Rondon, R.; Marquez, D. T.; Lanterna, A. E.; Scaiano, J. C., How Fast Can Thiols Bind to the Gold-nanoparticle Surface? *Photochem Photobiol* **2018,** (94) 1109–1115.
11. Marquez, D. T.; Scaiano, J. C., Plasmon induced self-assembly of gold nanorods in polymer films. *Chem Commun (Camb)* **2015,** *51* (10), 1911-1913.
12. Domínguez-Villegas, V.; Clares-Naveros, B.; García-López, M. L.; Calpena-Campmany, A. C.; Bustos-Zagal, P.; Garduño-Ramírez, M. L., Development and characterization of two nano-structured systems for topical application of flavanones isolated from Eysenhardtia platycarpa. *Colloids Surf B* **2014,** *116*, 183-192.
13. Elizarova, I. S.; Luckham, P. F., Layer-by-layer encapsulated nano-emulsion of ionic liquid loaded with functional material for extraction of Cd. *J Colloid Interface Sci* **2017,** *491*, 286-293.
14. Mie, G., Sättigungsstrom und Stromkurve einer schlecht leitenden Flüssigkeit. *Annelen der Physik* **1908,** *331* (8), 597-614.
15. Pacioni, N. L.; González-Béjar, M.; Alarcón, E.; McGilvray, K. L.; Scaiano, J. C., Surface plasmons control the dynamics of excited triplet states in the presence of gold nanoparticles. *J Am Chem Soc* **2010,** *132* (18), 6298-6299.
16. Carter, K. P.; Young, A. M.; Palmer, A. E., Fluorescent sensors for measuring metal ions in living systems. *Chem Rev* **2014,** *114* (8) 4564-4601.
17. Swierczewska, M.; Lee, S.; Chen, X., The design and application of fluorophore-gold nanoparticle activatable probes. *Phys Chem Chem Phys* **2011,** *13* (21), 9929-9941.
18. Mijatovic, D.; Eijkel, J. C.; van den Berg, A., Technologies for nanofluidic systems: top-down vs. bottom-up-a review. *Lab Chip* **2005,** *5* (5), 492-500.
19. Lu, W.; Lieber, C. M., Nanoelectronics from the bottom up. *Nat Mater* **2007,** *6* (11), 841-850.

20. von Freymann, G.; Kitaev, V.; Lotsch, B. V.; Ozin, G. A., Bottom-up assembly of photonic crystals. *Chem Soc Rev* **2013,** *42* (7), 2528-2554.
21. Claridge, S. A.; Liao, W. S.; Thomas, J. C.; Zhao, Y.; Cao, H. H.; Cheunkar, S.; Serino, A. C.; Andrews, A. M.; Weiss, P. S., From the bottom up: dimensional control and characterization in molecular monolayers. *Chem Soc Rev* **2013,** *42* (7), 2725-2745.
22. Dávila-Ibáñez, A. B.; Salgueiriño, V., Chemical and Kinetically Controllable Nucleation, Aggregation-Coalescence, and Ostwald Ripening Processes in the Synthesis of Magnetic Co–B Nanoparticles. *J Phys Chem* **2013,** *117* (9), 4859-4865.
23. Dennis, N. W.; Muhoberac, B. B.; Newton, J. C.; Kumbhar, A.; Sardar, R., Correlated Optical Spectroscopy and Electron Microscopy Studies of the Slow Ostwald-Ripening Growth of Silver Nanoparticles under Controlled Reducing Conditions. *Plasmonics* **2014,** *9*, 111-120.
24. Chikan, V.; McLaurin, E. J., Rapid Nanoparticle Synthesis by Magnetic and Microwave Heating. *Nanomaterials (Basel)* **2016,** *6* (5), 85.
25. Vanegas, J. P.; Scaiano, J. C.; Lanterna, A. E., Thiol-Stabilized Gold Nanoparticles: New Ways To Displace Thiol Layers Using Yttrium or Lanthanide Chlorides. *Langmuir* **2017,** *33* (43), 12149-12154.
26. Yin, Y.; Alivisatos, A. P., Colloidal nanocrystal synthesis and the organic-inorganic interface. *Nature* **2005,** *437* (7059), 664-670.
27. Witten, K. G.; Bretschneider, J. C.; Eckert, T.; Richtering, W.; Simon, U., Assembly of DNA-functionalized gold nanoparticles studied by UV/Vis-spectroscopy and dynamic light scattering. *Phys Chem Chem Phys* **2008,** *10* (14), 1870-1875.
28. Häkkinen, H., The gold-sulfur interface at the nanoscale. *Nat Chem* **2012,** *4* (6), 443-455.
29. Lanterna, A. E.; Coronado, E. A.; Granados, A. M., When Nanoparticle Size and Molecular Geometry Matter: Analyzing the Degree of Surface Functionalization of Gold Nanoparticles with Sulfur Heterocyclic Compounds *J Phys Chem C* **2012,** *116*, (11) 6520-6529.
30. Link, S.; El-Sayed, M. A., Size and Temperature Dependence of the Plasmon Absorption of Colloidal Gold Nanoparticles. *J. Phys. Chem. B* **1999,** *103*, 4212-4217
31. McGilvray, K. L.; Decan, M. R.; Wang, D.; Scaiano, J. C., Facile photochemical synthesis of unprotected aqueous gold nanoparticles. *J Am Chem Soc* **2006,** *128* (50), 15980-15981.
32. Xue, Y.; Li, X.; Li, H.; Zhang, W., Quantifying thiol-gold interactions towards the efficient strength control. *Nat Commun* **2014,** *5*, 4348.
33. Love, J. C.; Estroff, L. A.; Kriebel, J. K.; Nuzzo, R. G.; Whitesides, G. M., Self-assembled monolayers of thiolates on metals as a form of nanotechnology. *Chem Rev* **2005,** *105* (4), 1103-1169.
34. Li, C.; Yue, Y., Fluorescence spectroscopy of graphene quantum dots: temperature effect at different excitation wavelengths. *Nanotechnology* **2014,** *25* (43), 435703.
35. Jaffe, H. H.; Miller, A. L., The fates of electronic excitation energy. *J Chem Educ* **1966,** *43* (9), 469.
36. Kasha, M.; McGlynn, P., Molecular Electronic Spectroscopy. *Annu Rev Phys Chem* **1956,** *7* (1), 403-424.
37. Abbyad, P.; Childs, W.; Shi, X.; Boxer, S. G., Dynamic Stokes shift in green fluorescent protein variants. *Proc Natl Acad Sci U S A* **2007,** *104* (51), 20189-20194.
38. Braun, F.; Schwolow, S.; Seltenreich, J.; Kockmann, N.; Röder, T.; Gretz, N.; Rädle, M., Highly Sensitive Raman Spectroscopy with Low Laser Power for Fast In-Line Reaction and Multiphase Flow Monitoring. *Anal Chem* **2016,** *88* (19), 9368-9374.

39. Stamplecoskie, K. G.; Scaiano, J. C., Optimal Size of Silver Nanoparticles for Surface-Enhanced Raman Spectroscopy. J Phys Chem: 2011; Vol. 115, pp 1403–1409.
40. Hooijschuur, J. H.; Verkaaik, M. F. C.; Davies, G. R.; Ariese, F., Will Raman meet bacteria on Mars? An overview of the optimal Raman spectroscopic techniques for carotenoid biomarkers detection on mineral backgrounds *Neth J Geosci* **2015,** *95* (2), 141-151.
41. Gold Nanoparticle Properties. http://www.cytodiagnostics.com/store/pc/viewcontent.asp?idpage=3 (accessed October 28, 2019)

Chapter 2: Experimental Details

Table of Contents

2. Experimental

The following section describes the experimental methods and materials used throughout the work of my thesis. The characterization methods of nanoparticles will also be elaborated in the following section.

2.1 Materials and Instrumentation

All reagents have been purchased from Sigma Aldrich and have been used without any modifications unless otherwise mentioned. S-methyl-7-mercapto-4-methylcoumarin (C-SMe) was previously synthesized following Lanterna *et al.* methodology [1] and AuNPs were synthesized using the Turkevich method.[2]

2.1.2 TEM Image

Transmission electron microscopy (TEM) images were collected with a FEI Tecnai Twin TEM with a LaB6 emitter, operating at an acceleration of 120 kV. TEM imaging was used to confirm size and polydispersity of the synthesised batch of AuNP.

2.1.3 Fluorescence Spectroscopy Measurements

Steady-state absorbance and fluorescence measurements were recorded using a Cary 100 spectrophotometer and a Photon Technology International (PTI) fluorimeter. The following two fluorophores were used in the fluorometer; 7-mercapto-4-methylcoumarin and 7-Methoxy-4-methylcoumarin Fluorescence testing was done to determine proper concentrations of 7-mercapto-4-methylcoumarin. Samples were excited at 358 nm and the emission spectra taken from 380-550 nm. Spectra were taken before and after a 1.5-hour kinetic run.

Kinetic reactions were run with 900 µL of the 13 nm AuNP placed with various amounts of 7-mercapto-4-methylcoumarin, from 0.2 µM to 20 µM dissolved in DMSO in a reduced volume cuvette (1.5 mL). All samples contained 10% DMSO:H_2O. Samples were all prepared in the same fashion; to ensure uniformity in the mixtures of samples a constant ratio of dimethyl sulfoxide (DMSO) and water are used. Kinetics runs were begun only after the addition of the fluorophore. Initial kinetics runs were followed at either 380 nm or 370 nm for concentrations surpassing the monolayer maximum. Upon optimizations, it was shown that at the lower concentrations, that are closer to those of the monolayer concentration, the peak maximum was at 430 nm.

2.2 Synthesis of AuNP

Three sizes of AuNP were tested in the bio-barcode assay testing, two in-house synthesised particles, sodium borohydride and citrate reduced and finally a commercially available AuNP. The citrate synthesised AuNP were utilized for all kinetic bonding assays.

2.2.1 Citrate

To begin the synthesis of gold nanoparticles, previously noted by Gao *et al.* [3, 4], 20 mg of gold(III) chloride hydrate salt ($HAuCl_4 \bullet 3H_2O$) were dissolved in 20 mL of milli-Q water. The gold salt solution was added to 210 mL of milli-Q water. The solution was refluxed for 20 minutes under constant stirring and 20 mL of 39 mM sodium citrate solution was added slowly; following the addition of the citrate the solution was stirred under reflux another 2 hours. Two batches of AuNP were synthesized and resulted in 13 nm and 17 nm particles respectively (shown in Figure 2.1).

2.2.2 Sodium Borohydride ($NaBH_4$)

Another method used to synthesis nanoparticles was with sodium borohydride reduction, which had been previously described by Lanterna *et al.* [6] following the Turkevich method [2], in which 10 mL of 2 mM $NaBH_4$ solution was cooled down to 0 ºC and added to 10 mL of 0.25 mM $HAuCl_4$ aqueous solution. The solution was stirred for 15 min in an ice bath, and produced 4 nm particles.

2.2.3 Commercial

Finally, a 50 nm commercial nanoparticle purchased from Cytodiagnostics with manufacturer reported surface area of 7800 nm^2 and re-suspended in water using the method described in section 2.4.2.1.

2.3 Nanoparticle Characterization

2.3.1 Calculation of AuNP Concentration

Following Pacioni *et al.* [5] the concentration of nanoparticles can be estimated when assuming that during synthesis all Au(III) ions are reduced to Au(0). To begin one must first calculate the number to gold atoms per nanoparticle. In the case of large spherical clusters is can be assumed the volume of a cluster (V_{NP}) is equal to N times the volume of the individual atom $(V_A)^3$.

$$V_{NP} = \frac{3}{4}\pi {R_{NP}}^3 \tag{2.1}$$

The equation can be simplified to the equation below (with the assumption that a particle takes up the same area as a cube):

$$N = \left(\frac{R_{NP}}{r_A}\right)^3 \tag{2.2}$$

where N is the number of atoms in a nanoparticle, R_{NP} is the radius of the nanoparticle and r_A is the atomic radius of Au (0.144 nm for fcc Au). Thus, for a 14 nm particle:

$$N = \left(\frac{7\times10^{-9}}{0.144\times10^{-9}}\right)^3 \tag{2.3}$$

$$N = 114870$$

Once the number of gold atoms are determined, the concentration of the AuNP solution can be estimated with the following equation:

$$[AuNP] = \frac{N_{NP}}{N_A} = \frac{N_{atoms}}{N\times N_A} = \frac{moles\ Au^{3+}/l\times\cancel{N_A}}{N\times\cancel{N_A}} \tag{2.4}$$

$$[AuNP] = \frac{0.286\times10^{-3}}{114870}$$

$$[AuNP] = 2.49\ nM$$

2.3.2 Size and Shape of AuNP

2.3.2.1 UV-Vis Analysis

UV analysis was used to estimate the AuNP size and functionalization. A sample of 1 mL AuNP was added to a reduced quarts cuvette. The UV-Vis spectra was taken from 200 nm to 800 nm, a distinct peak was seen at 522 nm. In order to confirm the functionalization of the AuNP surface UV-Vis was used to monitor the shift in absorbance. Upon the addition of the C-SH probe the absorbance peak shifts to 528 nm.

2.3.2.2 TEM Analysis

A drop of the particle suspension, 2.4 nM, was placed on a carbon coated copper TEM grid and evaporated at room temperature. For the size measurement, the diameter of approximately 100 particles were counted calculated from a representative image of AuNP using Image J software. The image was prepared in the Image J software such that the contrast/ brightness allowed the particles to stand out clearly form the background. Image J measures the area of the particle image

from the number if pixels in the particle, from which the size is calculated. The nanoparticles were found to be an average of 13 nm diameter, and demonstrate a relative dispersion of particles.

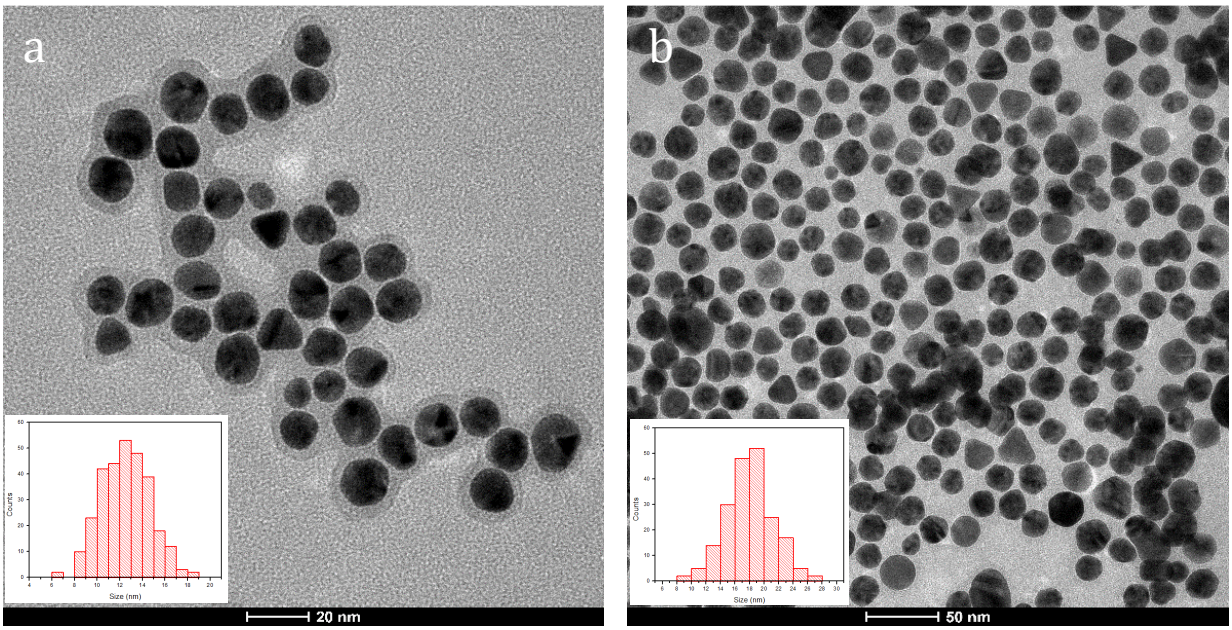

Figure 2.1: TEM images of citrate synthesised AuNP a) batch 1 synthesis b) batch two synthesis.

2.4 Bio Barcode Assay

2.4.1 DNA loading

2.4.2.1 Conjugation of DNA to Gold Nanoparticles

Commercial OligoREADY gold nanoparticles were purchased from Cytodiagnostics. The freeze-dried particles were re-suspended in 868 µL of Milli-Q water, (0.07 nM) and the sample split into two Eppendorf tubes with 434 µL each. In the Eppendorf tube there were two preparations, 1X and 4X, where the number before X represents the ratio of DNA to be loaded on the surface. The DNA, purchased from Integrated DNA Technologies, was functionalised with Rhodamine dye to facilitate quantification with fluorometer In the 1X (35 ng/ µL) preparation there was sufficient DNA to cover the surface of the AuNPs in a monolayer and 4X (105 ng/ µL) was a four-time excess of DNA . These calculations are taking into account that a double stranded DNA generally has a footprint of approximately 2-3 nm^2. For the 1X preparation 8 µL of DNA (870 ng/µL) and 24 µL of water whereas for 4X preparation add 32 µL of DNA (870 ng/ µL) was added. Both preparations had 10 µL of 1M NaCl added and repeated four times for a total of 50 µL. Samples were then incubated for 1 hour after which 0.125 µL Tween20 (0.025% v/v) was added followed by an overnight incubation (~18 hours). Samples were then centrifuged at 2000

rpm for 20 min, supernatants were collected and the pellet resuspended in 200 µL of 0.3X PBS giving a final concentration for the AuNP of 0.145 nM. The samples were centrifuged four times repeating the resuspensions in PBS to remove loose DNA.

2.4.2.2 In-house Citrate Coated Gold Nanoparticles Suspended in 0.3X PBS

A 10 mL aliquot of the citrate coated gold nanoparticle stock (2.5 nM) was centrifuged at 10 000 rpm for 20 min and resuspended in 6 mL of 0.3X PBS. In two Eppendorf tubes with 434 µL of 0.3XPBS gold nanoparticles was added to 20 µL (2%w/w) PEG (1.5 mg/mL) followed by both preparation methods. For the 1X preparation add 8 µL of (870 ng/µL) and 24 µL of water and for 4X preparation add 32 µL of DNA (870 ng/µL). Both preparations had 10 µL of 1M NaCl added and repeated four times for a total of 50 µL, followed by overnight incubation (~18 hours). Samples were then centrifuged at 10 000 rpm for 25 min, supernatants were collected and the pellet re-suspend in 200 µL of 0.3X PBS. The samples were centrifuged four times repeating the resuspensions in PBS to remove loose DNA.

2.4.2 UV and Fluorescence Measurements for DNA

Initial UV testing was done to monitor the attachment of DNA on the surface of AuNP. This was done by following the peak intensities at 260 nm for DNA and 520 nm for AuNPs. UV spectrum were taken using a Cary.

Due to the limited quantity of the sample, after centrifugation and resuspension the final sample has a total volume of 200 µL. Thus we used a reduced volume cuvette 3 mm by 3 mm by 48 mm to obtain a fluorescence signal. Large cuvettes required the dilution of samples resulting in low signal.

A PTI spectrofluorimeter was used to measure the fluorescence of rhodamine labelled DNA (Rh-DNA) by exciting the sample at 480 nm and measuring the emission spectra from 510 nm to 630 nm. With the Rhodamine peak of we are able to use the peak area found from 510 nm to 630 nm to calculate and quantify DNA. To ensure the Rh-DNA gave consistent results a calibration curve was established as seen in Figure 2.2. A calibration curve was made using the peak area of emission spectra of 8 concentrations of Rh-DNA from 1 to 10 nM. For consistency a water control as well as a PBS buffer control, were measured before each experiment to ensure there was no fluctuations in the fluorimeter.

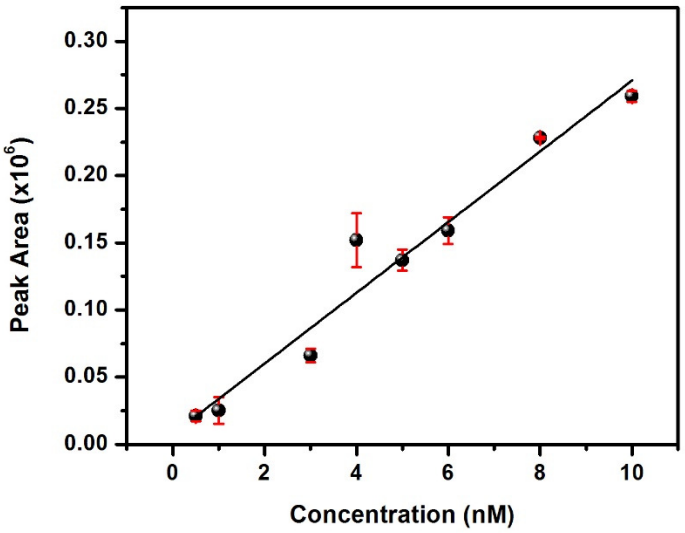

Figure 2.2: Calibration curve of Rh-labelled dsDNA based on the fluorescence of Rh from 510 nm to 630 nm upon excitation at 480 nm.

2.4.3 Raman Spectroscopy

Raman spectra were recorded in a Horiba Xplora microscope configured with 532 nm (at 24 µW) and 785 nm (at 50 µW) laser lines at 100% power. Data analyses were done using LabSpec 6 software. Initial Raman sampling was completed on various concentrations of rhodamine dye. Spectra were monitored between 1000 cm^{-1} to 150 cm^{-1} to verify the distinct binding of Rh to AuNP

2.4.4 Eppendorf Retention Testing

To monitor the DNA retention of the Eppendorf test tubes, samples of Rh-DNA were prepared at two concentrations (10 nM and 20 nM). The samples were left to incubate in the Eppendorf tubes and monitor over time, DNA loss resulted in reduced fluorescence signal. Fluorescence intensity measurements were taken in 15 minutes time intervals, samples were excited at 480 nm and spectra taken from 510 nm to 630 nm. Using software analysis the peak area of the emission peak was analysed and plotted over time. Prior to any sampling a control spectrum of water along with a control run of buffer were completed to ensure that the cuvette did not have residual particles from a previous run. Following issues with large quantities of DNA sticking to the surface of the polyallomer tubes, various coatings were used to reduce the amount of DNA lost to the surface. Coatings such as Bovine serum albumin (BSA) and sample diluent

(composition listed below) were incubated overnight and allowed to dry before adding DNA solution. Each of the following tubes were designed to result in reduced attraction of sample onto the surface of the test tube; Beckman Coulter polyallomer (PA) microfuge tubes, Eppendorf DNA LoBind Tubes 1.5 mL (022431021), VWR non-stick surface (NS) micro-centrifuge tubes 1.5 mL (20170-650), and 3D printed tubes (Formlabs clear resin, roughly 1.5 mL design).

Sample diluent: H_2O, 90-100%, Sodium phosphate, dibasic, 0.1-1.0%, Potassium phosphate, monobasic, 0.01-0.1%, Sodium chloride, 0.5-5.0%, Potassium chloride, 0.01-0.1%, EDTA sodium salt dihydrate, 0.1-1.0%, BSA, 0.01-0.1%, A mixture of antimicrobials (3(2H)-isothiazolone, 5-chloro-2-methyl- with 2-methyl-3(2H)-isothiazolone), 0.1-1.0%, Tween 20, 0.1-1.0%, and Interference blockers, no percentage listed.

2.4.5 Gel Electrophoresis

A 4% agarose gel was prepared by the Tabard-Cossa group. Samples were then run in 50 mL of Tris-acetate-EDTA (TAE) at a voltage of 5V/cm, 4 wells were filled with quadruplicate runs of 60 nM 50 base pair DNA and 4 wells were filled with quadruplicate runs of 60 nM Rh-labelled double stranded DNA. Each well contains a total of 24 µL, 20 µL DNA solution and 4 µL of loading.

2.4.6 Cuvette Cleaning

In order to ensure there was no cross contaminations between runs, the cuvettes were washed with 3 consecutive rinses with milli-Q water. In the event that nanoparticles stuck to the surface of the cuvette, the cuvette would be washed with aqua regia and rinsed 5 consecutive times with milli-Q water to avoid any residual acid presence and to avoid introducing any particulate.

2.6 References

1. Lanterna, A. E.; González-Béjar, M.; Frenette, M.; Scaiano, J. C., Photophysics of 7-mercapto-4-methylcoumarin and derivatives: complementary fluorescence behaviour to 7-hydroxycoumarins. *Photochem Photobiol Sci* **2017,** *16* (8), 1284-1289.
2. Kimling, J.; Maier, M.; Okenve, B.; Kotaidis, V.; Ballot, H.; Plech, A., Turkevich method for gold nanoparticle synthesis revisited. *J Phys Chem B* **2006,** *110* (32), 15700-15707.
3. Vanegas, J. P.; Scaiano, J. C.; Lanterna, A. E., Thiol-Stabilized Gold Nanoparticles: New Ways To Displace Thiol Layers Using Yttrium or Lanthanide Chlorides. *Langmuir* **2017,** *33* (43), 12149-12154.
4. Gao, J.; Huang, X.; Liu, H.; Zan, F.; Ren, J., Colloidal stability of gold nanoparticles modified with thiol compounds: bioconjugation and application in cancer cell imaging. *Langmuir* **2012,** *28* (9), 4464-4471.
5. Pacioni, N. L.; González-Béjar, M.; Alarcón, E.; McGilvray, K. L.; Scaiano, J. C., Surface plasmons control the dynamics of excited triplet states in the presence of gold nanoparticles. *J Am Chem Soc* **2010,** *132* (18), 6298-6299.
6. Lanterna, A. E.; Coronado, E. A.; Granados, A. M., When Nanoparticle Size and Molecular Geometry Matter: Analyzing the Degree of Surface Functionalization of Gold Nanoparticles with Sulfur Heterocyclic Compounds *J Phys Chem C* **2012,** *116*, (11) 6520-6529.

Chapter 3: How Fast Can Thiols Bind to the Gold Nanoparticle Surface?

Table of Contents

3. Kinetic Studies

Kinetic studies surrounding the formation of self-assembled monolayers (SAM) are of great importance for the stabilization of nanoparticles. The functionalization of gold surfaces with thiol compounds has been well studied as one of the most efficient gold surface passivation methods. [1, 2] In particular the focus of my study was the creation of thiolated monolayers on gold nanoparticles (AuNP). While most studies have focused on the thermodynamic efficiency, the complex kinetic aspects are often overlooked. In the area of thiol stabilized gold nanoparticles there is a fundamental question that needs to be answered: How long does it take for the functionalization to occur? Current literature demonstrated that the reaction time to obtain proper functionalization of the particle surface is in minutes or simply do not mention an incubation time. [1, 3] The modification of flat gold surface with thiolated molecules is a well understood method of stabilization and functionalization, but these studies reflect to a lesser extent the understanding of AuNP. The goal of the following work is to determine a timeline in which surface functionalization occurs, as well as the adequate time required to have proper functionalization of thiols on the surface of gold nanoparticles. This chapter focuses on kinetic studies to determine the minimum time one should wait prior to using AuNPs after functionalization. We will be utilizing fluorescent spectroscopy techniques in order to monitor the surface functionalization with the aid of a thiolated probe.

An example of how important incubation time and surface coverage is a study by Ansar *et al.*, where they showed the influence of thiolate derivatization on the catalytic reduction of 4-nitrophenol coverage on the catalytic performance. The free catalytic site density determines the activity of the material. Interestingly, considerable catalytic activity is retained even when the coverage on the surface is 90 %.[3] Surface coverage has a great importance on reactivity, thus determining a standard incubation time for such applications is of importance. AuNP are often used for these catalytic purposes and no standard incubation time has been established.

AuNP solutions are often polydisperse and have irregularities on the surface, as well as curvature variations depending on size and shape making the formation of SAMs more difficult and harder to have generalized conclusions on the particle reaction with various ligands. The stabilization of AuNP with thiols is mostly a result of the gold-sulphur bonding on the surface and creating a monolayer protecting the gold surface. It has been extensively investigated [1, 4-8] ; however, what most studies lack is any mention of an incubation time to avoid working with

nanostructures that were still undergoing derivatization. My work has shown that, unlike the standards that are currently used, the process of Au-S bonding can take upwards of an hour for completion; currently most studies simply mix thiols with AuNPs and assume the derivatization occurs instantaneously. With the aid of fluorescent spectroscopy, 7-mercapto-4-methylcoumarin (C-SH) was used as a "convenient" probe. It is a commercially available dye; allowing rapid and inexpensive control of fluorescence signal to ensure incubation time for functionalization of the AuNP surface. The time required for a Au-S bond to form can allow us to establish a recommended time to incubate AuNP for proper thiol coating.

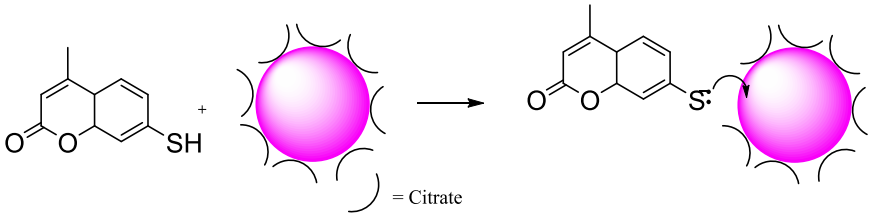

Scheme 3.1: Formation of strong Au-S bonds cause the displacement of citrate from the surface of the AuNP. Upon binding to the surface of the AuNP C-SH emits a fluorescent signal.

Since the citrate is not covalently bound to the surface of the AuNPs the addition of C-SH will bind covalently, removing the citrate off the surface [9], Scheme 3.1 illustrates the displacement of citrate that is expected upon the addition of C-SH.

3.1 7-mercapto-4-methylcoumarin as a Fluorescent Probe

7-mercapto-4-methylcoumarin has been widely used and studied as a fluorescent probe in the literature [10]. Given the characteristics of the molecule on its own, coumarin is not fluorescent on its own, it requires functionalization to allow it to fluoresce (pink structure is coumarin and black is functionalization allowing fluorescence in Scheme 3.2).

Scheme 3.2 Coumarin derivation structure

Many have reported on similar hydroxyl derivatives and their strong emissive properties, linked with the systems unprotected hydroxyl group. [11] However, for the purpose of this work the use of a thiolated coumarin is necessary to be able to monitor the self-assembling monolayers of

Au-S bonding. The use of a thiolated coumarin allows for a change in fluorescent signaling which can be monitored with emission signals. When bound to the AuNP the molecule fluoresces, whereas unbound C-SH is not strongly fluorescent.

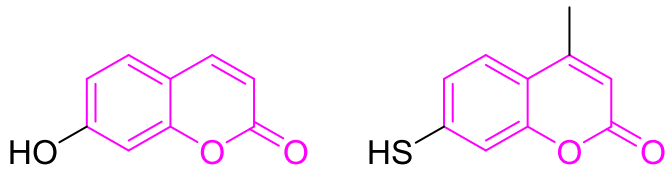

Scheme 3.3: Addition of thiol functional group to coumarin derivatives.

Replacing the hydroxyl group for a thiol can dramatically affect the fluorescence properties. It should be noted that the inclusion of an SH thiol group removes almost all fluorescent properties due to non-radiative deactivation. One of the main reasons behind this is that the modification plays a key role in the dominant resonance structure. [10]

Scheme 3.4: Excited C-SH deprotonates and creates the thione-like resonance structures' which have a potential fluorescence capacity. Adapted from Ref (10)

The thione-like resonance structure (depicted in black) removes the molecule's fluorescence capacity. [11] However in the presence of an AuNP, the C-SH sees plasmon enhancement giving the molecule a small fluorescence signal. Any modifications that remove the molecules ability to form the thione structure, such as methylation, will restore the fluorescent signal.

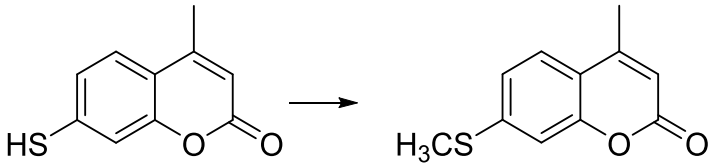

Scheme 3.5: Methylation of thione structure increases fluorescence of coumarin derivative.

The change in fluorescent signal is well demonstrated by the methylation of the 7-mercapto-4-methylcoumarin. Upon methylation, the thione-like resonance structure becomes unavailable, increasing fluorescence.[10] We employed a similar strategy when using AuNP, similarly to methylation, we are removing the thione resonance when C-SH is bound to a AuNP. When considering these factors one must also keep in mind the quenching and enhancement capabilities of the AuNP. As described in chapter one there is a crucial point to which the attachment of a fluorophore will result in quenching or enhancement. The interaction of the C-SH

with the AuNP, as mentioned previously the 7-mercapto-4-methylcoumarin on its own does not have strong fluorescent properties. Upon coordination with a AuNP the S-H bond is broken to form the S-Au bond; removing the thione resonance and allowing a fluorescence peak centered at 430 nm. It is with this in mind that we developed a method to determine the time required for the Au-S bond to form.

3.1.1 Fluorescence Emission in the Presence of AuNP

In order to confirm whether or not AuNP can quench fluorescence of coumarin that are in close proximity to the particle surface, we first run the emission spectra of C-SMe in the presence and in the absence of AuNP. Previously, Gonzalez-Bejar *et al.* have reported the use of 7-mercapto-4-methylcoumarin as a strong marker for thiol binding. [12] Due to the high fluorescence emission properties of the C-SMe (red), upon excitation it gives a fluorescence spectrum that is 30 fold more intense than that of the same concentration of C-SH (black). The presence of AuNP shows a modest enhancement on the C-SMe dye emission, which is seen in Figure 3.1, this is due to the plasmon enhancement explained in Chapter 1. This enhancement at a certain critical distance has previously been explained by Novotny *et al* [13] developing also on the relationship between AuNP and the fluorophore.

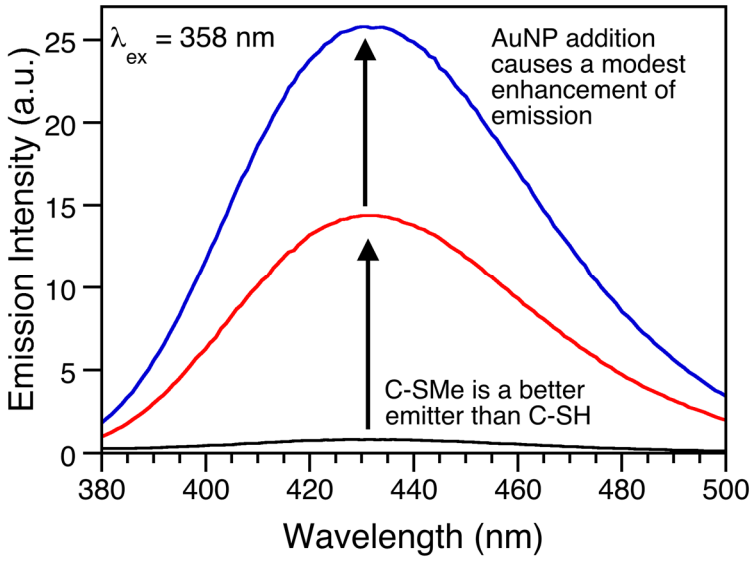

Figure 3.1: Emission spectra of 0.52 µM of C-SH (black), 0.052 µM of C-SMe (red) and the C-SMe sample after addition of 1.2 nM AuNP (blue) and a 5 min wait. All in 10% DMSO:H_2O.

This effect has previously been explained by Lanterna *et al.*[10] in an earlier contribution using Scheme 3.4 to rationalize the change in fluorescence. Additionally, a modest fluorescence enhancement of the C-SMe is detected due to the presence of AuNP, in contrast to typical plasmonic enhancements reported to be an order of magnitude larger.[13] It is known that while proximity enhances the signal, surface contact results in emission quenching; the experimental observation depends on the balance of these two effects, on the system as well as on the experimental conditions. [13, 14] Studies by Pacioni *et al.* [14] have shown the key role that the distance between the AuNP and the fluorophore is playing. Through Laser flash photolysis (LFP) experiments they were able to determine a correlation between distance and if enhancement or quenching will be seen.

Studies show at an infinite distance from the nanoparticles the fluorescence intensity of methylene blue is constant.[14] Quenching and enhancement are competing effects that are related through the distance of the fluorophore to the particle. A large increase in fluorescence is seen as the fluorophore approaches the AuNP surface (d < 20 nm). Moreover, upon approaching the surface (< 1 nm) the resulting fluorescence is completely quenched following the binding of the fluorophore on the surface.

Similarly, in the present work the concept of distance of the fluorophore was used to be able to monitor the attachment of thiols to the surface of AuNPs. Due to the structure of the fluorophore, when the C-SH bound to the surface, the fluorescent signal was enhanced. As has seen before, derivatization of the SH group can restore the emission of the coumarin, we expect the functionalization of AuNP with the C-SH, through a Au–S bond, can also increase the emission properties of the molecule.

3.1.2 UV-Vis Spectroscopy

UV-Vis spectroscopy was often used to confirm the binding of molecules on the surface of NP as well as the stability of the AuNP to ensure the solution did not have a large shift in absorbance. The shift in the plasmon band is a good measure to confirm binding has occurred as well as to see changes in the state of the AuNP (presence of agglomeration). Figure 3.2 demonstrates absorption spectra of AuNP alone and in the presence of C-SH.

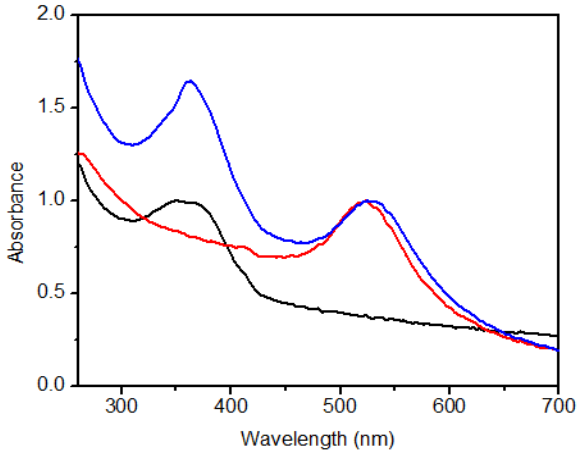

Figure 3.2: Normalized absorption spectra of C-SH alone (Black), AuNP without C-SH (Red) and in the presence (Blue) of 160 µM C-SH. A shift in the plasmon band maximum from 522 to 528 nm can be seen for the AuNP

The changes in Figure 3.2 are attributed to modifications on the surface of the AuNPs, as well as changes in the dielectric media, as a consequence of the presence of C-SH. Since C-SH was dissolved in DMSO, changes produced by the addition of the different solvent was ruled out. Pure DMSO was added to AuNP under the same conditions, and no deviations in the absorption spectrum were detected.

3.1.3 Fluorescence Spectroscopy

Fluorescence spectroscopy was used as a suitable tool to study different combinations of AuNP and various sensing molecules seen in Scheme 3.6. While analyzing the obtained data to extract kinetic and mechanistic information, we used a pragmatic approach to answer the question on hand: How fast can thiols bind to the gold nanoparticle surface?

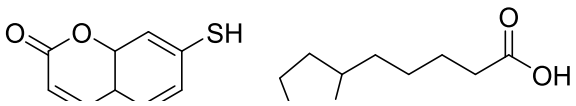

Scheme 3.6: Thiol compounds used in this study

Lipoic Acid (LA), thiophenol (PhSH) and 2-mercaptoethanol (ME) were used as competitive reactants to C-SH. Initial testing was completed to determine the baseline scattering of AuNP alone and in the presence of C-SH such that the signal from the fluorescence could be well detected. Figure 3.3 shows AuNP in the presence of dye and its effect on the fluorescence spectra.

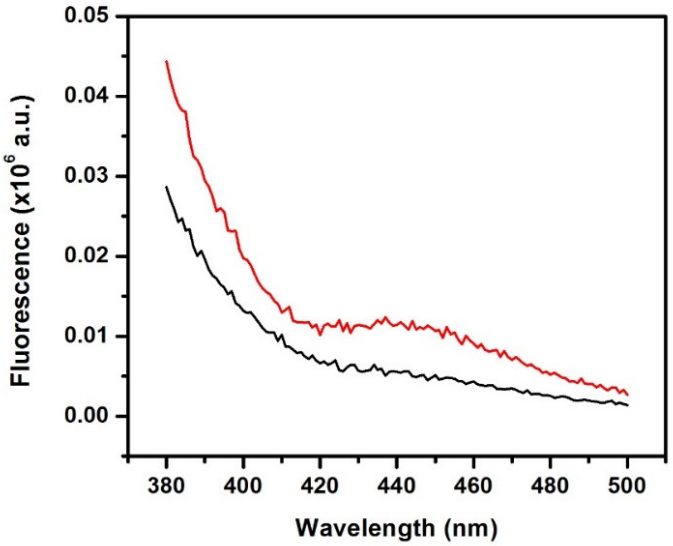

Figure 3.3: Fluorescent spectra of 2.4 nM AuNP (Black) and in the presence of 4 µM of C-SH (Red) after 120 minutes.

The black spectrum demonstrates the scattering of light seen when AuNP alone are excited at 358 nm. In comparison to the red spectrum, where AuNP are in the presence of C-SH dye, a distinct peak from 430-440 is clearly visible, and represents the C-SH fluorescent emission. Results of initial signal testing can be seen in Figure 3.4 where the concentration of C-SH ranged from 1 to 40 µM in the presence of AuNP.

From Figure 3.4, we were able to choose the proper concentrations to continue kinetic testing without having any issues of saturation of the PTI fluorimeter detector. The sample at 40 µM demonstrated large fluctuations whereas; concentrations below 10 µM demonstrated more uniform spectra and were chosen to complete kinetic testing described in Chapter 2.

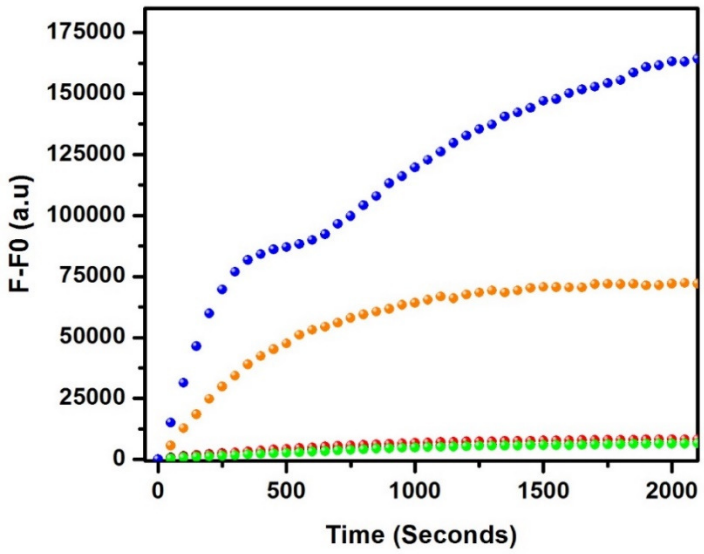

Figure 3.4: Kinetic fluorescence intensity monitored at 430 nm versus time for different concentrations of C-SH (blue 40 µM, Orange 20 µM, Black 8 µM, Red 6 µM, Green 4 µM) added to 1.2 nM AuNP in 10% DMSO:H2O.

Upon examining the initial kinetic testing, seen in Figure 3.4, samples at high concentrations showed high variability likely due to an excess of C-SH used to cover the surface of AuNP. Samples were hypothesised to no longer be creating a single monolayer but to be creating multilayers, which could be the reason for the creation of the second increase in fluorescence seen after 1500 seconds. For the 20 µM sample the plateau starting at 500 seconds is most likely due to the creation of the initial monolayer. However due to the high concentration of C-SH there is an excess of C-SH in solution allowing for the attachment of subsequent layers to the surface of the AuNP which is seen in the 40 µM sample. Upon the discovery of this tendency, lower concentrations of samples were used to avoid the creation of multilayer and focus on the creation of monolayers of thiols onto the AuNP.

3.2 Experimental Testing

To conclude a proper time of functionalization of the AuNP surface various parameters were tested to see the potential effect on binding. To begin, the concentration of the nanoparticles were varied to see the effect on the overall functionalization of their surface. During initial testing two concentrations were selected, 2.4 nM and 1.2 nM of AuNP, as seen in Figure 3.5. Following results from Figure 3.5, samples were reduced to an AuNP concentration of 1.2 nM. The sample

gave a higher fluorescence intensity than the samples with the same concentration of dye at a higher concentration of AuNP (2.4 nM).

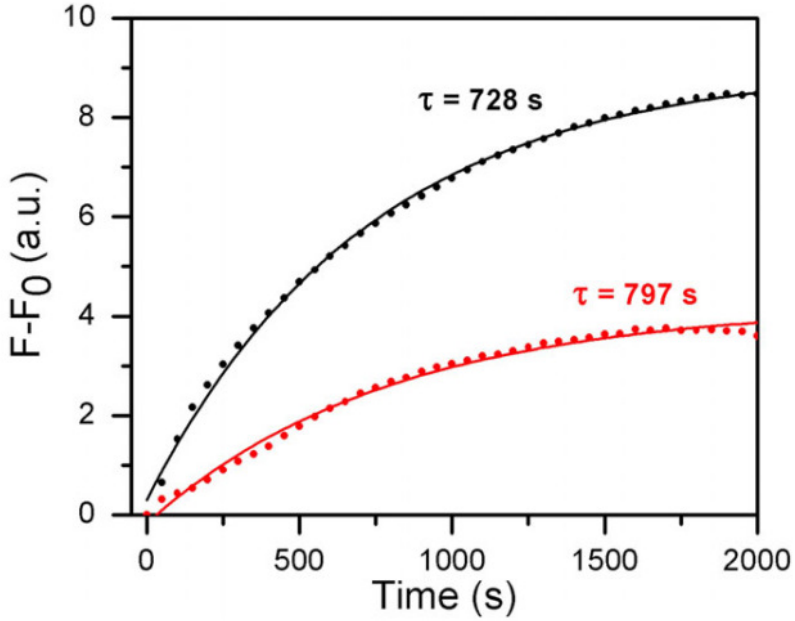

Figure 3.5: A fluorescence intensity monitored at 430 nm versus time with 1.2 nM (Black) and 2.43nM AuNP (Red) after the addition of 4 µM C-SH, samples were excited at 358 nm and emission followed at 430 nm.

It was noted that the rate constants, calculated using equation 3.2, of C-SH binding to the surface of the AuNP for both concentrations of AuNP (1.2 nM and 2.4 nM) are similar, 728 s and 797 s respectively. Moreover, the emission at 430 nm signal for the lower concentration of AuNP resulting in a higher signal was attributed to better light penetrations and minimal light reabsorption from the particles.

To optimise fluorescence signaling a tenfold dilution was chosen from initial tests in Figure 3.4, which placed samples in the range of 1 to 6 µM C-SH. Uniform and reproducible results, were obtained at the lower concentration of dye; this is most likely related to issues with surface saturation. The fluorescence kinetics data were analysed in two different ways; one method considered the absolute fluorescence intensity and the other considers the change in fluorescence intensity relative to time zero, both methods can be seen in Figure 3.6.

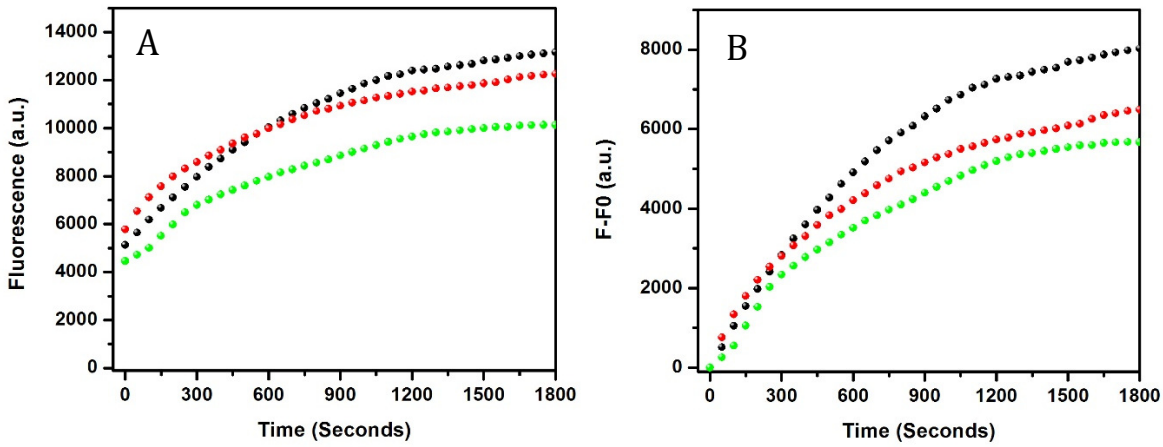

Figure 3.6: Kinetic fluorescence intensity monitored at 430 nm versus time for 3 µM (green), 4 µM (red) and 6 µM (black) C-SH added to 1.2 nM AuNP in 10% DMSO:H_2O where A) illustrates the absolute fluorescence over time and B) illustrates the fluorescence change over time

An example of the uncorrected traces is shown in Figure 3.6 A. Following the optimization of the AuNP concentration and the interpretation of the fluorescence change over time, various concentrations of C-SH were investigated in order to determine the bonding time of C-SH to the surface of AuNPs. The data presented in Figure 3.6 B allowed for better analysis, as it removes any of the fluctuation caused by the fluorometer. Furthermore, to ensure a global consistency of the analysis, samples were analysed following the change in fluorescence upon addition of AuNP and were globally fitted using equation (3.2). As seen in Figure 3.6 B utilising the change in fluorescence intensity demonstrates clearly a trend in the binding of C-SH on the surface of the AuNP. This emission is probably slightly enhanced by non-reactive initial interaction with the gold surface. A simple visual inspection of Figure 3.7 shows that about 30 min is required for 90% of the reaction to take place. The surface of each AuNP must present sites with different reactivity, further; the material size distribution is not monodisperse, as shown in Figure 2.1 from Chapter 2. Under these conditions, it is remarkable that the plots of Figure 3.7 can be reasonably fitted with a monoexponential growth; in other words, they follow excellent Langmuir-type first order kinetics. In fact, it was possible to use a kinetic global fitting approach to fit the data in Figure 3.7 using Equation (3.2)

$$A = A_0(1 - e^{-kt}) \tag{3.2}$$

where k is the observed rate constant ($k=1/\tau$ where τ is lifetime) for the growth of A (enhanced Raman or emission signal. k was obtained as the value that minimizes the mean squared error between the fitted and the observed kinetic curves with different values of A_0.

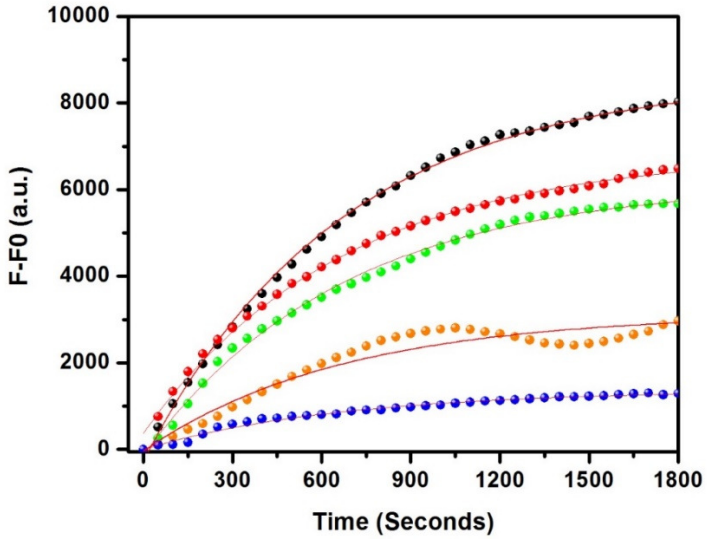

Figure 3.7: Fluorescence intensity change (F-F0) monitored at 430 nm versus time with 1.2 nM AuNP after the addition of 1µM (blue), 2 µM (orange), 3 µM (green), 4 µM (red) and 6 µM (black) C-SH

The surface of the nanoparticles were well-functionalized and remained stable during the kinetic testing. Figure 3.7 illustrates the effect of the increasing the concentration of C-SH. The kinetic tests were monitored overtime and demonstrated a minimum incubation time of 90 minutes is necessary for thiols to cover the surface of AuNP properly. The lifetimes of each kinetic test was measured and is shown in Table 3.1.

Table 3.1: Kinetics for the binding C-SH, at varying concentrations, to the surface of AuNP

[C-SH] (μM)	τ (s)
6	715
4	630
3	701
2	467
1	651

†Samples were excited at 358nm and monitored over time at 430nm in the presence of 1.2nM AuNP in 10% DMSO:H_2O

As seen in Table 3.1, the lifetime for binding remains similar for all cases regardless of the concentration of dye used. All samples have a τ in the range of 630-715 s, which can be considered relatively the same. Following the results from the individual runs, global kinetic analysis was conducted and yielded a lifetime (s) of 735 s, considering that three lifetimes corresponds to 95% completion, the visual estimate of 30 min mentioned above appears quite reasonable. Beyond a single lifetime or rate constant, global analysis also yields a projected plateau value for the signal (A_0). These values were recorded and plotted against concentration in Figure 3.8. The plot reaches a plateau that implies the mercaptan and not the AuNP surface is the likely limiting reagent in this system. At the highest C-SH concentration, this corresponds to ~3300 thiolate bonds per nanoparticle.

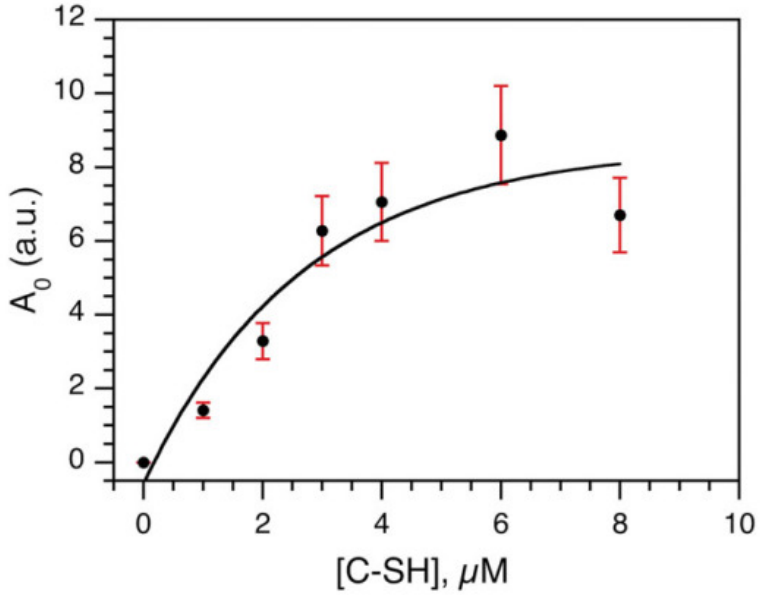

Figure 3.8: Fluorescence intensity change (A_0) determined from the calculated plateau in Figure 3.7 versus concentration C-SH with errors estimated as 15%.

3.2.1 Different Batches of AuNP

Another aspect investigated was the reproducibility of the methodology over various batches of AuNP, since different batches have some variations as seen in TEM image in Chapter 2. Batch 2 AuNPs (~17 nm) were synthesized in the same method batch 1 and prepared for kinetic analysis. Due to polydispersity and variances between batches of AuNP, we wanted to establish that there were no drastic changes in results and to be able to demonstrate reproducibility.

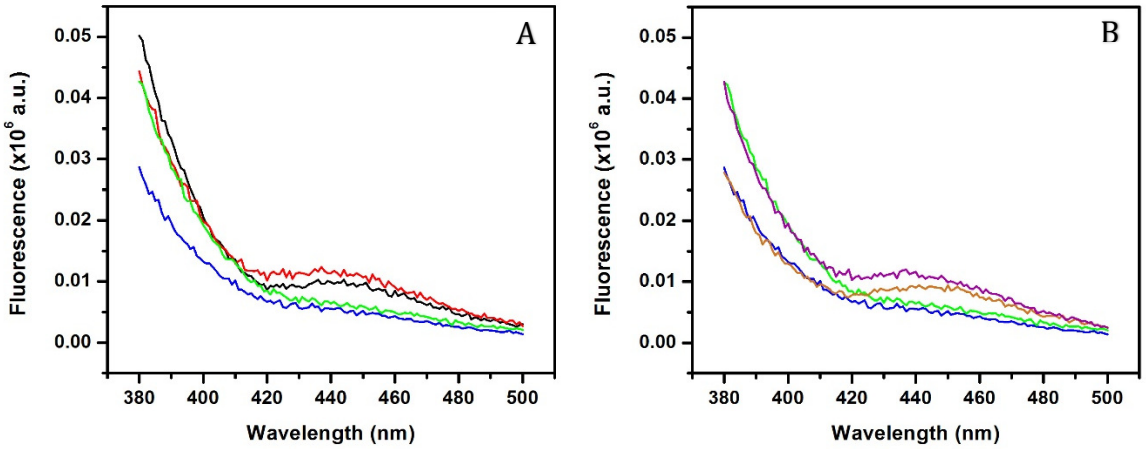

Figure 3.9:A) Fluorescent spectra of AuNP in the presence of 4 μM C-SH where batch 1 at time 0 (black), 120 min (red) and batch 2 at time 0 (blue) and 120min (green.) B) Fluorescent spectra of AuNP in the presence of 4 μM C-SH where batch 2 at time 0 (blue) and t=120min (green) and batch 2 in presence of 40 μM NaOH at t=0 (orange) and 120 min (purple).

In Figure 3.9, the fluorescence spectra of two different batches of AuNP were measured and illustrates the difference between batch polydispersity. For each batch of AuNP, the pH was measured using pH paper and was adjusted accordingly with NaOH. Obtaining AuNP at the proper pH was crucial for the fluorescence signal. When looking at Figure 3.10 the presence of NaOH has a minor effect on the fluorescence properties of the C-SH.

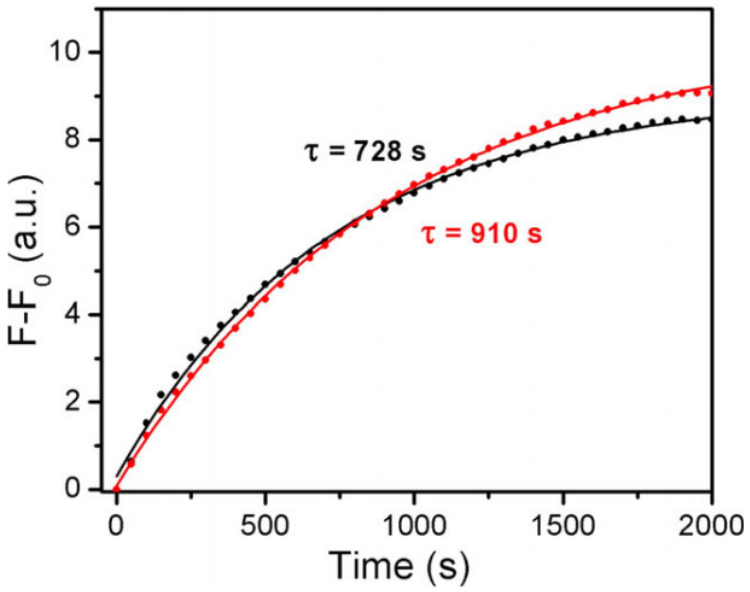

Figure 3.10: Fluorescence intensity change (F-F0) monitored at 430 nm versus time with 1.2 nM AuNP Batch 1 in the presence of 4 µM C-SH (black) Batch 2 in the presence of base 40 µM NaOH (red).

To ensure that no fluctuation of the fluorescence intensity was present, a second batch AuNP was synthesized in the same method as those above, giving an average size of 17 nm. Figure 3.9 and 3.10 demonstrate the results of the reproducibility testing both with the same concentration as well as with a second batch of AuNP. Both batches provided reproducible results thus demonstrating the method's reproducibility

3.3 Competitive Reactants

In an attempt to understand the different properties of thiol gold bonding, we investigated other types of thiols, which could not be monitored by fluorescence but are commonly used, shown in Scheme 3.6. Some other thiols, which are more difficult to monitor by SERS and fluorescence spectroscopy, but also have interesting biological applications were tested, such as 2-mercaptoethanol (ME) and lipoic acid (LA). From SERS data we know that PhSH follows a similar binding to C-SH.[15] We hypothesised that other thiols should have incubation times that resemble

those of C-SH. If this is to be proven true, there should be a decrease in fluorescence intensity upon the addition of a competing reactant (ME, LA or PhSH). To begin, reactions were done with aliphatic molecules, 2-mercaptoethanol was added in similar concentration to C-SH. In a vial the C-SH, DMSO and water are mixed together to ensure a homogenous system. It was noted that if the solutions were not properly mixed there would appear to be two phases. Both molecules were mixed together with DMSO and water followed by the addition of AuNP seconds prior to the start of kinetics run, all reaction components were placed in a reduced volume cuvette (1.5 mL). The solution was homogenous upon irradiation. The addition of a competing molecule, depending on its affinity and ability to reach the surface of the AuNP, should result in a change in fluorescence intensity of the reaction which is seen in Scheme 3.7.

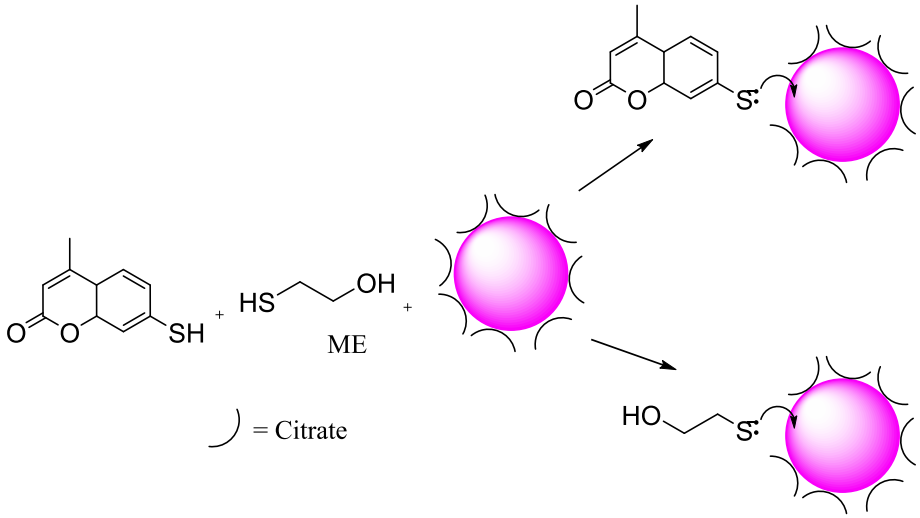

Scheme 3.7: Formation of strong Au-S bonds cause the displacement of citrate from the surface of the AuNP by C-SH in the presence of a competitive reactant (2-mercaptoethanol). Both ME and C-SH displace citrate from the surface of the AuNP.

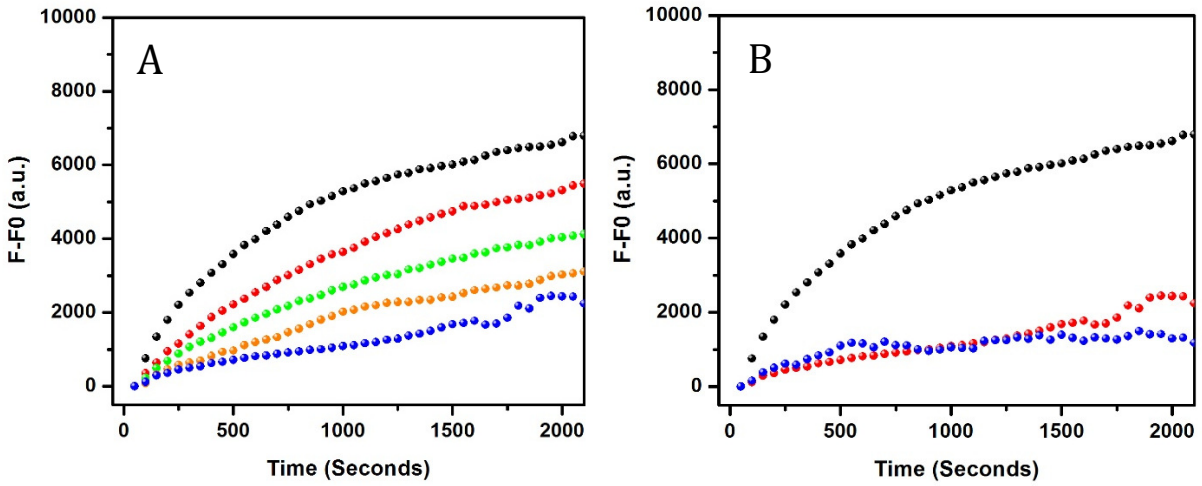

Figure 3.11: A) Fluorescence intensity change (F-F0) monitored at 430 nm versus time with 1.2 nM AuNP after the addition of 4 µM C-SH (Black) in the presence of a competitive reactant 2-Mercaptoethanol (ME) 0.05, 0.1, 0.25, 0.52 µM. B) Fluorescence intensity change (F-F0) monitored at 430 nm versus time with 1.2 nM AuNP after the addition of 4 µM C-SH (black) 4 µM C-SH and 0.52 µM ME (red) and 4 µM C-SH added to a solution of AuNP previously incubated with 1.5 µM ME (Blue).

2-mercaptoethanol linear structure it allowed for easy binding to the surface of AuNP. As a competing reactant, the 2-mercaptoethanol sees much less steric hindrance on the surface of the AuNP. Due to its shape and size the ME has a higher likelihood of reaching the surface of the AuNP than the C-SH, which is a bulky aromatic molecule. The fluorescence intensity was dramatically affected by the presence of the ME, which is seen in Figure 3.11 A. The change in fluorescence intensity reflects the hypothesis that ME had a similar kinetics bonding to the surface of the AuNP as the C-SH. As the ME binds to the surface there is a decreased surface area for the C-SH to bond. In the presence of higher concentration of ME the fluorescence intensity of the fluorophore decreased. A second study was also done to see the effect of having a competitive reactant already on the surface of the AuNP prior to the addition of a fluorophore, Figure 3.11 B. In this case, the ME was incubated with the AuNP for 24 hours prior to the addition of the C-SH. We investigated the possibility of the C-SH to displace the ME, however since a covalent bond was created the C-SH could not displace the ME that was already attached to the surface which resulted in an overall decreased fluorescence. This was reflected by similar fluorescence intensity for a sample where both reactants (ME and C-SH) were added simultaneously.

We further scoped the competitive reactants by choosing other thiol molecules to investigate the potential effects of thiol molecules. Lipoic acid was chosen as an ideal candidate to demonstrate that thiol structure can also effect the functionalization time of the AuNP. Lipoic

acid should behave similarly to disulfides, however the cyclic structure allows LA to have two possible binding sites. In order for lipoic acid (LA) to be viable to bind with the AuNP, an S-S bond of the cyclic ring must be broken. The breaking of the S-S bond requires both time and energy, which is why it is hypothesised that the LA would require a longer incubation period to functionalize the surface. Once the S-S bond is broken, the LA is a bidentate ligand that can bind to the AuNP. Scheme 3.8 demonstrates the bond cleavage that is required for LA to become a bidentate ligand and be able to bind to the AuNPs.

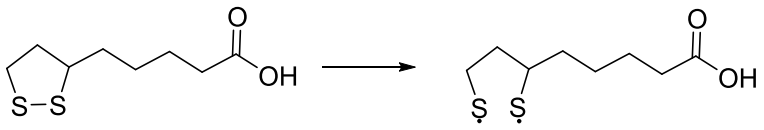

Scheme 3.8: Breaking S-S bond is required concurrently to the creation of Au-S bond to be created on the surface of the AuNP.

When considering the size of the LA in comparison to the ME, the lipoic acid will have a greater steric hindrance at the surface of the AuNP, making it more difficult for the thiol to reach the surface. It is for this reason there is a smaller affect on the fluorescence intensity upon initial testing of direct competitive reactants seen in Figure 3.12.

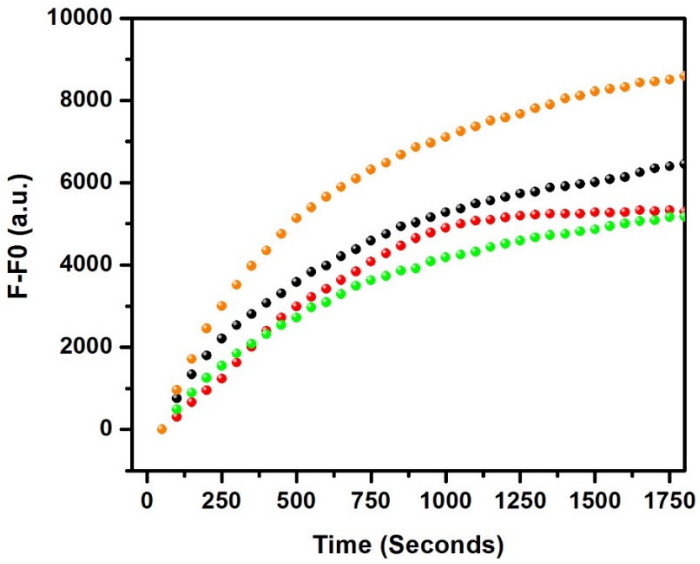

Figure 3.12: Fluorescence intensity change (F-F0) monitored at 430 nm versus time with 1.2 nM AuNP after the addition of 4 µM C-SH (Black) in the presence of a competitive reactant Lipoic Acid (LA) 0.5 (red), 1 (Green) and 8 µM (Orange).

In the case of LA, we noted, at high concentrations, the solution became cloudy and we saw solubility issues with LA. The change in solution resulted in issues of reproducibility for higher concentrations of LA as light could not properly penetrate the sample. As seen in Figure 3.12 where the 8 µM (Orange) sample was completely white and opaque, it showed a higher fluorescent signal than those with lower concentrations. The higher fluorescent signal is linked to the higher level of light scattering by the opaque solution; moreover, there was a white precipitate that formed over the course of the kinetic run. The issues with precipitation of the LA were linked to the low solubility of LA in water and for further studies, the concentation of LA was no higher than 2 µM.

Subsequent testing of LA overnight incubation was completed using 1.5 µM to avoid reproducibility issues. LA was incubated with AuNP for 24 hours prior to the addition of C-SH and compared to the simultaneous addition of LA and C-SH. In Figure 3.13 only a slight decrease in fluorescence intensity meaning the C-SH is "favored" kinetically when in direct competition with LA. Moreover, upon further examination samples that had been incubated with LA in the presence of AuNP overnight, which allowed LA time to break down the cyclic S-S bond and bind to the surface of the AuNP, show changes in fluorescence intensity.

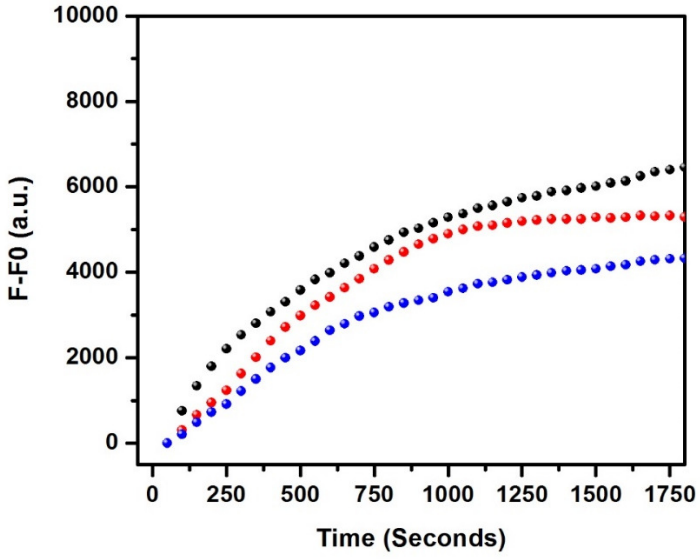

Figure 3.13: Fluorescence intensity change (F-F0) monitored at 430 nm versus time with 1.2 nM AuNP after the addition of 4 µM C-SH (Black) 4 µM C-SH and 4 µM LA (Red) and 4 µM C-SH added to a solution of AuNP previously incubated with 1.5 µM LA (Blue).

Results seen in Figure 3.13 show that the samples incubated overnight result in lower fluorescent intensity than samples in direct competition. This change is a representation of the

amount of available active sites on the AuNP surface for the C-SH dye to bind. Since the surface is functionalized with the LA it is no longer available for the C-SH to bind.

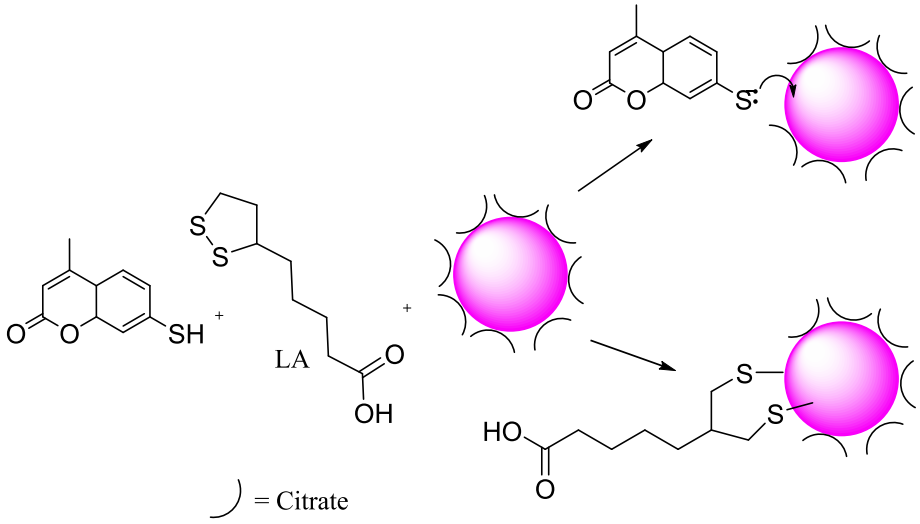

Scheme 3.9: Formation of strong Au-S bonds cause the displacement of citrate from the surface of the AuNP of mercapto-coumarin in the presence of a competitive reactant (lipoic acid).

The presence of LA does not dramatically affect the fluorescence intensity, which could be due to the slower reactivity. In the case of LA slower reactivity further studies were done to understand the binding kinetics further. The AuNP were incubated in the presence of LA at a concentration of 1.5 µM overnight for 24 hrs. Following the incubation the sample had 4 µM C-SH added concentration and evaluated the kinetics of the binding.

The competition of C-SH with LA shows that thiols are more reactive than disulfides, however once LA is bound it is difficult to remove and hinders the binding of any other thiols. From these studies we can note that the incubation time of simple (linear) thiols is approximately 90 minutes; however for disulfides, one should allow the samples to be incubated overnight, upwards of 24 hours if possible. Surface enhanced Raman Spectroscopy (SERS) has previously been used to monitor structural and kinetics of thiol-AuNP interactions which confirm that aromatics such as thiophenol require approximately 90 minutes to bind to the AuNP surface.[15] Moving forward with the competitive reactants, finally a larger aromatic thiol was tested to see if a molecule with similar characteristics to the C-SH would also be as competitive as the ME. Following studies conducted by SERS we investigated the use of thiophenol (PhSH) as a competitive reactant shown in Scheme 3.10.

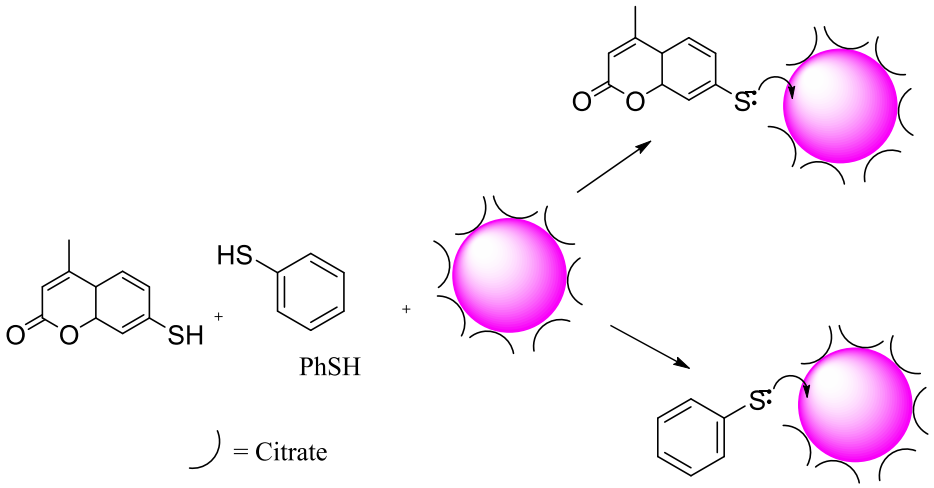

Scheme 3.10: Formation of strong Au-S bonds cause the displacement of citrate from the surface of the AuNP of Mercapto-Coumarin in the presence of a competitive reactant (thiophenol).

As with the other competitive reactants we monitored simultaneous addition of PhSH as well as overnight incubation, these results are demonstrated in Figure 3.14 below.

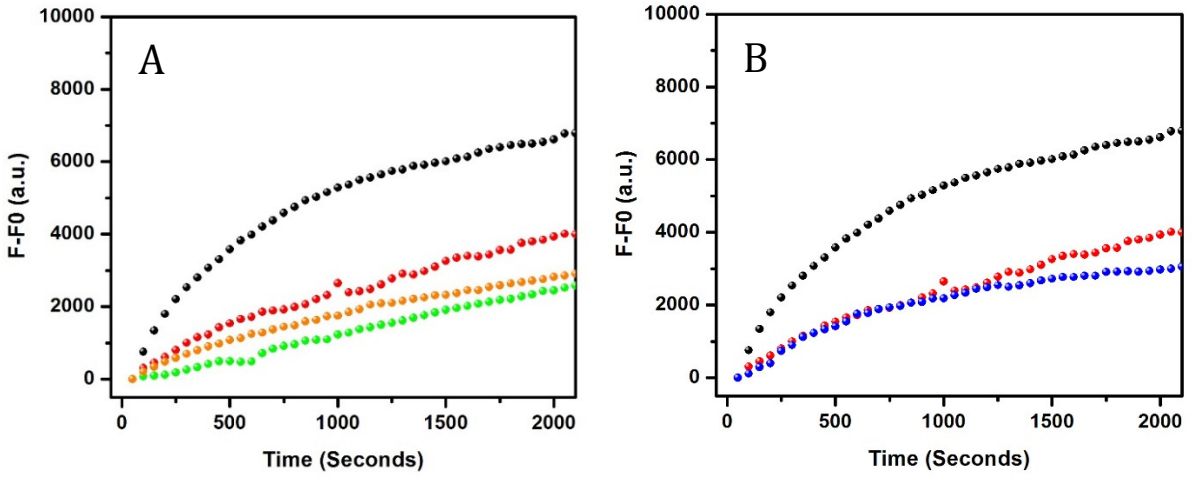

Figure 3.14 A) Fluorescence intensity change (F-F0) monitored at 430 nm versus time with 1.2 nM AuNP after the addition of 4 µM C-SH (Black) in the presence of a competitive reactant Thiophenol (PhSH) 0.1 µM (Green), 0.17 µM (Orange), 0.35 µM (Red). B) Fluorescence intensity change (F-F0) monitored at 430 nm versus time with 1.2 nM AuNP after the addition of 4 µM C-SH (Black) 4 µM C-SH and 0.1 µM PhSH (Red) and 4 µM C-SH added to a solution of AuNP previously incubated with 1.5 µM PhSH (Blue).

As demonstrated in Figure 3.14 A the rate at which the C-SH binds to the surface of the gold nanoparticles is significantly less in the presence of thiophenol in comparison to the dye on its own without a competitive reactant. These results match those of previous studies, with the use of SERS, showing an average of 90 minutes for an incubation time. A summary of the lifetimes for the competitive reactants is shown in Table 3.2. In Figure 3.14 B the change in fluorescence intensity over time is shown in the presence of thiophenol (PhSH), the fluorescent signal of the C-

SH is significantly less in the presence of thiophenol in comparison to the dye. However there is not as large a difference in fluorescence between the simultaneous addition and the overnight incubation in comparison to results with LA as a competitive reactant.

Table 3.2: Reaction rate (seconds) of 4 μM C-SH binding to AuNP in the presence of competitive reactants (4 μM).

	Control	Simultaneous	Overnight Incubation
C-SH	680±70	-	-
LA	-	560±70	620±70
PhSH	-	2000±200	760±70
ME	-	2500±300	380±70

†Samples were excited at 358 nm and monitored over time at 430 nm in the presence of 1.2 nM AuNP in 10% DMSO:H_2O

The various competitive reactants were tested to see how their structure would affect the competitive potential. We have noted that the structure of the thiol has an impact on the speed at which it will bind to the surface. We discovered that thiol structure and size can play a role in reactivity, competitive reactants such as aromatic and aliphatic can be considered within the same incubation period however, disulphides (such as LA) should be considered differently. When using aromatics and aliphatic thiols one can assume that after 90 minutes the surface of the AuNP has been properly functionalized, however disulphides such as LA require a longer incubation time to have a complete functionalization, closer to 24 hours if possible. Further development will be required to properly understand and evaluate the kinetic bonding of the competitive reactant. It should be noted that results with PhSH and ME require further development as the effect of a competing reactant should not affect the initial rate at which C-SH can bind to the surface of the AuNP. When looking at Figure 3.11 and Figure 3.14, we do see this trend.

In conclusion, the study has shown that the thiol composition as well as the particles all play a role in the creation of the Au-S bond. In the case of thiols such as disulfides (LA) an overnight incubation would be required to allow time for the S-S bond to break concurrently to the functionalization of the surface with the creation of Au-S bond. We also noted that various batches of similar sized nanoparticles did not affect the rate at which the Au-S bond is made. The results from Chapter 3 prove the reactivity of several thiols occurs within the same timescale; however, disulfides (such as LA) react much more slowly. To answer the title question, we recommend one

to two hour wait for thiol binding to be essentially complete, while for disulfides, overnight incubation is recommended. Any “ready-mix” strategy is bound to lead to results obtained while the formation of thiolate bonds was still in progress.

3.4 References

1. Pensa, E.; Cortés, E.; Corthey, G.; Carro, P.; Vericat, C.; Fonticelli, M. H.; Benítez, G.; Rubert, A. A.; Salvarezza, R. C., The chemistry of the sulfur-gold interface: in search of a unified model. *Acc. Chem Res* **2012,** *45* (8), 1183-1192.
2. Goldmann, C.; Lazzari, R.; Paquez, X.; Boissière, C.; Ribot, F.; Sanchez, C.; Chanéac, C.; Portehault, D., Charge Transfer at Hybrid Interfaces: Plasmonics of Aromatic Thiol-Capped Gold Nanoparticles. *ACS Nano* **2015,** *9* (7), 7572-7582.
3. Ansar, S. M.; Kitchens, C. L., Impact of Gold Nanoparticle Stabilizing Ligands on the Colloidal Catalytic Reduction of 4-Nitrophenol. *ACS Catalysis* **2016,** *6* (8), 5553–5560.
4. Xue, Y.; Li, X.; Li, H.; Zhang, W., Quantifying thiol-gold interactions towards the efficient strength control. *Nat Commun* **2014,** *5*, 4348.
5. Häkkinen, H., The gold-sulfur interface at the nanoscale. *Nat Chem* **2012,** *4* (6), 443-455.
6. Stamplecoskie, K. G.; Yousefalizadeh, G.; Gozdzialski, L.; Ramsay, H., Photovoltaics as an experimental tool for determining frontier orbital energies and photocatalytic activity of thiol protected gold clusters. *J Phys Chem C* **2018,** *122*, 13738-13744.
7. Reimers, J. R. F., M. J.; Marcuccio, S. M.; Ulstrup, J.; Hush, N. S., Competition of van der Waals and chemical forces on gold – sulfur surfaces and nanoparticles *Nat Rev Chem* **2017,** *1*, 0017.
8. Yousefalizadeh, G.; Stamplecoskie, K. G., Norrish type I photochemistry as a powerful tool in the isolation of thiol protected Au25SR18 clusters *J Photochem Photobiol* **2018,** *A 353*, 251-254.
9. Vanegas, J. P.; Scaiano, J. C.; Lanterna, A. E., Thiol-Stabilized Gold Nanoparticles: New Ways To Displace Thiol Layers Using Yttrium or Lanthanide Chlorides. *Langmuir* **2017,** *33* (43), 12149-12154.
10. Lanterna, A. E.; González-Béjar, M.; Frenette, M.; Scaiano, J. C., Photophysics of 7-mercapto-4-methylcoumarin and derivatives: complementary fluorescence behaviour to 7-hydroxycoumarins. *Photochem Photobiol Sci* **2017,** *16* (8), 1284-1289.
11. Demelo, J. S. S.; Becker, R. S.; Macanita, A. L., Photophysical Behavior of Coumarins as a Function of Substitution and Solvent - Experimental-Evidence for the Existence of a Lowest Lying $^1(n,\pi^*)$ State. *J Phys Chem* **1994,** *98* (24), 6054-6058.
12. González-Béjar, M.; Frenette, M.; Jorge, L.; Scaiano, J. C., 7-mercapto-4-methylcoumarin as a reporter of thiol binding to the CdSe quantum dot surface. *Chem Commun (Camb)* **2009,** (22), 3202-3204.
13. Anger, P.; Bharadwaj, P.; Novotny, L., Enhancement and quenching of single-molecule fluorescence. *Phys Rev Lett* **2006,** *96* (11), 113002.
14. Pacioni, N. L.; González-Béjar, M.; Alarcón, E.; McGilvray, K. L.; Scaiano, J. C., Surface plasmons control the dynamics of excited triplet states in the presence of gold nanoparticles. *J Am Chem Soc* **2010,** *132* (18), 6298-6299.
15. Bard, A.; Rondon, R.; Marquez, D. T.; Lanterna, A. E.; Scaiano, J. C., How Fast Can Thiols Bind to the Gold-nanoparticle Surface? *Photochem Photobiol* **2018,** (94) 1109–1115.

Chapter 4: Nanopore Barcode Assay Development

Table of Contents

4. Nanopore Barcode Assay Work: Clinical Diagnostic Sensing

Clinical diagnosis has been developed with the aid of more sensitive sensing methods. Sensing techniques are being pushed further to their limits in attempts to be able to detect a target analyte at the fM level, utilizing multiple amplification methods to reach such low detection levels. Current assays can accurately read concentrations in the pM range. Many techniques have used DNA-modified particles to increase system sensitivity via the amplification of signal, which is a result of the level of DNA loading.[1-3] Nanoparticles are bridging the gap between the uses of chemistry in an aid to develop biological applications. The present project's overall goal is to establish an assay in which the target analyte can be measured at the sub-picomolar level with the aid of a nanopore structure.

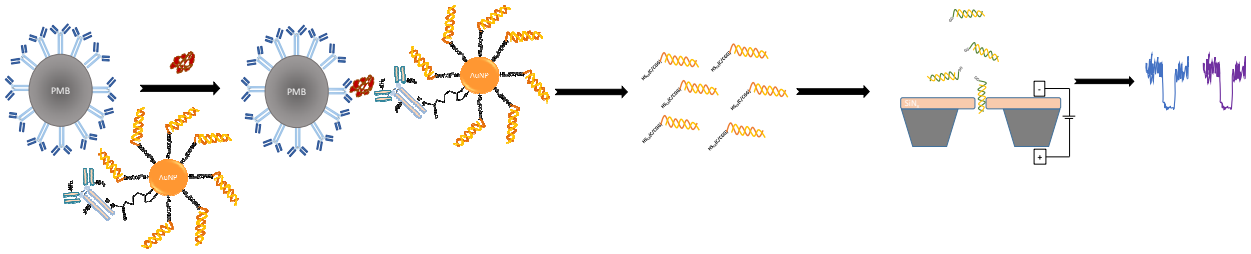

Scheme 4.1: Typical nanopore system where target analyte (red) is bound between two antibodies, one loaded to a magnetic micro particle (MMP) and the other one to a gold nanoparticle (AuNP). The AuNP has DNA barcodes bound to the surface that are released and read by a silica nanopore, which will produce an electrical signal every time a single DNA molecule passes through it.

The assay depicted in Scheme 4.1 is a simplified model for the project's assay assembly. A target protein (red) is bound between a magnetic micro particle (MMP) functionalised with specific antibodies and a gold nanoparticle (AuNP) functionalized with specific antibodies and DNA barcodes. In this case, DNA barcodes are used to amplify and quantify a specific target protein. Each DNA acts as a "barcode" to be able to count and quantify a target protein. When the target protein is trapped between the antibodies attached to the MMP and the AuNP, the target protein can be isolated via magnetic separation of the MMP. After the target protein is isolated, the DNA barcodes are released and read by the nanopore detector, which produces an electrical signal every time a single DNA molecule passes through it.

Reaching fM level can be challenging for common quantification techniques; therefore, we have explored the nanopore assay, where DNA is used as a marker to be able to detect a target analyte that would otherwise be too difficult to measure. The nanopore detector is a silica-based

pore material with passageways that allow molecules of a given size (nm) to pass through. The nanopore detector can be used to measure specific sequences of DNA and give an electrical output for each DNA strand that passes through the pore. Various DNA sizes will give slightly different signals from the nanopore, as noted by Tabard-Cossa *et al*., smaller DNA strands do not interact with the nanopore as well and result in a lower signal. [4] In the present work all DNA was of a fixed length of 50 base pairs.

The nanopore is utilised to quantify the amount of a target analyte, which is a reflection of the electrical signals produced by the DNA barcodes. The goal is to be able to quantify a specific number of DNA to a single target protein. In this case the target analyte is the thyroid stimulating hormone (TSH) which is a glycoprotein consisting of two subunits. TSH is a pituitary gland that stimulates the thyroid to produce thyroxine (T_4) and triiodothyronine (T_3) which regulates the metabolism of most tissues in the body.[5] What makes the system a good candidate for the nanopore assay is that TSH is in low concentration but is immune-detectable in the blood, and allows testing from a simple blood sample to be taken and amplified. The nanopore system can detect any target analyte; however, the main issue is the amount of target analyte available. In a given blood sample TSH is at such low concentrations that it is negligible in the measurement system. Therefore, the target protein concentration must be amplified. A common method to obtain signal amplification involves the use of gold-nanoparticles. AuNPs allow an indirect amplification of the target analyte signal.[6] In a basic nanopore system, one antibody is attached to a single DNA barcode, meaning the ratio of target analyte to DNA is 1:1. However, if an antibody is attached to an AuNP, the nanoparticle can have 100-1000 DNA barcodes attached to a single NP, as depicted in Scheme 4.2. Thus, when the target analyte is trapped between the antibody of the AuNP and the antibody attached to the MMP, the amount of DNA associated to a single target analyte is greater causing signal amplification.

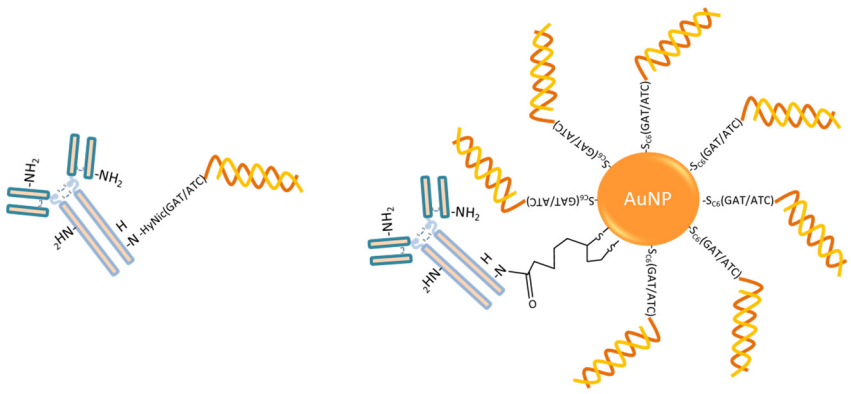

Scheme 4.2: Basic detection system with one DNA molecule associated to a single antibody (left), and amplification system using multiple DNA strands attached to a AuNP and associated to a single antibody (right).

The amplification from the AuNP allows the bio-barcode system to attain sensitivity at very low concentrations. The MMP is used as a filtering tool for the target protein that has been sandwiched with the DNA loaded AuNP. The MMP can be filtered with the aid of a strong magnet. Since the MMP is bound to the AuNP via the trapped target analyte, the DNA attached can be quantified. Once the trapped analyte (THS) has been isolated from a sample, release mechanisms are used to cleave the DNA from the AuNP. Upon the release of the DNA that was loaded on the surface of the AuNP, the nanopore can sense the DNA and depict an electrical signal. Therefore, each electrical signal represents the passage of a DNA barcode through the nanopore as seen in Scheme 4.3. Once the number of DNA are calculated, the ratios between target analyte to DNA can be used to indirectly calculate the concentration of target analyte (THS).

Silica nanopores are commonly made with thin silicon nitride or silicon oxide membranes, between 10 to 50 nm thick. The silica membranes can be tailored to a wide variety of sizes and are robust. Their fabrication and cleaning are well illustrated by Beamish *et al.*[7]

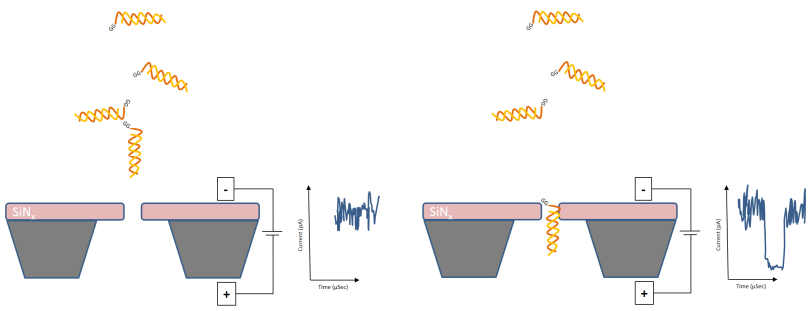

Scheme 4.3: Silica nanopore system, where DNA is filtered from AuNP prior to being exposed to the nanopore. Isolated DNA is pushed through the nanopore and an electrical signal is produced for each DNA molecule that passes through the nanopore. Adapted from ref (8) with permission from ACS Nano Copyright (2009).

DNA-covered AuNP are often building blocks of an assembly system. The use of DNA-loaded AuNP to increase sensing of a given target analyte is known as a bio-barcode method. [8] The AuNP could play a key role in the amplification and sensitivity of the nanopore assay, the possibility of quantification is directly related to the AuNP ability to bind to thiolated DNA. Upon cleavage of the DNA, the solution is placed into the nanopore and when the DNA passes through the nanopore an event is recorded. These events can be counted; thus, DNA can be quantified. Events are measured via the change in current, which is generated when a single DNA molecule passes through the pore (see Scheme 4.3).[8]

4.1 DNA Loading Quantification

In order to ensure the validity of the assay, the amount of DNA loaded onto the surface of the AuNP must be quantified prior to the DNA being put through the nanopore assay. Gold nanoparticles have been used as vessels to carry DNA; [9] they are often chosen due to their chemical inertness, low cost and size controlled preparations. What makes them interesting for applications in biology is their easily manipulated surface chemistry, in particular, the functionalization with thiol molecules to form self-assembled monolayers (SAM). The simplicity of SAMs in this case makes the use of AuNP an ideal candidate for the loading and quantification of thiol DNA. [10, 11]

Maximizing the amount of DNA loading per particle becomes crucial to obtain proper signal amplification of target analyte since it needs to be in the sub picomolar scale. The AuNP are used as a carrier vessel for the target DNA and allow signal amplification, when comparing to a basic target system, which would have a single DNA per antibody. However, utilising the higher

surface area of AuNP can allow for up to 1000X amplification. Particle size can also have an effect on the amount of DNA that can be loaded onto a given NP.[6]

When using the bio-barcode assay there is a direct correlation with the amount of DNA and the amount of amplified analyte signal. Being able to find a system that allows for accurate quantification is necessary for this project to be accomplished.

Validation methods often include the use of fluorescent marker and quantification methods. The main objective of my work was focused on the loading and quantification of DNA on AuNP. This is a small portion of a larger project centered on the development of ultra-sensitive detection system capable of monitoring sub-pico molar concentration of DNA. The other part of the project was conducted by the Tabard-Cossa group, which consisted of the design of the nanopores, the DNA preparation and the final DNA quantification through the nanopore assay.

4.1.1 Estimation of DNA Loaded per AuNP

Many methods have been developed to quantify DNA loaded on the surface of AuNP; however, most of them are based on indirect quantification of the material, which results in less accurate results. Methods such as measuring excess DNA by UV analysis in the wash supernatants and subtracting the residual concentration from that added to the AuNP solution give an idea of DNA on the surface by the indirect measurement of unbound DNA. In this work, initial tests were done using UV measurement as an indirect method. These methods required samples to be centrifuged down and use of the supernatant to measure excess DNA that did not properly attach to the surface of the AuNP. The initial test was used to approximate the quantity of unbound DNA.

The initial DNA testing was carried out, first to choose the type of terminated DNA, as well as to select proper concentrations for particle loading. Initial tests were established taking the absorbance of the samples at various concentrations to establish calibration curves as well as the limit of detection.[13] Specific DNA sequences for our given tests were designed as barcodes for their facile attachment to the surface of AuNP.[14] The ideal sequence was chosen to be able to give clear readings as well as sufficient event readings on the nanopore without causing blockages or to pass without signal. DNA sequences 10-base pair or less produce minimal signal, since the smaller chains are under the limit of detection of the nanopore and can go undetected. After optimization, the Tabard-Cossa group chose a length of 50 base pairs to be ideal for the nanopore system. Following the choice of DNA length testing related to the DNA termination to use. Amino

and thiolated terminated DNA (NH_2-DNA and SH-DNA, respectively) were tested for both binding capability as well as stability. Both the NH_2-DNA and SH-DNA strands have different type of interactions with the surface of AuNPs, where NH_2-DNA is electrostatically attached to the surface of the AuNP and the SH-DNA is covalently bound. The primary amine group allows for easy loading, however, there are issues with the reproducibility of the system, since NH_2-DNA is not covalently bound. The dynamics of the system equilibrium make the DNA quantification very challenging Furthermore, any amount of mechanical work resulted in a large loss of DNA on the surface of the AuNP.

A 200 nM NH_2-DNA solution was added to the AuNP solution in order to yield an approximate loading of 1000 DNA strands per NP. The free DNA was separated from the AuNP by a series of centrifugation and washing cycles using milli-Q water. The supernatant was evaluated to determine the residual DNA that did not bind to the surface of the AuNP. The initial method using UV-Vis spectroscopy was used as a qualitative method to ensure that the majority of the DNA was bound to the AuNP. The absorption spectrum of the supernatant from each wash was measured to monitor the amount of DNA not-bound to the AuNP and the value was subtracted from the DNA amount initially added to the AuNP solution.

Figure 4.1 illustrates initial UV testing of NH_2-DNA; the UV-visible spectra tests were used as controls to verify if NH_2-DNA would have electrostatic interactions with the surface of the AuNP.

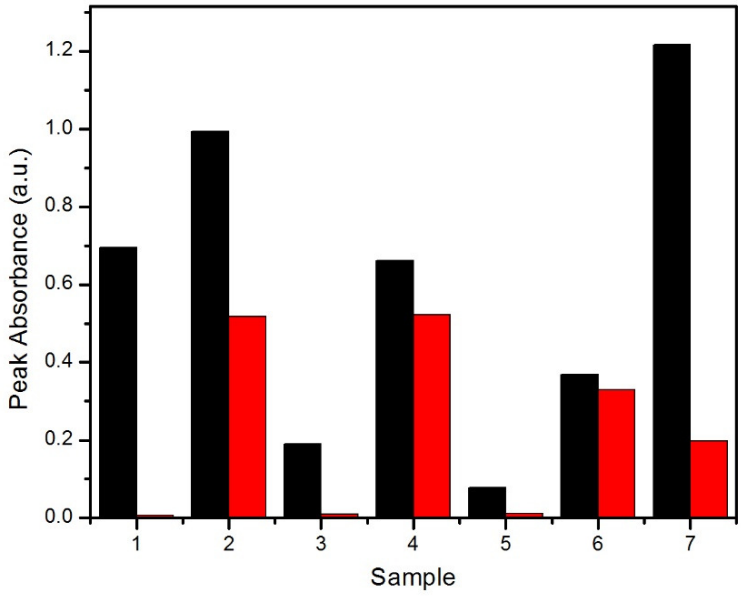

Figure 4.1: DNA UV absorbance measurements at 260 nm (black) and AuNP at 530 nm (red). An initial control of NH_2-DNA at 200nM (1), AuNP(1.7nM) in the presence of 200nM DNA (2), the supernatant of the AuNP and DNA solution centrifuged at 2000 rpm (3), the resuspension of the AuNP pellet formed upon centrifugation at 10 000 rpm(4), supernatant of a second centrifugation (5), resuspension of a second pellet (6), sample 6 sonicated (7).

The absorbance at 260 nm was taken to measure the level of DNA present and the absorbance at 530 nm was measured to verify the AuNP stability throughout the various processes. Throughout the washing cycles there was a drastic increase in the absorbance peak at 260 nm that can be associated with the absorption of NH_2-DNA. NH_2-DNA does not bind covalently, thus, as the AuNP were washed by centrifugation, each subsequent wash supernatant contained DNA. As a final verification, the sample was sonicated to examine the release of NH_2-DNA. The NH_2-DNA allows for a dynamic system which relies on the diffusion of DNA on the surface of the AuNP. The absorbance spectra of AuNP alone and AuNP in the presence of DNA can be seen Figure 4.2

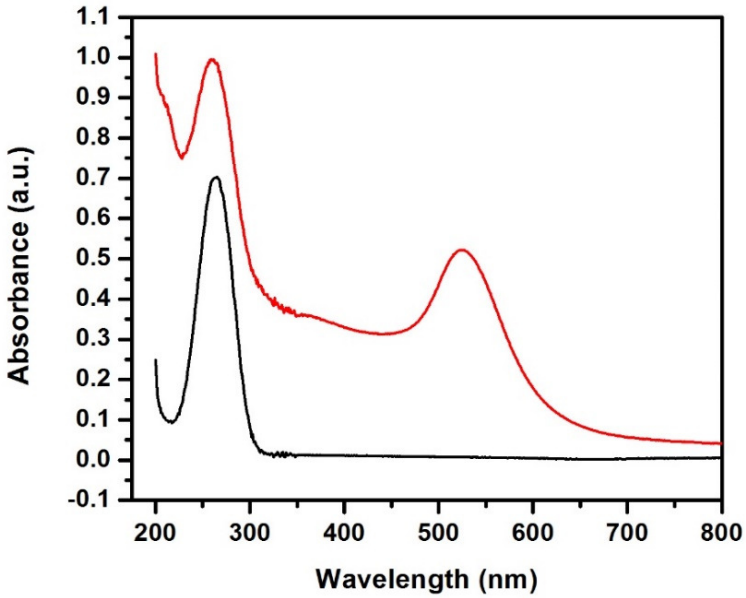

Figure 4.2: Absorbance spectra of AuNP at 1.7nM with NH_2-DNA 200nM (red) and NH_2-DNA 200nM (black)

Additionally, upon the resuspension of the AuNP pellet created from washing cycles, there is a loss of DNA due to the agglomerated particles on the surface of the polymer test tube. The agglomeration of AuNP is most prominent during the first and second resuspension. To avoid the loss of AuNP on the surface of the polymer test tube the centrifugation speed was reduced from 10,000 to 2,000 rpm. Changing the speed of the centrifuge allows for the AuNP to be re-suspended more easily and with more consistency, reducing the loss of AuNP to the polymer test tubes. The loss can be visually identified by a residual purple-black color on the surface of the plastic.

It is important to note that the changes seen depend on the medium used (PBS) as well as the state of the AuNP, (washed/centrifuged). Un-centrifuged samples showed little change over time in comparison to samples centrifuged and resuspended in water. As mentioned in Chapter 3, changes in the dielectric medium can be monitored easily by the shift of maximum absorption of the plasmon band.

In order to follow the state of the AuNP, UV analysis was followed at 530 nm and 700 nm, monitoring the peak at 700 nm follows the AuNP stability. As the AuNP agglomerate there is a peak that appears in the 700 nm region. Following the peak at 530 nm will also monitor the stability of the AuNP, and 260 nm monitors the DNA peak.

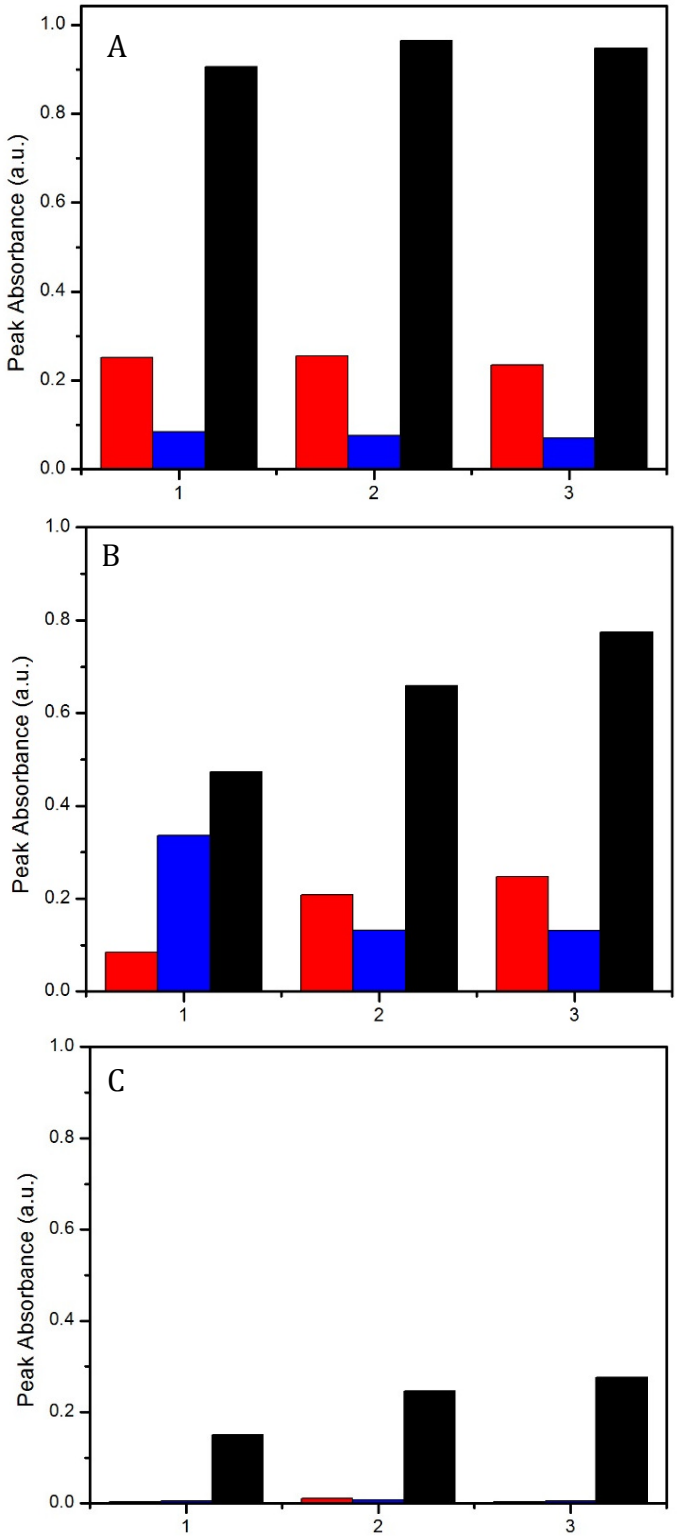

Figure 4.3: UV analysis of AuNP DNA mixture was measured at 530 nm (red), and 700 nm (blue) for potential agglomeration and finally at 260 nm for DNA (black) after sequential loadings 1, 2 and 3 corresponding to the number of DNA loadings completed (0.05 µM) for A) samples before centrifugation, B) after centrifugation, C) supernatant.

Sequential loading allows for a large concentration of DNA to be loaded in 3 sequential aliquots, allowing for the system to equilibrate to the change in environment. It also allows for a gradual addition of DNA on the surface of the nanoparticles which reduces the potential for agglomeration. As seen in Figure 4.3 maximum absorbance at three key wavelengths were monitored to see the effects of sequential loading, measurements were taken at 525 nm and 700 nm to monitor the stability of the AuNP. The increase in absorbance intensity at 700 nm represents the agglomeration of the AuNP and is often the result of insufficient surface coverage allowing the AuNP to agglomerate together. For the purpose of these experiments, the surface coverage of the AuNP needs to be maximized. Upon agglomeration of the nanoparticles, there is a reduced surface area available for loading. In an effort to avoid further losses, various concentrations of DNA were used on the surface of AuNP as well as the two types of binding methods. Once the loading method was established as 3 sequential loadings to increase the likelihood of DNA binding to the surface a long-term test was completed to determine the stability of both binding methods for the DNA.

Utilising the bond strength of Au-S allows the system to be more robust and more consistent; each particle has a similar coverage, however as mentioned in Chapter 3 there is an incubation time required to ensure the full coverage of the AuNP. Consistency was essential to have quantitative and qualitative results for the nanopore project. In-house AuNP had severe issues with stability due to the loss of particles on the walls of microfuge tubes. Many have noted that the use of stabilizing materials in solution such as PEG and the presence of salt could help avoid the loss of AuNP to agglomeration. [6, 15] To avoid the risk of sample agglomeration, some studies have shown that agglomeration can be avoided by loading DNA sequentially. The salt aging technique has been used to gradually change the dielectric media giving time for the AuNP to adjust and allow the DNA to functionalize the surface of the AuNP. [16] Following studies with the binding effects of amino and thiol terminated DNA other parameters were tested to ensure the optimal conditions for the highest possible loading of DNA on the surface of the AuNP. Firstly, we looked at two sources of AuNP, a commercial AuNP OligoREADY 50 nm AuNP and a citrate reduced 14 nm AuNP made in house. Both particles were loaded with two concentrations of 50 base pair double stranded DNA. The concentration of DNA was based on the potential surface coverage, 1X concentration (8 ng/L) allows for a single monolayer to assemble on the surface of the in-house AuNP and 4X concentration (32 ng/L) was a four-time excess of DNA. For further

analysis, the NH_2-DNA stability was tested on both a short term and long-term basis (24 hrs and 2 weeks). The two-week timeframe was chosen to model the time delay required to process samples in the barcode assay. Both types of DNA were tested for long-term stability, as often samples for the nanopore system would be required to have a shelf life of approximately 2 weeks, it is for this reason that the timeline of 2 weeks was chosen for testing. Figure 4.4 shows the results of the long-term stability testing of NH_2-DNA and SH-DNA.

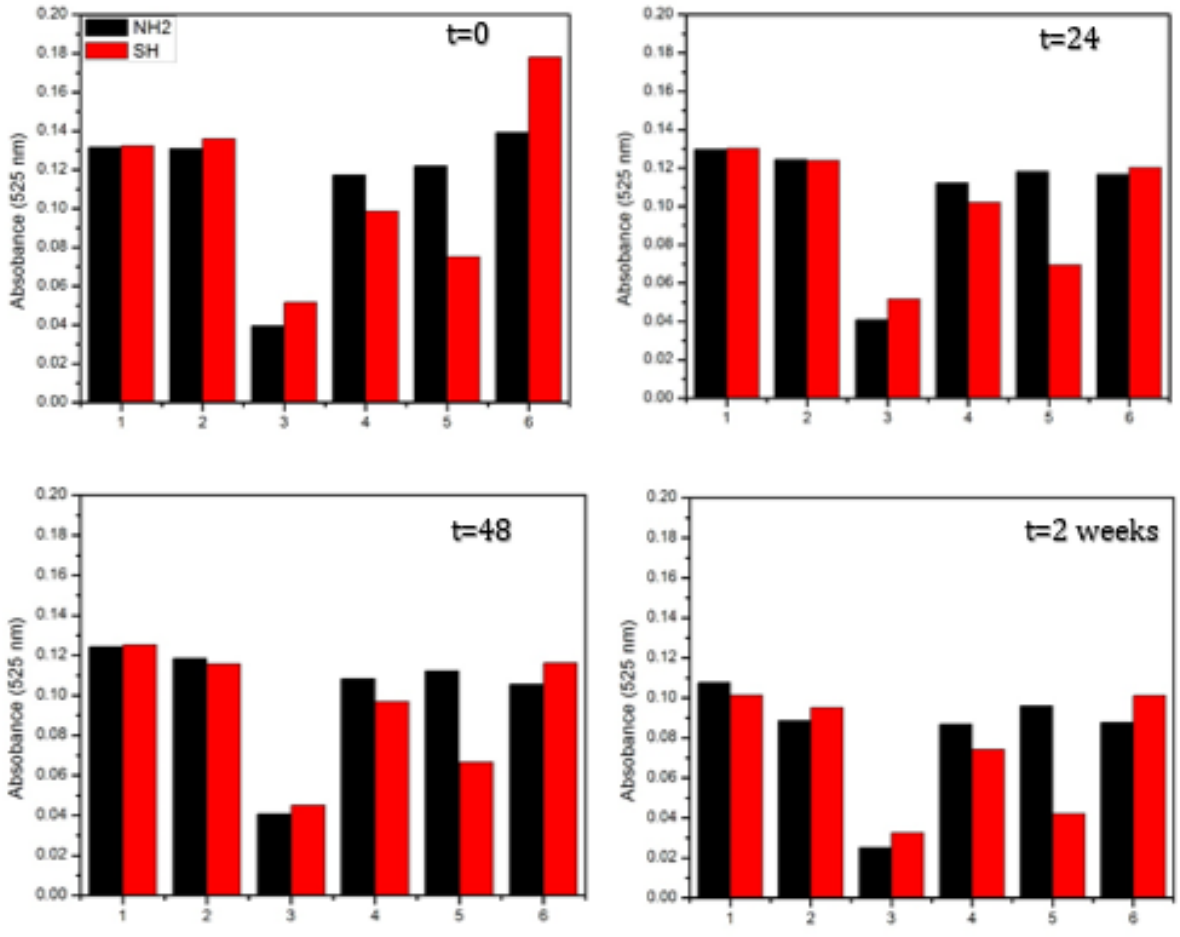

Figure 4.4: All samples were run with 200 nM DNA (where black is NH_2-DNA and red is SH-DNA) in the presence of in-house AuNP (1.8 nM) at time 0, 24 hours, 48 hour, 2 weeks, where in 1) samples were suspended in water and centrifuged, 2) suspended in 1X PBS and centrifuge, 3) samples were re-suspended in water and centrifuged a second time, 4) samples were re-suspended in 1X PBS and centrifuged a second time, 5) samples were suspended in water and finally re-suspended in 1X PBS and centrifuged and second time, and 6) un-centrifuged samples.

The use of thiol terminated DNA allows a strong gold-sulphur bond to ensure that the DNA was not lost to mechanical work done in the system, in particular there was minimal loss upon centrifugation of samples. In comparison to the NH_2-DNA, the thiols created a covalent bond with Au, which has shown to be stronger than the Au-Au bond itself.[17] Thiol terminated DNA was chosen due to the well-studied Au-S binding used in sensing applications. It is commonly known the stability and strength of the Au-S is around 130 kcal/mol.[17]

After initial testing which demonstrated that both NH_2-DNA and SH-DNA represented a general level of stability, SH-DNA was chosen as the ideal DNA due to the covalent bonding which is resistant to mechanical stress such as centrifugation and demonstrated a greater stability. In an effort to increase accuracy from initial UV testing further investigations were continued with the aid of fluorescent-labelled DNA. A fluorescent probe such as rhodamine was added to the DNA in order to produce a fluorescent signal, which would increase accuracy and sensitivity in comparison to UV-Vis spectroscopy. Fluorescence spectroscopy allows for a high quality signal at lower concentrations. The DNA was composed of the 50 base pair length strand with a 6-carbon chain attached to rhodamine dye (shown in Scheme 4.4).

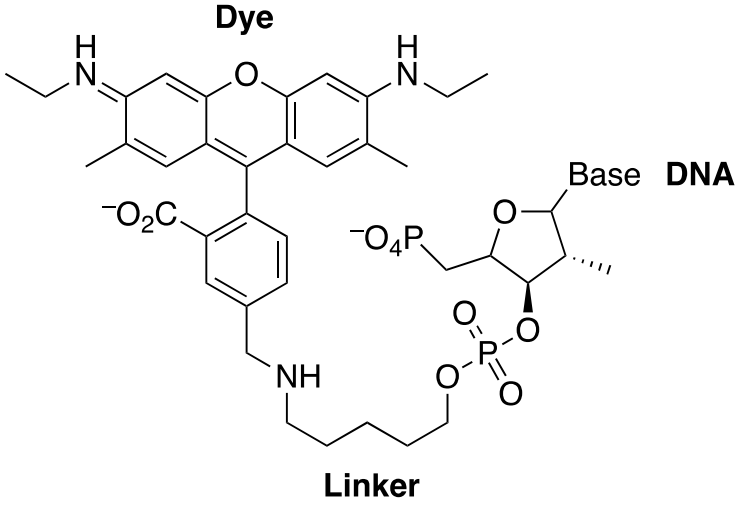

Scheme 4.4: Rhodamine-Labelled DNA.

The amount of Rh-labelled DNA was determined by fluorescence spectroscopy using the Rh emission band between 515 nm to 560 nm. Each DNA had a Rh label which then allowed for quantification of the sample.

We also investigated different DNA strands. The use of single- or double-stranded DNA (ssDNA and dsDNA, respectively) was a parameter that we varied in an attempt to increase surface coverage and nanopore signal. Due to the inherent nature of ssDNA to hybridize to a double stranded helix, the assay uses dsDNA for the majority of the testing. The dsDNA showed a greater resilience to manipulation throughout the various steps and stability testing. However, the ssDNA was also tested to verify the effect ssDNA could have on the system. Exploratory tests were conducted with a standard reduced volume cuvette (1.5 mL), however, due to the limited sample size produced by DNA loading experiments; another reduced-volume quartz cuvette was required (300 µL). Once we established the cuvette was precise, accurate further testing was continued to be able to determine the loading of Rh-labelled dsDNA on the surface of commercial AuNP.

From the initial fluorescence testing in Figure 4.5, the amount of DNA loaded on the surface is seemingly higher when a higher concentration of DNA is used. However, upon the cleaning and resuspension of the sample, Figure 4.6, the overall DNA that remains on the surface is no more than 10% of the potential loadings. The higher loadings result in higher loss of signal, which represents the surface saturation of the AuNP. One of the main issues with the loading was that the DNA did not seem to be adhering to the surface of the AuNP. Thus, further studies require the implementation of various techniques to increase loading and maintain stability. The use of sequential loadings of DNA as well as the aid of salt aging showed some improvements on the samples.

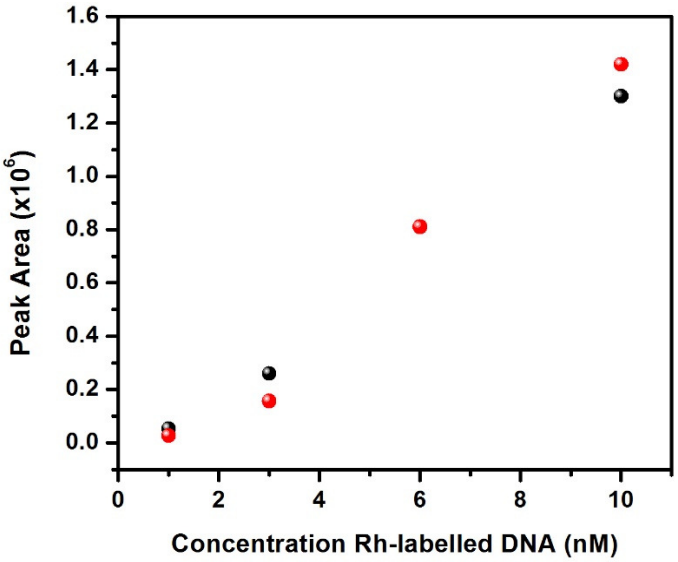

Figure 4.5: Fluorescence peak of dsDNA with the peak integrated between 515 nm and 560 nm upon excitation at 480 nm, before (black) and after 18-hour incubation (red) in the presence of 1.7 nM AuNP.

Results from Figure 4.6 show that only the sample supernatant had a level of detectable fluorescence. This was primarily due to the loss of AuNP as well as the concentration of DNA loaded on the surface was close to the limit of detection of the fluorimeter making the integration of the sample peak area very low. Due to the length of the DNA strands, excessive quenching of the fluorophore can be ruled out. As mentioned in Chapter 1, the distance of the fluorophore to the AuNP plays a key role in the AuNP potential to quench. The 50 base pair DNA strands that were used were approximately 15 nm long. The distance between the rhodamine attached to the end of the DNA strand should be far enough away from the AuNP to limit quenching. Thus, the low signal seen in Figure 4.6 is from little to no DNA binding on the surface of the AuNP.

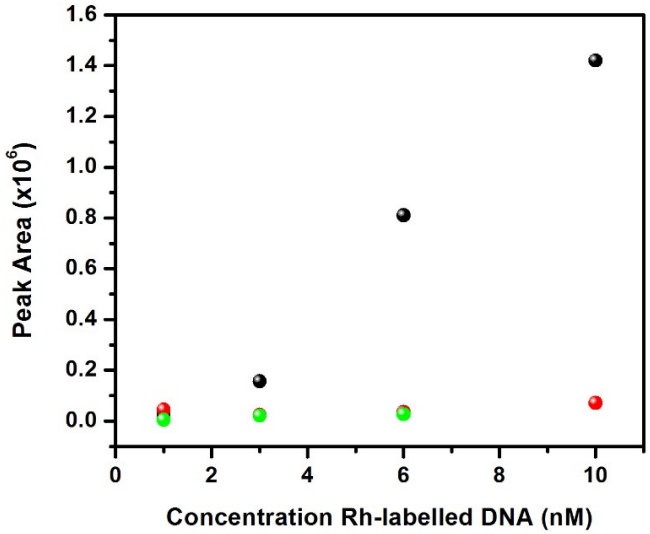

Figure 4.6: Fluorescence peak integrated between 515 nm and 560 nm upon excitation at 480 nm, of dsDNA with Commercial 50 nm AuNP (red), Supernatant of the centrifugation wash cycle (black) Resuspension of centrifugation washing pellet of DNA and AuNP (green) with varying concentration of Rh-labelled DNA.

In an attempt to increase potential loading on the surface of AuNP, we investigated ssDNA as a way to reduce steric problems in the system. ssDNA resulted in a much lower fluorescence signal (Figure 4.7). Unfortunately, the peak area of the samples is smaller for the ssDNA, most likely due to the losses to the test tube walls. At the highest concentration, 10 nM, the ssDNA had a fluorescence signal less than half that of the dsDNA. As a method of confirmation, emission spectra of both ssDNA and dsDNA were taken (Figure 4.7).

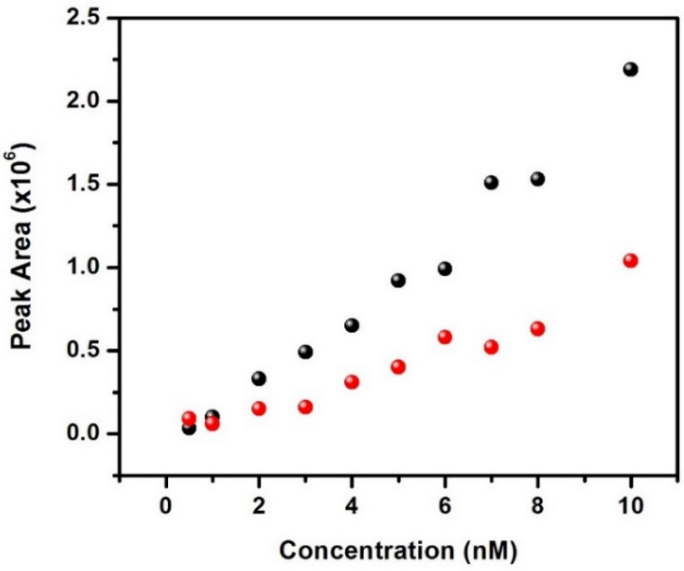

Figure 4.7: Fluorescence peak area of ssDNA (Red) and dsDNA (Black) with the peak integrated between 515 nm and 560 nm upon excitation at 480 nm, in the presence of 1.7 nM AuNP (14 nm).

The emission spectra are illustrated in Figure 4.8, showing further that the dsDNA produced approximately double the signal of ssDNA when comparing samples with the same concentration. The distinct peak of the dsDNA allowed for a clearer analysis between runs and it was easier to establish any changes. Furthermore, the rigidity of the dsDNA facilitates keeping the rhodamine dye away from the surface of the AuNP, which can reduce the quenching of the fluorophore. Due to a higher and more distinct signal along with the overall stability of the dsDNA, it was chosen as the ideal candidate to continue studies involving release and an environment that resemble largely that of the nanopore system the DNA would see in the final assay.

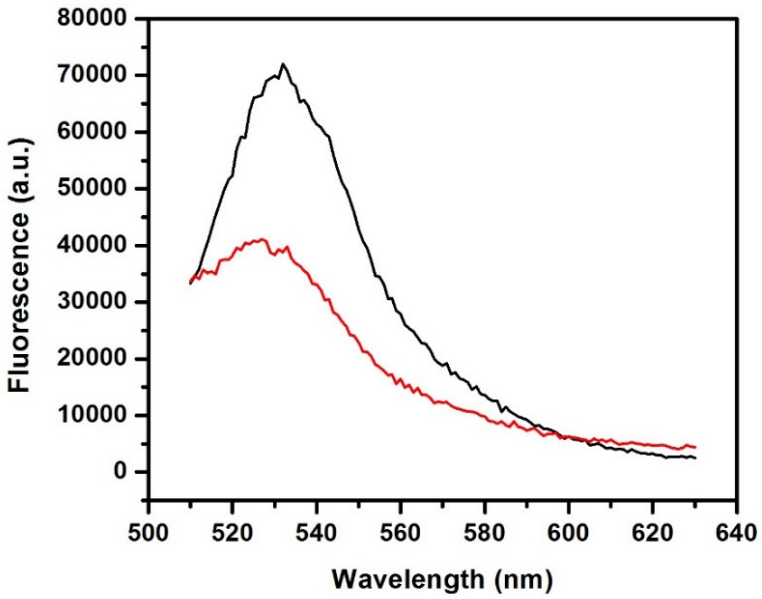

Figure 4.8: Fluorescence spectra of 10 nM dsDNA (Black) and 10 nM ssDNA (Red) upon excitation at 480 nm.

4.2 DNA Release

To be able to have a proper signal amplification, the release of DNA attached to the surface must be as efficient as possible. The cleavage of DNA has been tested with various methods; many studies have shown a variety of ways to cleave DNA off the carrier vessel; those that are common are enzymatic cleavage, dissolution of AuNP, and salt crashing shown in Scheme 4.5. [18, 19] Different methods were chosen for the two different types of DNA used. Methods which required the breaking of bonds were necessary for SH-DNA. However for the NH_2-DNA simple displacement methods could be used.

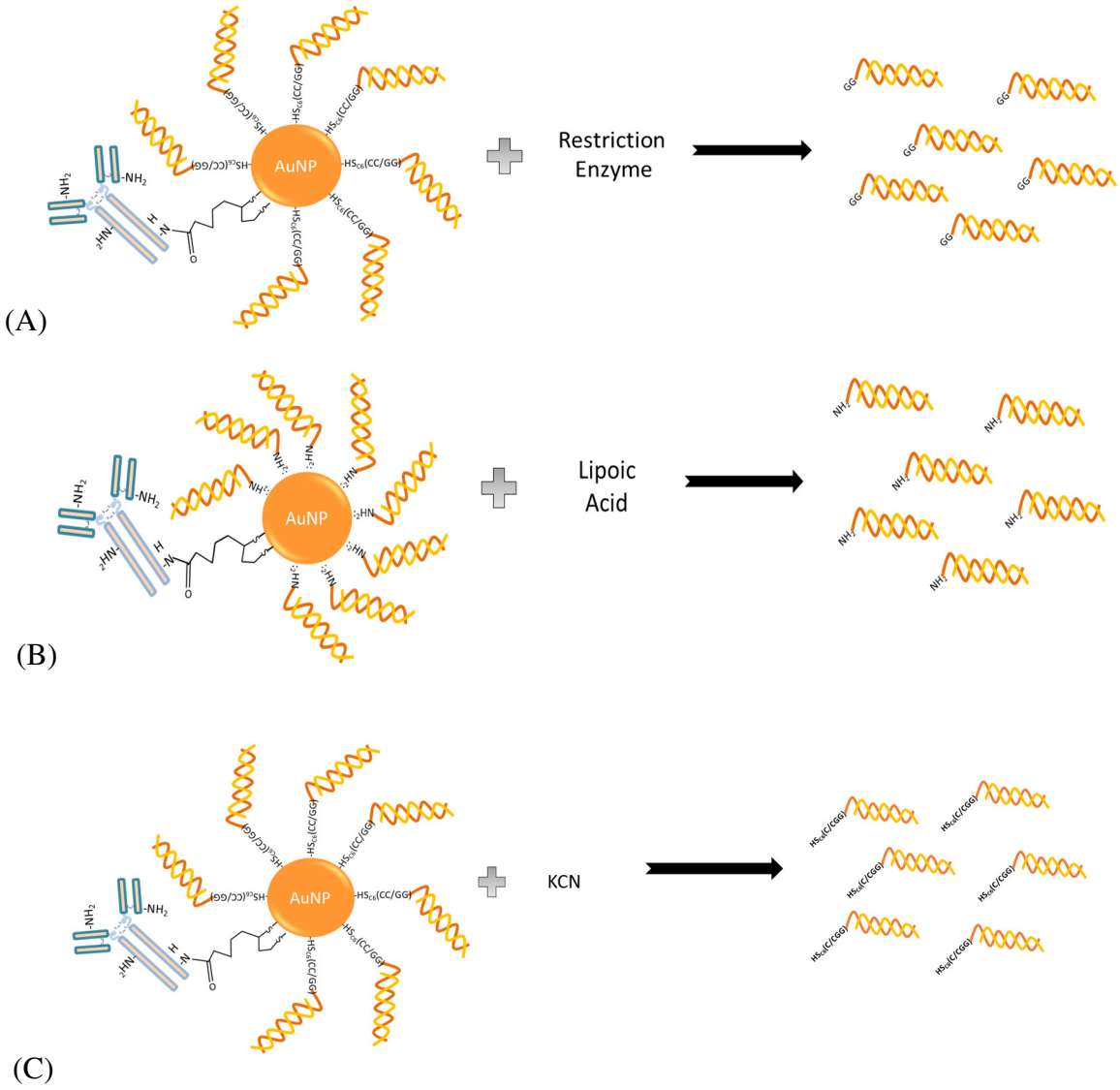

Scheme 4.5: DNA release techniques tested: (A) Enzymatic release requires DNA strands to have an extra 6 carbon chain to allow space for restriction enzyme to cut DNA sequence. (B) Lipoic acid can displace NH_2-DNA electrostatically bound to the surface of the AuNP. (C) KCN can dissolve the AuNP releasing the thiol bound DNA.

The cleavage of DNA must be efficient to ensure proper quantification. One common method to remove DNA from the surface is the release via an enzymatic cleavage. The DNA used has a specific cut sequence for which the enzyme can cleave the DNA from the AuNP, and then the DNA can be quantified in the nanopore. However, the nanopore must not be blocked by larger elements such as the AuNP. It is crucial to remove or precipitate the nanoparticles to ensure the pores ability to have clear readings. It is for this reason that methods that dissolve and release the DNA simultaneously were also investigated; they include the use of KCN as well as those that

keep the AuNP intact but release the DNA bound such as lipoic acid (LA). LA, as mentioned in chapter 2 created covalent bonds which can displace the NH_2-DNA electrostatically bound to the surface of the AuNP. A quantification method that has been used, follows the UV spectra of the colloidal solutions. However there have been issues with the UV measurements producing distinct peaks, Baldock *et al*. have utilised the area in which DNA absorbs around 260 nm. Issues arise with the scattering of light due to Au salts and/or Au clusters, which results in a greater lever of difficulty quantifying the 260 nm measurement.[19] The scattering of the AuNP can cause inconsistencies around the 260 nm range.

To overcome the issues with peak overlap, experiments were conducted to remove the gold nanoparticles, the use of KCN was employed to dissolve all gold, creating $KAu(CN)_2$ which has distinct peaks separate from the DNA peak at 260 nm as shown in Figure 4.9.

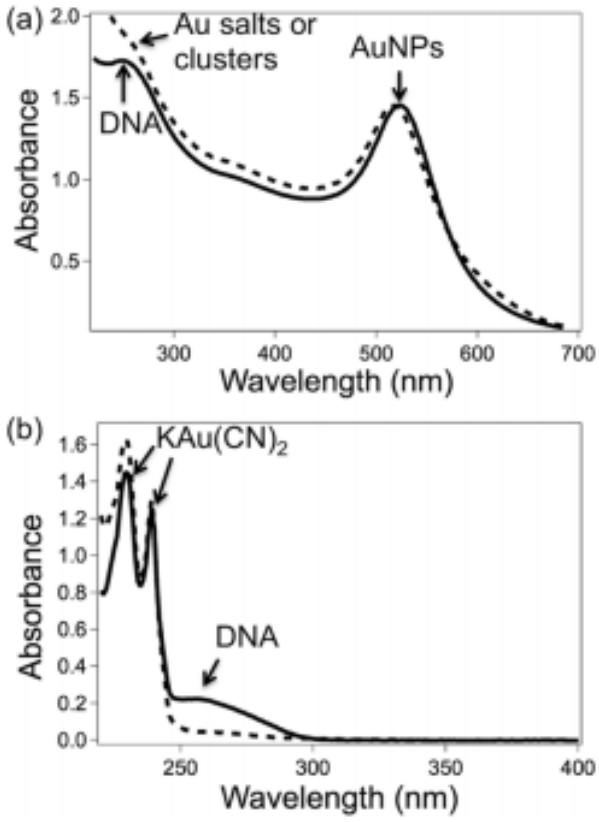

Figure 4.9: UV spectra of KCN dissolution of AuNP. Reprinted with permission from Anal Chem Copyright (2016).

The addition of cyanide results in the complex with gold giving significant peak shift which allowed for analysis of the DNA absorbance peak. The prescence of CN^- could indeed release the

DNA loaded onto the surface of the AuNP, which is dissolved in the process. In the studies presented in Chapter 4 NaCN was used to dissolve AuNP and release the DNA loaded on the surface of the particles. The use of cyanide to dissolve metals is also known as cyanide ethching.

Initial testing has shown that DNA is not significantly affected by the presence of the NaCN; furthermore the addition of NaCN to AuNP demonstrates the removal of the peak at 520 nm which is characteristic of AuNP and the appearance of the peaks at 230 nm and 240 nm (Figure 4.10).

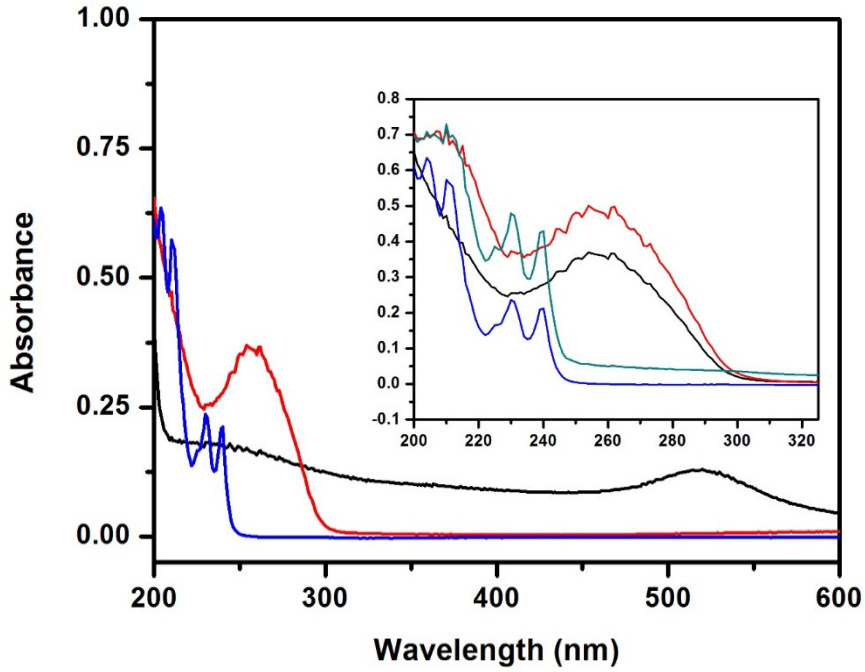

Figure 4.10: UV spectra were taken to demonstrate DNA (red), AuNP (black), and finally AuNP in the presence of KCN (blue). Inset: UV spectra of dsDNA (Black), DNA in the presence of 100 µM NaCN (red), 14 nm AuNP suspended in water in the presence of 100 µM NaCN (green), 14 nm AuNP suspended in 1X PBS in the presence of 100 µM NaCN (blue).

A visual colour change was seen in the AuNP solution, going from a ruby red to clear. Due to the overlapping issues of the DNA and the dissolution product of the AuNP, as seen in Figure 4.10, this method was no longer pursued. The use of lipoic acid as a method to displace DNA was deployed as a way of displacing NH_2-DNA from the surface of the AuNP, since the NH_2-DNA did not involve the formation of a covalent bond on the surface. Further, the addition of the LA was hypothesised to displace the NH_2-DNA, with the formation of two covalent Au-S bonds (130

kcal/mol) in its place. [17] In comparison to NaCN, the use of LA is a process that requires longer incubation times as showed in Chapter 3.

4.2.1 SERS

Surface Enhanced Raman Spectroscopy (SERS) has also grown in interest, with applications in clinical sensing. SERS takes advantage of the increases in Raman signal intensity for molecules adsorbed on the surface of NPs. The experiment relies on the scattering of light, and thus rough surfaces are required for there to be significant enhancement. SERS can be utilised similarly to fluorescence to follow bonding kinetics on the particle surface based on peak intensity. When considering the bonding of a SH-DNA onto the AuNP the most prominent peaks are from the Au-S bonding. Samples of rhodamine dye and AuNP were tested to first see if the system would be sensitive enough to measure low concentration samples in the nanomolar range. Upon testing of multiple concentrations of rhodamine dye, shown in Figure 4.11, many inconsistencies were noted and it was determined that SERS would not be a valid method to quantify the DNA bound to the surface of AuNP for the given concentrations.

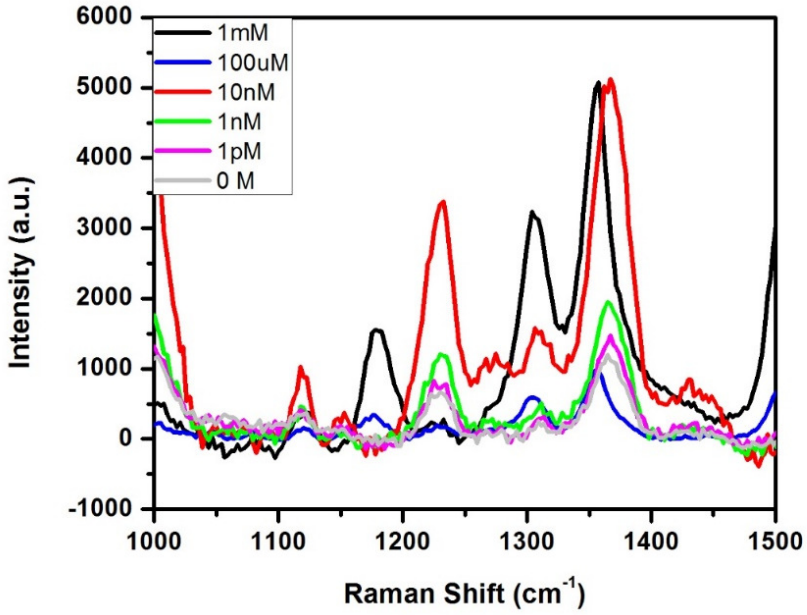

Figure 4.11: SERS spectra of increasing concentration of rhodamine dye 0-1mM.

4.2.2 Antibody Loading

Antibodies are common linkers used to recognize target proteins, which make them ideal candidates to be bound to AuNP. The nanopore's amplification relies on the use of antibody to

capture the given target protein (TSH). Firstly, there are two antibodies required to capture the target protein, one attached to a paramagnetic bead and the other one is attached to the AuNP. The antibodies capture/sandwich the target protein, which can then be separated via the paramagnetic bead with a powerful magnet.

The orientation of the antibody should be monitored to ensure proper binding and surface coverage of the nanoparticle. Ideally, to maintain quantifiable and reliable system the MMP should bind 1:1 to the antibody attached to the AuNP. When considering the reliability of the amplification, one aspect to consider is the loading of antibodies on the surface of the AuNP. To ensure a high DNA loading, it is ideal to have a single antibody on the surface of the AuNP. Having a single antibody also reduces errors related to binding the target analyte. If multiple antibodies are bound to the AuNP, multiple target analytes could be bound to a single AuNP, thus reducing the amplification. Another aspect to consider is the orientation of the antibody and the type of interaction that it may have with the surface of the AuNP. As seen in Figure 4.12 there are three common orientations adopted by the antibody. In orientation A the antibody is adsorbed onto the surface of the nanoparticle, however in a horizontal orientation there is a larger loss of surface area than if the antibody was attached vertically (Orientation C). In orientation B, we see the antibody is electrostatically bound to the surface of the AuNP and finally, in orientation C the antibody is covalently bound to the surface of the AuNP. Both orientations A and B can lead to lower binding of DNA on the surface of the AuNP which will in turn reduce the number of events detected by the nanopore. Furthermore, orientations A and B lead to a higher degree of steric interactions between the two particles when binding to the target protein, it is for this reason these two were avoided for testing. An antibody with a thiol-terminated end was chosen to allow a vertical orientation C that allows the target protein to be more readily bound and optimal DNA loading on the surface of the AuNP.

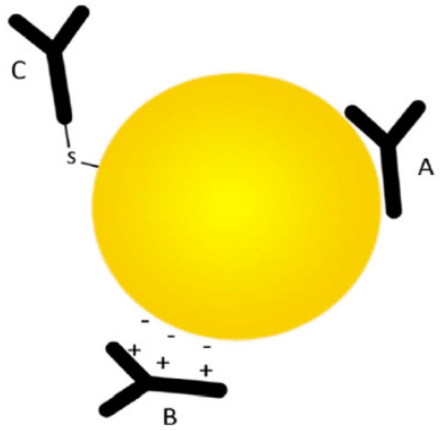

Figure 4.12: Illustration of potential binding of antibodies onto the surface of a AuNP From ref. 20 Reprinted with permission from Sensing and Bio-Sensing Research Copyright (2016).

Following the functionalization of antibodies on the surface of the AuNP, no testing was completed due to the lack of stability of the solution. After an overnight incubation period the AuNP were lost to the wall of the test tubes. This in conjunction with the low results from the fluorescence quantification lead to the testing of various test tube materials.

4.3 Tube testing

Low signals and inconsistencies in preliminary testing of Rh-DNA sparked interest in determining the source of test fluctuations. Upon running multiple trials of the same concentration, many inconsistencies were seen in consecutive trials as well as trials run at an earlier time. It is for this reason that studies to test the DNA binding to the surface of the containers was looked at in more detail. A long-term incubation study was conducted to monitor the loss of DNA to the surface of the microfuge tube. A microfuge tube was incubated with Rhodamine-6G dye labelled DNA and the fluorescence of the sample was monitored over time, exciting the sample at 480 nm and integrating the emission peak from 510 nm to 630 nm. The solution was pipetted out of the microfuge tube into a quartz cuvette for measurement in intervals of 15 minutes, once the scan was completed the sample was returned to the microfuge tube and the process was continued over the course of 4 hours. We noted that over the course of a few hours the samples fluorescence signal decreases. Figure 4.13 shows the results of the sample loss over time, there was a 50% signal loss in the span of 4 hours. A final sample was taken after 24 h to verify if any further loss would occur, the test tubes showed minimal loss after the initial 4h-incubation period.

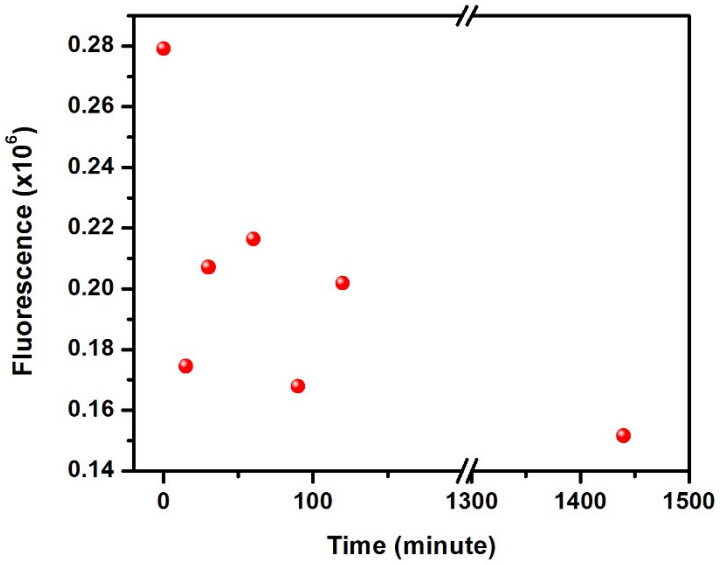

Figure 4.13: Fluorescence peak area integrated from 515 nm to 560 nm upon excitation at 480 nm, of 10 nM rhodamine DNA incubated over time in polyallomer tube testing at 10nM.

Since samples in the nanopore assay will remain on a shelf overnight and up to periods of two weeks, the stability of the DNA is crucial. The standard Eppendorf used were the Beckman Coulter polyallomer microfuge tubes (PA), they demonstrated significant loss of DNA, which can be seen in Figure 4.13. Following the results in Figure 4.13 different variables such as concentration and wall coating were investigated as a potential way to reduce loss of material to the test tube walls, (shown in Figure 4.14).

Polyallomer test tubes were run to test the loss of DNA; samples were incubated over time and monitored to measure the fluorescence intensity loss. When looking at Figure 4.14 the intensity of both concentrations of Rh-DNA (10 and 20 nM) without the presence of salt, have a similar final fluorescence intensity. We investigated further by looking at the percentage of DNA loss for the 20 nM concentration shown in Table 1. In an attempt to clarify results, we tried to verify the effects of various aspects; the main aspects researched in my study were the use of a wall coating as well as the presence of salt. The use of a wall coating was established by incubating and washing test tubes with standard protein solutions such as BSA (Bovine Serum Albumin) and Sample Diluent (see Chapter 2). High salt concentrations were commonly used in the bio barcode system, thus to emulate the environment of the assay high salt concentrations were verified when

testing test tubes for DNA binding to plastic. Since the standard polyallomer tubes, which had been regularly used in testing, showed large signal inconsistencies related to the loss of DNA on the surface, we began to investigate other types of test tubes available on the market.

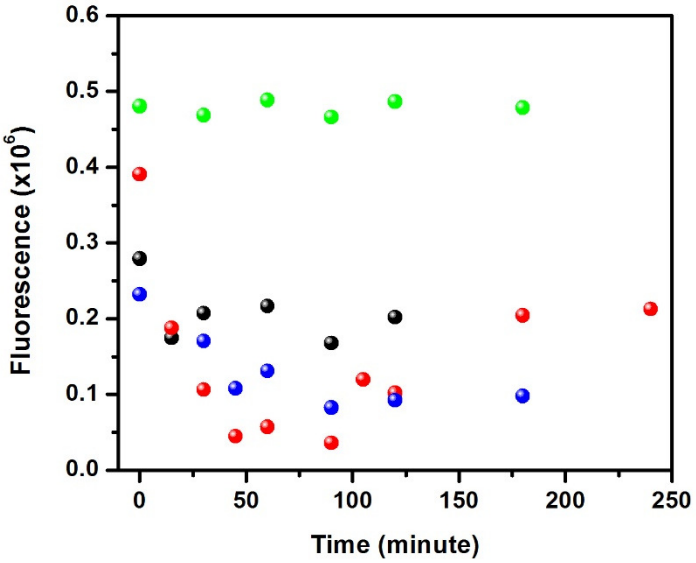

Figure 4.14: Fluorescence peak area integrated from 515 nm to 560 nm upon excitation at 480 nm of rhodamine DNA incubated over time in polyallomer tube testing at 10 nM (Black) and 20 nM (red) as well as in the presence of 2M KCl 10 nM (Blue) and 20 nM (Green).

A variety of commercial "bind" resistant Eppendorf tubes were tested along with one fabricated in house with a 3D printed material that resembles that used in the nanopore system. As results from Table 4.1 show, the adhesion resistant marketed tubes resulted in a similar loss of DNA. Following results found with PA, other tubes were investigated because multiple companies offer non-stick or low binding materials such as Eppendorf DNA LoBind Tubes, VWR non-stick surface micro-centrifuge (NS), and 3D printed tubes. Each of these tubes were designed to result in reduced attraction of sample onto the surface of the test tube.

Table 4.1: Tube retention testing parameters and results.

Tube	Wall Coating	KCl	% loss
PA			45
		2M KCl	64
			89*
		2M KCl	5*
	BSA		60ŧ
	Sample Diluent		24
3D Printed			37
Low Bind			86
NS			53
Glass			64ŧ

*Samples contained 20 nM dye. ŧ No DNA.

Higher concentrations of Rh-DNA still lead to a similar final fluorescence intensity, which demonstrates the attachment of the DNA on the surface had either not reached saturation or the DNA was creating a multilayer on the tube surface. However, further research would be required to confirm this.

Results seen in Figure 4.15 show that the three new materials for the test tubes demonstrated a similar loss to the PA microfuge. Many of the test tubes were commercially marketed as "bind" resistant. Tests with the use of both rhodamine labelled and standard unlabelled DNA were run and incubated in the test tubes, which lead to the discovery that the use of Rh-labelled DNA, was the cause of the loss to the walls of the materials. This was confirmed with gel electrophoresis, which was run by the Tabard-Cossa group, which can be seen in Figure 4.16. However in all cases the test tubes from the three different sources resulted in high loss.

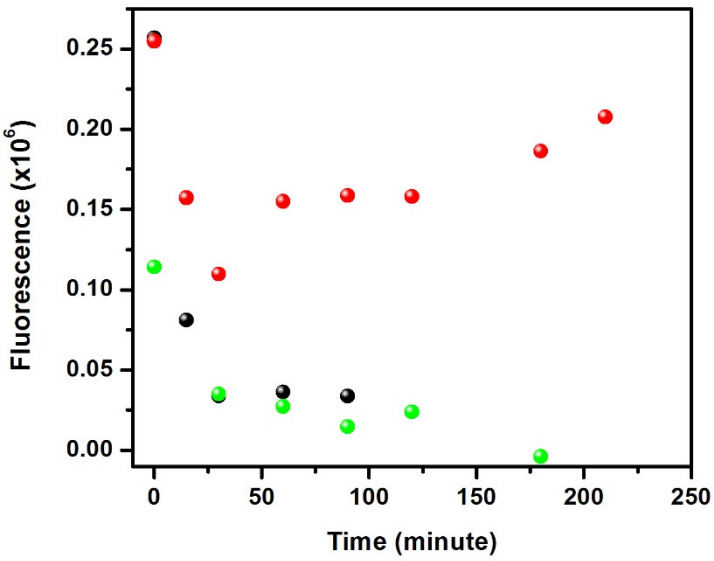

Figure 4.15:Fluorescence peak integrated from 515 nm to 560 nm upon excitation at 480 nm of alternative plastic test tube were tested for incubation with 10 nM Rh-DNA low bind (Black), 3D printed (Red), and NS(Green) tubes.

The gel electrophoresis results demonstrate the effect of adding a rhodamine dye label to 50 base pair DNA. Gel electrophoresis is used to be able to measure the level of DNA present in a sample by the density of DNA in the wells, which is visually seen by the darker shades. Both samples were run in duplicate trials, where in which Rh-50BP DNA as well as 50 BP DNA were incubated for an hour in a PA tube as well as mixed directly and injected into the gel. As seen in Figure 4.16 the addition of the rhodamine label results in a decrease in signal intensity after an hour of incubation in the PA tubes. Whereas in comparison the non-labelled 50 BP DNA did not show a decrease in signal intensity. Since the Rh-labelled DNA resulted in lower yields than anticipated, combined with the loss of DNA to the surface of experimental equipment, this avenue of research was stopped. The issues related to the Rh-labelled DNA resulted in the development of other types of amplification methods to be investigated by the Tabard-Cossa group in an effort to further increase the signal amplification of the nanopore assay.

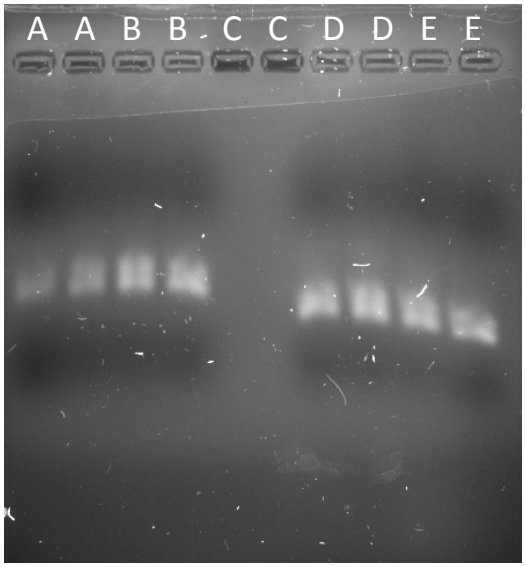

Figure 4.16: Gel electrophoresis of A)Rh-labelled DNA (1h incubation), B) Rh-labelled DNA, C) Empty, D) dsDNA (1 h incubation), and E) DNA.

In conclusion, many studies for the nanopore assay through the use of SH-DNA on the surface of AuNP as an amplification method may require further development. It was concluded that the use of ssDNA would not be an efficient way to measure signal amplification due to low fluorescent signal. In comparison the dsDNA resulted in an overall higher fluorescent signal, which allowed some tests to be completed; however, results were not conclusive. In an attempt to understand the different pathways of the rhodamine DNA, we ran various controls to determine what caused the lack of signal. Following control test with dsDNA, it was noted that there is a significant loss of DNA to plastic materials. Furthermore, we have discovered that the use of many test tubes, which are considered low binding, should be reviewed as most have shown over 50% loss of dye to the wall surface at nanomolar concentrations (20 nM). Moreover, my results showed that the use of surfactants on the surface of the test tube walls could be used as a method to reduce loss, though the use of bulkier materials such as BSA is not recommended, as it is difficult to remove from solution and can block the nanopore at later stages in the assay. Incubating test tubes overnight with surfactants such as sample diluent (see Chapter 2) and the use of high salt concentrations (2M KCl) showed significant increased stability of the DNA in solution.

4.4 References

1. Yu, H.; Xu, X.; Liang, P.; Loh, K. Y.; Guntupalli, B.; Roncancio, D.; Xiao, Y., A Broadly Applicable Assay for Rapidly and Accurately Quantifying DNA Surface Coverage on Diverse Particles. *Bioconjug Chem* **2017,** *28* (4), 933-943.
2. Nam, J. M.; Thaxton, C. S.; Mirkin, C. A., Nanoparticle-based bio-bar codes for the ultrasensitive detection of proteins. *Science* **2003,** *301* (5641), 1884-1886.
3. Thaxton, C. S.; Nam, J. M.; Mirkin, C. A., PCR-like sensitivity for proteins with bio-bar-code amplification. *Discov Med* **2003,** *3* (19), 58-60.
4. Tabard-Cossa, V.; Karau, P., Capture and Translocation Characteristics of Short Branched DNA Labels in Solid-State Nanopores. *ACS Sensors* **2018,** *3*, 1308-1315.
5. Sarapura, V. D.; Wood, W. M.; Gordon, D. F.; Ridgway, E. C., A cell line that produces the glycoprotein hormone alpha-subunit contains specific nuclear factors similar to those present in thyrotropes. *Thyroid* **1992,** *2* (1), 31-38.
6. Hurst, S. J.; Lytton-Jean, A. K.; Mirkin, C. A., Maximizing DNA loading on a range of gold nanoparticle sizes. *Anal Chem* **2006,** *78* (24), 8313-8318.
7. Beamish, E.; Kwok, H.; Tabard-Cossa, V.; Godin, M., Fine-tuning the size and minimizing the noise of solid-state nanopores. *J Vis Exp* **2013,** (80), e51081.
8. Tabard-Cossa, V.; Wiggin, M.; Trivedi, D., Single-Molecule Bonds Characterized by Solid-State Nanopore Force Spectroscopy. *ACS Nano* **2009,** *3* (10), 3009-3014.
9. Giljohann, D. A.; Seferos, D. S.; Patel, P. C.; Millstone, J. E.; Rosi, N. L.; Mirkin, C. A., Oligonucleotide loading determines cellular uptake of DNA-modified gold nanoparticles. *Nano Lett* **2007,** *7* (12), 3818-3821.
10. Pensa, E.; Cortés, E.; Corthey, G.; Carro, P.; Vericat, C.; Fonticelli, M. H.; Benítez, G.; Rubert, A. A.; Salvarezza, R. C., The chemistry of the sulfur-gold interface: in search of a unified model. *ACC Chem Res* **2012,** *45* (8), 1183-1192.
11. Goldmann, C.; Lazzari, R.; Paquez, X.; Boissière, C.; Ribot, F.; Sanchez, C.; Chanéac, C.; Portehault, D., Charge Transfer at Hybrid Interfaces: Plasmonics of Aromatic Thiol-Capped Gold Nanoparticles. *ACS Nano* **2015,** *9* (7), 7572-7582.
12. Pacioni, N. L.; González-Béjar, M.; Alarcón, E.; McGilvray, K. L.; Scaiano, J. C., Surface plasmons control the dynamics of excited triplet states in the presence of gold nanoparticles. *J Am Chem Soc* **2010,** *132* (18), 6298-6299.
13. Teo, Y. N.; Wilson, J. N.; Kool, E. T., Polyfluorophores on a DNA Backbone: A Multicolor Set of Labels Excited at One Wavelength. *J Am Chem Soc* **2009,** *131* (11), 3923-3933.
14. Liu, Y.; Xu, J.; Wang, Q.; Li, M. J., Coupling coumarin to gold nanoparticles by DNA chains for sensitive detection of DNase I. *Anal Biochem* **2018,** 555, 50-54.
15. Stiufiuc, R.; Iacovita, C.; Stiufiuc, G.; Florea, A.; Achim, M.; Lucaciu, C. M., A new class of pegylated plasmonic liposomes: synthesis and characterization. *J Colloid Interface Sci* **2015,** *437*, 17-23.
16. Zhang, X.; Servos, M. R.; Liu, J., Surface science of DNA adsorption onto citrate-capped gold nanoparticles. *Langmuir* **2012,** *28* (8), 3896-3902.
17. Xue, Y.; Li, X.; Li, H.; Zhang, W., Quantifying thiol-gold interactions towards the efficient strength control. *Nat Commun* **2014,** *5*, 4348.
18. Vanegas, J. P.; Scaiano, J. C.; Lanterna, A. E., Thiol-Stabilized Gold Nanoparticles: New Ways To Displace Thiol Layers Using Yttrium or Lanthanide Chlorides. *Langmuir* **2017,** *33* (43), 12149-12154.

19. Baldock, B. L.; Hutchison, J. E., UV-Visible Spectroscopy-Based Quantification of Unlabeled DNA Bound to Gold Nanoparticles. *Anal Chem* **2016,** *88* (24), 12072-12080.
20. Jazayeri, M. H.; Amani, H.; Pourfatollah, A. A., Various methods of gold nanoparticles (GNPs) conjugation to antibodies. *Sensing and Bio-Sensing Research* **2016,** *9*, 17-22.

Chapter 5: Conclusions and Future Work

Table of Contents

5. Conclusions

5.1 Summary

The work in this thesis was inspired by two projects. The motivation behind the first project was our interest in understanding the delay required between reagent mixing and completion of the S-Au derivatization process. In order to address this issue involved the use of fluorescence spectroscopy.

The second project explored the feasibility of using Au-S bonding as an application to amplify signal in a nanopore assay; developed in a clinical diagnostic tools. Nanoparticles are bridging the gap between the uses of chemistry as an aid in the development of materials for biological applications. The overall goal was to establish an assay in which the target analyte can be measured at the sub picomolar level with the aid of a nanopore structure.

The study has shown that, unlike industrial and research common practices, an incubation time of 90 minutes is recommended to ensure proper surface functionalization of the thiols onto the AuNP. Furthermore, thiol composition and the particles used all play a role in the creation of the Au-S bond. In the case of disulfides, such as lipoic acid (LA) an overnight incubation would be required to allow time for the S-S bond to break concurrently to the functionalization of the surface with the creation of Au-S bond. We also noted that various batches of similar sized nanoparticles did not affect the rate at which the Au-S bond is made. These results prove the reactivity of several thiols occurs within the same timescale; however, disulfides (such as LA) react much more slowly. For simple thiols, we recommend one to two hour wait for thiol binding to be essentially complete, while for disulfides, overnight incubation is recommended. Any "ready-mix" strategy is bound to lead to results obtained while the formation of thiolate bonds was still in progress.

We also noted that the environment of the nanoparticles affects the fluorescence signal; for example, two different batches of AuNP were tested to illustrate the variability between different batches. As mentioned in Chapter 2 each batch of AuNP can have slight differences in the polydispersity and this has an effect on the fluorescent signal obtained. For each batch of AuNP, the pH was measured using pH paper and was adjusted as needed with NaOH. Obtaining AuNP at the required pH was crucial for the reproducibility of the fluorescence signals. When looking at Figure 3.9 the presence of NaOH has an effect on the fluorescence properties of the C-SH. To ensure that no fluctuation of the fluorescence intensity was present, a second batch AuNP was

synthesized in the same method as those above, giving an average particle size of 17 nm. Figure 3.9 demonstrates the results of the reproducibility testing both with the same concentration as well as with a second batch of AuNP.

In the bioassay project, the main issues limiting the development of the project are low quantity of sample and signalling issues due to the inherent nature of the DNA to "stick" to the surface of the material at the extremely low concentrations used. However, from results in Chapter 4 we were able to establish that thiolated DNA binds more readily to the surface of AuNPs than Amino terminated DNA presumably because Au-S creates a covalent bond whereas Au-N is an electrostatic interaction on the surface of the AuNP. Following testing of termination for the DNA strands, ssDNA and dsDNA were tested. The use of ssDNA would not be an efficient way to measure signal amplification due to a lack of fluorescent signal. In comparison the dsDNA resulted in an overall higher fluorescent signal, which allowed some tests to be completed. However, results were not conclusive. In an attempt to understand the different pathways of the rhodamine-DNA, we ran various controls to determine what caused the lack of signal. This work has shed light on a larger issue with the inherent nature of the DNA to stick on the surface as seen in Figure 4.15 and 4.16, multiple tubes that were labeled and marketed as non-stick, or low binding, showed losses over 50% at nanomolar concentrations (20 nM). This issue can be circumvented with the use of proteins or surfactants (BSA and sample diluent) on the walls of the microfuge tubes. However, the presence of the larger molecules such as BSA in the final solutions resulted in blockages in the later stages of the nanopore assay. Incubating test tubes overnight with surfactants such as sample diluent and the use of high salt (2 M KCl) showed significant increased stability of the DNA in solution.

Future Work

5.2 Future Work

5.2.1 How Fast Can Thiols Bind to the AuNP Surface

Further investigation with the use of various competitive reactants was utilised to demonstrate how structure would affect their competitive potential. We have noted that the structure of the thiol has an impact on the speed at which it will bind to the surface. We discovered that thiol structure and size can play a role in reactivity, competitive reactants such as aromatic and aliphatic, can be considered within the same incubation period; however, disulphides (such as

LA) should be considered differently, as mentioned above. When using aromatics and aliphatic thiols, one can assume that after 90 minutes the surface of the AuNP has been properly functionalized. Further development will be required to properly understand and evaluate the kinetic bonding of the competitive reactant. The effect of a competing reactant should not affect the initial rate at which C-SH can bind to the surface of the AuNP.

5.2.2 Nanopore Barcode Assay

A significant drawback of the nanopore assay is the low concentrations of samples, which require systems to be able to measure extremely dilute samples with minimal loss. In the nanopore assay further investigation is required to determine an efficient way to reduce the loss of DNA on the surface of plastic tubing. In an attempt to avoid issues with DNA loss, finding DNA that has a strong enough signal on its own may warrant further research. There is potential to develop a DNA strand that generates a fluorescent signal without the addition of a fluorescent probe as the probe could be one of the causes for DNA sticking to the surface of the microfuge tubes. A method to circumvent the agglomeration and loss of nanoparticle would also be required, studying a larger scope of different sized nanoparticles. Different coating agents could allow larger amounts of DNA to bind with greater ease while maintaining nanoparticle stability.